

Università degli Studi dell'Insubria
DIPARTIMENTO DI SCIENZA E ALTA TECNOLOGIA

Ph.D. Thesis / Dissertation

The Renormalization Scale Setting Problem in QCD

Author:

Leonardo Di Giustino

Advisor:

Prof. Philip G. Ratcliffe

Chair of the Doctoral Programme:

Prof. Giuliano Benenti

XXXIV CICLO - January 2022

Contents

Introduction	1
1 Quantum Chromodynamics	8
1.1 Introduction	8
1.2 The flavor symmetry: $SU(3)_f$	10
1.3 Hints for color	12
1.4 Quarks and gluons	12
1.5 Gauge theories	14
1.6 The QCD Lagrangian	15
1.7 Quark states and $SU(3)_c$	16
2 The Renormalization Group	19
2.1 Renormalization	19
2.2 The running coupling constant $\alpha_s(\mu)$	21
2.3 The evolution of $\alpha_s(\mu)$ in perturbative QCD	23
2.4 One-loop result and asymptotic freedom	25
2.5 Two-loop solution and the perturbative conformal window	27
2.6 α_s at higher loops	30
2.7 The β coefficients in different schemes	32
2.8 The Λ parameter and quark thresholds	33
2.9 The Renormalization Group Equations	37
2.10 The Extended Renormalization Group Equations	39

3	Renormalization Scale Setting in QCD	43
3.1	Conventional scale setting - CSS	44
3.2	The Principle of Minimal Sensitivity: PMS Scale-Setting	48
3.3	The Fastest Apparent Convergence principle - FAC scale setting	49
3.4	The BLM Scale-Setting	51
3.5	Phenomenological comparison	56
4	The Principle of Maximum Conformality - PMC scale setting	58
4.1	The multi-scale Principle of Maximum Conformality: PMCm	61
4.2	The single-scale Principle of Maximum Conformality: PMCs	63
5	Infinite-Order Scale-Setting using the Principle of Maximum Conformality: PMC_∞	65
5.1	Intrinsic conformality (iCF)	66
5.2	Comments on the iCF and the ordered scale invariance	71
5.3	The PMC_∞	73
5.4	iCF coefficients and scales: a new “How-To” method	74
5.5	PMC_∞ results for thrust and C-parameter	76
5.6	The PMC_∞ scales at LO and NLO	79
5.7	NNLO Thrust distribution results	81
5.8	NNLO C-parameter distribution results	85
6	The thrust distribution in the QCD perturbative conformal window and in QED	89
6.1	The thrust distribution according to N_f	89
6.2	The thrust distribution in the Abelian limit $N_c \rightarrow 0$	92
7	Precise determination of the strong coupling and its behavior from Event Shape variables using the PMC	96
7.1	Running behavior	97
7.2	$\alpha_s(Q)$ from mean values	99

7.3	$\alpha_s(M_Z)$ from χ^2 -fit	101
8	Heavy-quark pair production near the threshold region	105
8.1	The QCD process of the quark pair production in the $\overline{\text{MS}}$ scheme . .	106
8.2	Quark-pair production in the V-scheme	113
8.3	Lepton pair production	116
	Summary	119
	Conclusions	125
	Bibliography	128

Glossary

AF asymptotic freedom.

BLM Brodsky-Lepage-Mackenzie.

BSM beyond standard model.

CSR commensurate scale relation.

CSS conventional scale setting.

EW electroweak.

FAC fastest apparent convergence principle.

GCR generalized Crewther relation.

GM–L Gell-Mann–Low.

GUT grand unified theory.

HQ heavy quark.

iCF intrinsic conformality.

IR infrared.

mMOM minimal momentum-subtraction scheme.

MOM momentum-subtraction scheme.

MS minimal-subtraction scheme.

$\overline{\text{MS}}$ modified minimal-subtraction scheme.

NP new physics.

OPT optimized perturbation theory.

pQCD perturbative quantum chromodynamics.

PMC principle of maximum conformality.

PMCa alternative principle of maximum conformality scale-setting.

PM Cm multi-scale principle of maximum conformality scale-setting.

PMCs single-scale principle of maximum conformality scale-setting.

PMC_∞ infinite-order scale-setting using the principle of maximum conformality.

PMS principle of minimal sensitivity.

RG renormalization group.

RGE renormalization group equations.

RS renormalization scheme.

RSS renormalization scale setting.

SM standard model.

UV ultraviolet.

V-scheme scheme of the static potential between two heavy quarks.

xRGE extended renormalization group equations.

“In the perspective of a theory unifying all the interactions, electromagnetic, weak and strong nuclear, such as a so-called grand unified theory or GUT, we are constrained to apply the same scale-setting procedure in all sectors of the theory.”

Introduction

A key issue in making precise predictions in QCD is the uncertainty in setting the renormalization scale μ_R in order to determine the correct running coupling $\alpha_s(\mu_R^2)$ in the perturbative expansion of a scale invariant quantity. Other quantities such as the top and Higgs mass uncertainty, the strong coupling uncertainty also affect the theoretical predictions for perturbative QCD, but one of the most important sources of error is given by the renormalization scale and scheme ambiguities. These scale and scheme ambiguities are an important source of uncertainties for predictions in many fundamental processes in perturbative QCD, such as the gluon fusion in Higgs production [1], or bottom-quark production [2], which are essential for the physics investigated at the Large Hadron Collider (LHC) and at future colliders.

Precise predictions are crucial for both standard model (SM) and beyond the standard model (BSM) physics, in order to enhance sensitivity to new physics (NP) at colliders.

In principle, an infinite perturbative series is void of this issue, given the scheme and scale invariance of the entire physical quantities [3–7], in practice perturbative corrections are known up to a certain order of accuracy and scale invariance is only approximated in truncated series leading to so-called scheme and scale ambiguities [8–18]. On one hand, according to the conventional practice or conventional scale setting (CSS), this problem cannot be avoided and is responsible for part of the theoretical errors. Using the CSS approach the renormalization scale μ_R is set to the typical scale of a process Q , and errors are estimated by varying the scale over a range of two [$Q/2; 2Q$]. This method gives predictions with large theoretical

uncertainties comparable with the calculated order correction. Moreover, this procedure leads to results that depend on the renormalization scheme and on the initial scale choice, to a perturbative series that diverges as $\sim \alpha_s^{n+1} \beta_0^n n!$ [19], and does not agree with QED. Moreover, in several processes there is more than one typical scale and results can be significantly different for perturbative calculations according to the different choices of scale [20].

On the other hand, some strategies for the optimization of the truncated expansion have been proposed, such as the Principle of Minimal Sensitivity (PMS) proposed by Stevenson [10–13], the Fastest Apparent Convergence (FAC) criterion introduced by Grunberg [14–16]. These are procedures commonly in use for scale setting in perturbative QCD together with the CSS and an introduction to these methods can also be found in Refs. [21, 22]. However, as shown in Refs. [21], these methods not only have the same difficulties of CSS, but they also lead to incorrect and unphysical results [23] in particular kinematic regions.

In general a scale-setting procedure is considered reliable if it preserves important self-consistency requirements. All Renormalization Group properties such as: *uniqueness*, *reflexivity*, *symmetry*, and *transitivity* should be preserved also by the scale-setting procedure in order to be generally applied [24]. Other requirements are also suggested by known tested theories, by the convergence behavior of the series and also for phenomenological reasons or scheme independence.

It has been shown how all the theoretical requirements for a reliable scale-setting procedure can be satisfied at once, leading to accurate results by using the PMC (the Principle of Maximum Conformality [25–27]). This method is the generalization and extension of the original Brodsky-Lepage-Mackenzie (BLM) method [17] to all orders and to all observables. The primary purpose of the PMC method is to solve the scale-setting ambiguity, it has been extended to all orders [28, 29] and it determines the correct running coupling and the correct momentum flow according to RGE invariance [30, 31]. This leads to results that are invariant respect to the initial renormalization scale in agreement with the requirement of scale invariance

of an observable in pQCD [21]. This method provides a systematic way to eliminate renormalization scheme and scale ambiguities from first principles by absorbing the β terms that govern the behavior of the running coupling via the renormalization group equation. Thus, the divergent renormalon terms cancel, which improves convergence of the perturbative QCD series. Furthermore, the resulting PMC predictions do not depend on the particular scheme used, thereby preserving the principles of renormalization group invariance [24, 30]. The PMC procedure is also consistent with the standard Gell-Mann–Low method in the Abelian limit, $N_c \rightarrow 0$ [32]. Moreover, in a theory of unification of all forces, electromagnetic, weak and strong interactions, such as Grand Unified theories, one cannot simply apply a different scale-setting or analytic procedure to different sectors of the theory. The PMC offers the possibility to apply the same method in all sectors of a theory, starting from first principles, eliminating the renormalon growth, the scheme dependence, the scale ambiguity, and satisfying the QED Gell-Mann-Low scheme in the zero-color limit $N_c \rightarrow 0$.

We show in this thesis, how the implementation at all orders of the PMC simplifies in many cases by identifying only the β_0 -terms at each order of accuracy due to the presence of a new property of the perturbative corrections: the *intrinsic conformality* (iCF). First we recall that there is no ambiguity in setting the renormalization scale in QED. The standard Gell-Mann-Low scheme determines the correct renormalization scale identifying the scale with the virtuality of the exchanged photon [4]. For example, in electron-muon elastic scattering, the renormalization scale is the virtuality of the exchanged photon, i.e. the spacelike momentum transfer squared $\mu_R^2 = q^2 = t$. Thus

$$\alpha(t) = \frac{\alpha(t_0)}{1 - \Pi(t, t_0)} \quad (1)$$

where

$$\Pi(t, t_0) = \frac{\Pi(t) - \Pi(t_0)}{1 - \Pi(t_0)}$$

From Eq. 3.8 it follows that the renormalization scale $\mu_R^2 = t$ can be determined by the β_0 -term at the lowest order. This scale is sufficient to sum all the vacuum

polarization contributions into the dressed photon propagator, both proper and improper, at all orders. Again in QED, considering the case of two-photon exchange, a new different scale is introduced in order to absorb all the β -terms related to the new subprocess into the scale. Also in this case the scale can be determined by identifying the lowest-order β_0 -term alone. This term identifies the virtuality of the exchanged momenta causing the running of the scale in that subprocess. This scale again would sum all the contributions related to the β -function into the renormalization scale and no further corrections need to be introduced into the scale at higher orders. Given that the pQCD and pQED predictions match analytically in the $N_C \rightarrow 0$ limit where $C_F \alpha_{QCD} \rightarrow \alpha_{QED}$ (see Ref. [32]), we extend the same procedure to pQCD. In fact, in many cases in QCD the β_0 terms alone can determine the pQCD renormalization scale at all orders [33] eliminating the renormalon contributions $\alpha_s^{n+1} \beta_0^n n!$. Although in non-Abelian theories other diagrams related to the three- and four-gluon vertices arise, these terms do not necessarily spoil this procedure. In fact, in QCD, the β_0 terms arising from the renormalization of the three-gluon or four-gluon vertices as well as from gluon wavefunction renormalization determine the renormalization scales of the respective diagrams and no further corrections to the scales need to be introduced at higher orders. In conclusion, if we focus on a particular class of diagrams we can fix the PMC scale by determining the β_0 -term alone and we show this to be connected to the general scheme and scale invariance of an observable in a gauge theory.

This thesis is organized as follows: in **section I** we introduce QCD as a gauge theory based on the $SU(3)_c$ local symmetry; in **section II** we give a description of the renormalization group equations and their extended version, starting from the renormalization procedure of the strong coupling $\alpha_s(\mu)$ and its renormalization scale dependence; in **section III** we present the state of the art for the renormalization scale setting problem in QCD, introducing the basic concepts of scale setting procedures in use at present: conventional scale setting (CSS), FAC-scale setting, PMS-scale setting and BLM scale setting, highlighting their basic features

and showing some important physical results; in **section IV** we describe the PMC approach; in **section V** we introduce the newly developed method PMC_∞ and its new features; we show results for the application of the PMC_∞ to the event-shape variables: thrust and C-parameter comparing the results under the CSS and the PMC_∞ methods; in **section VI** we apply the PMC_∞ to thrust in the perturbative conformal window of QCD and we investigate the QED limit of the QCD thrust calculations; in **section VII** we show a novel method to determine the strong coupling and its behavior $\alpha_s(Q)$ over a wide range of scales, from a single experiment at a single scale, using the event shape variable results; in **section VIII** we apply the PMC/ PMC_∞ to a multi-renormalization scale process: heavy-quark pair production at threshold, comparing results in different schemes and taking the QED limit of the QCD calculations.

This thesis mostly summarizes results published in the following articles or conference proceedings:

- L. Di Giustino, Stanley J. Brodsky, Xing-Gang Wu and Sheng-Quan Wang, PMC_∞ : Infinite-Order Scale-Setting method using the Principle of Maximum Conformality and preserving the Intrinsic Conformality; Proceedings of the conference RADCOR 2021, arXiv:2110.05171 [hep-ph].
- L. Di Giustino, Francesco Sannino, Sheng-Quan Wang and Xing-Gang Wu, Thrust Distribution for 3-Jet Production from e^+e^- Annihilation within the QCD Conformal Window and in QED, Physics Letters B 823C (2021) 136728; arXiv:2104.12132[hep-ph];
- L. Di Giustino, Stanley J. Brodsky, Sheng-Quan Wang and Xing-Gang Wu, Infinite-order scale-setting using the principle of maximum conformality: A remarkably efficient method for eliminating renormalization scale ambiguities for perturbative QCD, Phys.Rev.D 102 (2020) 1, 014015: arXiv: 2002.01789[hep-ph];
- Sheng-Quan Wang, Stanley J. Brodsky, Xing Gang Wu, L. Di Giustino and Jian-Ming Shen, Renormalization scale setting for heavy quark pair production in e^+e^- annihilation near the threshold region, Phys.Rev.D 102 (2020) 1, 014005: arXiv: 2002.10993[hep-ph];
- Sheng-Quan Wang, Stanley J. Brodsky, Jian-Ming Shen, Xing-Gang Wu and L. Di Giustino A Novel Method for the Precise Determination of the QCD Running Coupling from Event Shapes Distributions in Electron-Positron Annihilation, Phys. Rev. D 100 (2019) 9, 094010 : arXiv:1908.00060[hep-ph];

- Sheng-Quan Wang, Stanley J. Brodsky, Xing-Gang Wu, L. Di Giustino Thrust Distribution in Electron-Positron Annihilation using the Principle of Maximum Conformality, Phys. Rev. D 99 (2019) 11, 114020: arXiv: 1902.01984[hep-ph];
- X. D. Huang, J. Yan, H. H. Ma, L. Di Giustino, J. M. Shen, X. G. Wu and S. J. Brodsky, Detailed Comparison of Renormalization Scale-Setting Procedures based on the Principle of Maximum Conformality, arXiv:2109.12356 [hep-ph];
- Sheng-Quan Wang, Chao-Qin Luo, Xing-Gang Wu, Jian-Ming Shen, Leonardo Di Giustino, New analyses of event shape observables in electron-positron annihilation and the determination of α_s running behavior in perturbative domain, arXiv:2112.06212 [hep-ph];

Chapter 1

Quantum Chromodynamics

1.1 Introduction

Quantum Chromodynamics is the theory of the strong interaction, which describes how elementary constituents such as quarks and gluons interact in order to bind together and form hadrons. In particular, the theory exhibits the symmetries observed experimentally and it explains why quarks interact strongly at low energies and weakly in processes at large momentum transfer, where quarks appear to be almost free.

Despite the many successful achievements, there are still several problems that need to be solved in order to test the theory to the highest precision. In particular, the confinement mechanism still remains unexplained, though some evidence of such phenomenon has been obtained in recent years by investigating gauge theories on the lattice and by studying the topology of the non-Abelian gauge theories. In order to overcome this obstacle, several alternative approaches have also been proposed, which so far unfortunately are not completely void of ambiguities and lead to results that are rather model dependent. The non-perturbative region is in fact affected by the peculiar infrared (IR) dynamics, which involves mechanisms like hadronization, soft radiation and confinement. In particular, in the IR region the behavior of the

strong coupling α_s is not yet predictable or explained in QCD. Recent studies of light front holographic QCD (LFHQCD) (i.e. AdS/CFT theory) suggest the presence of a finite limit of the coupling at zero momentum, which means the presence of an interacting fixed point in the β -function. This hypothesis has not been rejected by comparison with experimental data and the behavior of the coupling seems to be in agreement. At the moment the AdS/CFT correspondence with QCD is still under investigation and the LFHQCD can be considered only as a model or as an “ansatz” for the non-perturbative region of QCD. Despite the lack of a perturbative expansion at low energies, there are still several strong theorems that hold and that can be used to relate processes with analogous characteristics in the non-perturbative region and model parameters can be constrained by fits to data. Thus, if on one hand the dynamics at long distances is not yet totally revealed, on the other hand the dynamics at high energies reached its apex with the discovery of *asymptotic freedom* (AF), which perfectly explains experimental evidence of the weakly interacting partons inside hadrons at high momentum transfer. The perturbative nature of QCD at short distances is still affected by errors due to uncertainties, which in several cases can spoil the theoretical predictions and which are related to both the confining nature of the strong forces and the renormalization scale and scheme ambiguities. The latter are the main sources of errors in many processes where QCD corrections can be calculated perturbatively. In order to make reliable theoretical predictions and improve the precision, it is crucial to eliminate the scale and scheme ambiguities in order to improve the theoretical calculations in QCD enhancing the sensitivity to any possible signal of new physics (NP) at the large hadron collider (LHC). Furthermore, QCD is the most complex gauge theory we have ever dealt with, it represents the most difficult sector of the Standard Model (SM) for quantitative predictions. In fact, if in the electroweak (EW) sector, perturbation theory is always applicable, given the particular weak nature of the interaction at energies accessible in accelerators or in weak decays involving leptons and vector bosons, this is not always possible in QCD since the coupling $\alpha_s(Q) \gg \alpha_{QED}$ in a wide range of

scales Q and quarks cannot be observed as real states. Thus the complex nature of QCD can only be investigated by comparing its predictions with all possible results from different experiments in different kinematic regions. Given the vast variety of the phenomena and phenomenological applications, QCD is currently still a field of great interest and under continuous and active investigation.

1.2 The flavor symmetry: $SU(3)_f$

Neutron, proton, pions and the other particles listed in the Particle Data Group (PDG) [34] tables are classified as *hadrons* and have in common the particular property of interacting via the strong interaction. All these particles can be simply classified using global symmetries, in particular the $SU(3)$ symmetry. This was originally discovered by Gell-Mann and Neeman with the quarks *up*, *down*, *strange* (u, d, s) and was later expanded to include the quarks *charm* (c), *bottom* (b) and *top* (t). These symmetries apply, following the Gell-Mann and Zweig approach, starting from the assumption that light hadrons are formed by quarks, respectively three for baryons and two (a quark and an antiquark) for mesons. Quarks are fermions of spin 1/2 divided into six flavors. Three quarks, u, c, t, have charge $Q = 2/3$, while d, s, b have a charge of $Q = -1/3$. Following the original idea of the isospin $SU(2)_I$ symmetry of Heisenberg for the states of the nucleon, Gell-Mann introduced the group $SU(3)_f$ for the quarks: u, d, s. The $SU(3)_f$ symmetry applies straightforwardly assuming first that the three light quarks u, d, s transform as a fundamental representation 3 of the flavor symmetry group $SU(3)_f$. All other particles formed by the u, d, s quarks can be classified as higher representations of the group, which can be generated by taking multiple products of the fundamental representation:

$$3 = q_i = \begin{pmatrix} u \\ d \\ s \end{pmatrix}. \quad (1.1)$$

The $SU(3)_f$ group is a rank 2 Lie group and its representations are identified with two quantum numbers: by convention we take the third component of isospin T_3 and the hypercharge Y . The two quantum numbers strangeness and hypercharge are not independent, but are related by the Gell-Mann and Nishijima formula:

$$Q = T_3 + Y/2,$$

where $Y = B + S$, with B the baryon number, which for all quarks has the value $B = 1/3$, S is the strangeness and Q the electric charge. In this model, we expect mesons and light baryons to be classified according to the following representations:

$$\text{Mesons} = 3 \otimes \bar{3} = 8 \oplus 1, \tag{1.2}$$

$$\text{Baryons} = 3 \otimes 3 \otimes 3 = 10 \oplus 8 \oplus 8 \oplus 1. \tag{1.3}$$

The symmetry of Gell-Mann and Neeman predicts that mesons are arranged in terms of octets and singlets, with baryons in octets, decuplets and singlets. The fact that this simple representation can in fact classify the lightest mesons and baryons present in nature, was a remarkable achievement.

At present six different flavors of quarks are known, and in principle, one could think of generalizing $SU(3)_f$ to $SU(6)_f$. Unfortunately, the large differences among the heavier quark states, break the global $SU(6)$ symmetry strongly. In contrast, the original $SU(3)_f$ symmetry of the light quarks is nearly conserved, given that the u, d, s quarks have approximately the same masses. This justifies the approximation of the quasi-conserved chiral symmetries, under which the left-handed and right-handed fields transform independently of each other. Such chiral symmetries are given by the invariance of the Lagrangian under the group $SU(3)_L \times SU(3)_R$ or considering a better approximation, by the group $SU(2)_L \times SU(2)_R$, involving only the up and down quarks, which can be actually considered massless ($m_u, m_d \ll \Lambda_{QCD} \simeq 300\text{MeV}$).

1.3 Hints for color

The discovery of the $\Delta^{++}(J = 3/2)$ baryon in 1951 [35] provided a first indication of the existence of a new degree of freedom necessary to antisymmetrize its wavefunction. In fact, the particle is in a fundamental $L = 0$ state with all spins aligned along the same direction $u^\uparrow u^\uparrow u^\uparrow$, which leads to a symmetric wavefunction. This is in contrast with the Pauli exclusion principle and Fermi-Dirac statistics, given that baryons have semi-integer spin. In order to overcome this inconsistency, a new quantum number was introduced: *color*, with at least $N_c = 3$ number of colors and with each quark q^α , having a color index $\alpha = 1, 2, 3$. Thus, according to this assumption the wavefunction can be antisymmetric:

$$\Delta^{++} = \frac{1}{\sqrt{6}} \epsilon^{\alpha\beta\gamma} |u_\alpha^\uparrow u_\beta^\uparrow u_\gamma^\uparrow\rangle. \quad (1.4)$$

Other experimental evidence for color was provided by measurements of the decay width of the neutral pion, $\Gamma(\pi \rightarrow \gamma\gamma) \propto N_c^2$ and by the ratio $R_{e^+e^-} = N_c \sum_{f=1}^{N_f} Q_f^2$, that showed a neat N_c proportionality. These experimental hints were also supported by other theoretical indications like the anomaly cancellation and the U(1) problem of the η' meson mass.

1.4 Quarks and gluons

The “quark model” introduced by Gell-Mann, comprehensively explains the spectrum of hadronic states and in particular the spectra of states containing heavy quarks such as *charm* and *bottom*: charmonium, bottomonium respectively and also D and B mesons. The charmonium, bottomonium states appear as resonances of $c\bar{c}$ and $b\bar{b}$ quark states. Taking into account the reduced mass difference, these are in fact similar to the states of positronium (e^-e^+) and can be obtained assuming that the heavy quarks interact via a non-relativistic potential that at short-distances has the characteristics of an effective Coulomb-like static potential, while at large-distances diverges linearly according to the confinement mechanism. For the sake

of completeness, in order to complement the description of the interaction of heavy quarks, relativistic and pQCD corrections should be also taken into account. It was also found that, in processes with large momentum transfer, hadrons appear to be made up of almost free elementary constituents (i.e. weakly interacting with each other) called *partons* by Feynman.

After careful analysis and measurements of charges and spins, Feynman's partons were identified with Gell-Mann's quarks. It was deduced that these values are in agreement with those of the quark model. In particular, at the moment we know of 6 quark flavors: namely, u, d, s, c, b and t , where each flavor also corresponds to three different states of color (r, g, b). Quarks are then elementary particles that interact via strong forces exchanging other massless particles, i.e. *gluons*. However, quarks have never been observed as free particles in laboratories, so they cannot be represented as asymptotic states. They only exist as elementary constituents of hadrons, wherein they are confined. Moreover, also real states of single gluons cannot be directly observed. Gluons are the bosons that convey the strong forces inside hadrons analogously to photons in QED, but unlike photons they carry the color charge. In fact, they exist in the SU(3) octet configuration or *adjoint* representation. In this picture, quarks and gluons are carriers of the color quantum number, while baryons and mesons are colorless particles. This means that all hadrons are singlets under rotations in the color space and cannot exchange long range gluons. In order to avoid the existence of extra unobserved hadronic states, to therefore satisfy hadron spectroscopy, one must postulate furthermore that all asymptotic states are colorless. This assumption is known as the *hypothesis of confinement*; in fact, it implies the non-observability of free quarks and gluons, which excludes the color singlet gluon state.

1.5 Gauge theories

QCD is a non-Abelian *gauge theory*, i.e. a Lagrangian quantum field theory with the gauge symmetry given by the invariance of the Lagrangian under the local special unitary Lie group $SU(3)_c$ transformations. In general, gauge theories satisfy two fundamental requirements: invariance under the particular gauge group, which for the Standard Model is $SU(3)_c \times SU(2)_L \times U(1)_Y$ and *renormalizability*. These two requirements lead to a theory that is symmetric under the local transformation of the particular special unitary group and under the *renormalization group equations* (RGE). The groups $SU(3)_c$ and $SU(2)_L$ are non-Abelian special unitary groups related to the strong and weak forces. The $U(1)_Y$ is the Abelian group of hypercharge, which leads to QED after the *spontaneous symmetry breaking* (SSB) mechanism. Lie groups have the following Standard representations:

$$U = \exp\left\{i \sum_{i=1}^{n^2-1} \epsilon_i T^i\right\},$$

where ϵ_i are real parameters and T^i Hermitian traceless matrices defined as *group generators*. Special unitary groups have a total number of $2n^2 - n^2 - 1 = n^2 - 1$ generators, where “ n ” is the dimension of the fundamental representation of the group, and $n - 1$ generators are diagonal. The algebra of Lie groups is set by the commutation relations of the generators:

$$\left[\frac{\sigma_i}{2}, \frac{\sigma_j}{2}\right] = i\epsilon_{ijk} \frac{\sigma_k}{2} \quad (1.5)$$

and

$$\left[\frac{\lambda_i}{2}, \frac{\lambda_j}{2}\right] = if_{ijk} \frac{\lambda_k}{2}, \quad (1.6)$$

where ϵ_{ijk} and f_{ijk} are total antisymmetric tensors and are the *structure constants* of the group, while the σ_i with $i = 1, 2, 3$ and the λ_j with $j = 1, 2, \dots, 8$ are the adjoint representations of the $SU(2)$ and $SU(3)$ group given by the Pauli and the Gell-Mann matrices respectively.

1.6 The QCD Lagrangian

The QCD Lagrangian can be derived from the *Yang-Mills* Lagrangian by adding all flavor contributions. The Yang-Mills Lagrangian is itself a gauge invariant Lagrangian under local special-unitary transformations:

$$U_x U_x^\dagger = U_x^\dagger U_x = I, \quad \det U_x = 1. \quad (1.7)$$

Local gauge SU(3) matrices, U_x , can be parametrized using the form:

$$U_x = \exp[-ig_s \sum_A \theta^A(x) \lambda^A / 2], \quad (1.8)$$

where g_s is the coupling constant, which is related to α_s by: $g_s^2 = 4\pi\alpha_s$ and λ^A ($A = 1, 2, \dots, 8$) are the group generators of SU(3)_c, which are given by the Gell-Mann matrices:

$$\begin{aligned} \lambda^1 &= \begin{pmatrix} 0 & 1 & 0 \\ 1 & 0 & 0 \\ 0 & 0 & 0 \end{pmatrix}, \lambda^2 = \begin{pmatrix} 0 & -i & 0 \\ i & 0 & 0 \\ 0 & 0 & 0 \end{pmatrix}, \lambda^3 = \begin{pmatrix} 1 & 0 & 0 \\ 0 & -1 & 0 \\ 0 & 0 & 0 \end{pmatrix}, \\ \lambda^4 &= \begin{pmatrix} 0 & 0 & 1 \\ 0 & 0 & 0 \\ 1 & 0 & 0 \end{pmatrix}, \lambda^5 = \begin{pmatrix} 0 & 0 & -i \\ 0 & 0 & 0 \\ i & 0 & 0 \end{pmatrix}, \lambda^6 = \begin{pmatrix} 0 & 0 & 0 \\ 0 & 0 & 1 \\ 0 & 1 & 0 \end{pmatrix} \\ \lambda^7 &= \begin{pmatrix} 0 & 0 & 0 \\ 0 & 0 & -i \\ 0 & i & 0 \end{pmatrix}, \lambda^8 = \frac{1}{\sqrt{3}} \begin{pmatrix} 1 & 0 & 0 \\ 0 & 1 & 0 \\ 0 & 0 & -2 \end{pmatrix}. \end{aligned} \quad (1.9)$$

The $\theta^A(x)$ are arbitrary parameters depending on space-time coordinates. In order to preserve the gauge invariance locally, a new definition of the derivative occurs, the *covariant derivative*:

$$(D^\mu q_f)^\alpha = \left\{ \partial^\mu \delta^{\alpha\beta} - ig_s G_{\alpha\beta}^\mu(x) \right\} q_f^\beta, \quad (1.10)$$

where q_f^β is the fermionic field in its fundamental representation of the group $SU(3)_c$, with $f = 1, \dots, 6$ and $\beta = 1, 2, 3$, the flavor and color indices respectively, and:

$$G_{\alpha\beta}^\mu(x) = \sum_A \frac{\lambda_{\alpha\beta}^A}{2} G^{A\mu}(x) \quad (1.11)$$

the eight gauge fields relative to the eight gluons with $A = 1, \dots, 8$. Following these considerations we can write the QCD Lagrangian as:

$$\mathcal{L}_{QCD} = -\frac{1}{4} \text{tr}(F_{\mu\nu} F^{\mu\nu}) + \sum_f \bar{q}_f^\beta (i\gamma^\mu (D_\mu)_{\beta\alpha} - m_f \delta_{\beta\alpha}) q_f^\alpha, \quad (1.12)$$

where the gluon field strength tensor $F_{\mu\nu}^A$ is given by:

$$\begin{aligned} F^{\mu\nu}(x) &\equiv \partial^\mu G^\nu - \partial^\nu G^\mu - ig_s [G^\mu, G^\nu], \\ &\equiv (\lambda^A/2) F^{A\mu\nu}(x), \end{aligned} \quad (1.13)$$

with

$$F^{A\mu\nu}(x) = \partial^\mu G^{A\nu} - \partial^\nu G^{A\mu} + g_s f^{ABC} G^{B\mu} G^{C\nu}. \quad (1.14)$$

Due to the non-commutative nature of $SU(3)$, the trace of the field strength tensor introduces gluon cubic and quartic self interactions, which is the main difference between QCD and QED. These interactions are particularly important in the calculation of the β -function and lead to a fundamental property of QCD: asymptotic freedom. Eq. 1.12 is still missing two terms \mathcal{L}_{GF} and \mathcal{L}_{Ghosts} , respectively the Lagrangians for the gauge fixing and ghost terms, which must be introduced for consistency (for a review see Ref. [36]). However, these terms do not introduce extra real final or initial particle states, but fictitious particles; namely ghosts, which occur only in loop integration.

1.7 Quark states and $SU(3)_c$

According to the Lagrangian in Eq. 1.12, the strong force preserves the flavor quantum number. The interactions that change flavor stem from weak interactions. In

fact, flavor-changing transitions among different quarks have a lower intensity with respect to flavor conserving interactions. Moreover, intermediate bosons of the electroweak interactions (γ , Z^0 , W^\pm), do not couple via strong forces or to color charges. Thus, the $SU(3)_c$ color symmetry is well preserved by the strong forces and it can be considered the perfect candidate for the QCD symmetry group. Moreover, QCD includes the following features:

- color $SU(3)_c$ is an exact symmetry;
- $N_c = 3$;
- quarks and antiquarks have different fundamental representations: $\bar{3} \neq 3$, this leads to a complex representation;
- hadrons are colorless particles, so they must be represented as color singlets;
- asymptotic freedom.

These conditions exclude other groups, but lead straightforwardly to the $SU(3)$ group symmetry. Assuming the fundamental representations for quarks and antiquarks, 3 and $\bar{3}$ respectively, we can determine the other possible $SU(3)_c$ states considering multiple combinations of quarks and/or antiquarks:

$$\begin{aligned}
q\bar{q} & : 3 \otimes \bar{3} = 1 \oplus 8, \\
qqq & : 3 \otimes 3 \otimes 3 = 1 \oplus 8 \oplus 8 \oplus 10, \\
qq & : 3 \otimes 3 = \bar{3} \oplus 6.
\end{aligned}
\tag{1.15}$$

Simple color singlets result from $q\bar{q}$ and qqq and lead to mesons and baryons respectively. Recently other unstable particles assumed to be tetraquarks (e.g. $X(3872)$) and pentaquarks (e.g. Θ^+ (1540)) [37] have been observed by Belle, $D\emptyset$, BaBar and LHCb, while there is no evidence for a six quark state. A first six quark state, namely hexaquark, was introduced by Jaffe (H-dibaryon [38]) and recently by Farrar (sexaquark [39]). Actually color representations for mesons and baryons are

not the only color singlets possible that can be realized with multiple combinations of quarks and antiquarks. In fact, color singlets can also be formed considering the combinations: $qq\bar{q}\bar{q}$, $qqq\bar{q}$, $qqqqq$. Tetraquark and pentaquark states are both unstable, while the sexaquark is claimed to be stable. However, it is still under investigation if these novel quark states are simple bound states or molecules.

Chapter 2

The Renormalization Group

2.1 Renormalization

Renormalization is a procedure that applied quantum field theories (QFT) in order to cancel an infinite number of ultraviolet (UV) singularities that arise in loop integration absorbing them into a finite number of parameters entering the Lagrangian, like the mass or coupling constant and fields. This procedure starts from the assumption that the variables entering the Lagrangian are not the effective quantities measured in experiments, but are unknown functions affected by singularities. The origin of the ultraviolet singularities is often interpreted as a manifestation that a QFT is a low-energy effective theory of a more fundamental yet unknown theory.

The use of regularization UV cut-offs shields the very short distance domain, where the perturbative approach to QFT ceases to be valid.

Once the coupling has been renormalized to a measured value and at a given energy scale, the effective coupling is no longer sensitive to the ultraviolet (UV) cut-off nor to any unknown phenomena arising beyond this scale. Thus, the scale dependence of the coupling can be well understood formally and phenomenologically. Actually gauge theories are affected not only by UV, but also by infrared (IR) divergencies. The cancellation of the latter is guaranteed by the Kinoshita - Lee -

Nauenberg (KLN) theorem [40, 41].

Considering first the Lagrangian of a massless theory, which is free from any particular scale parameter, in order to deal with these divergences a regularization procedure is introduced. Referring to the dimensional regularization procedure [42–44], one varies the dimension of the loop integration, $D = 4 - 2\varepsilon$ and introduces a scale μ in order to restore the correct dimension of the coupling.

In order to determine the renormalized gauge coupling, we consider the quark-quark-gluon vertex and its loop corrections. UV-divergences arise from loop integration for higher order contributions for both the external fields and the vertex. The renormalization constants are related by:

$$Z_{\alpha_s}^{-1} = (\sqrt{Z_3 Z_2 / Z_1})^2, \quad (2.1)$$

where Z_{α_s} is the coupling renormalization factor, $Z_1(Q^2)$ is the vertex renormalization constant and $Z_3(Q^2)$ and $Z_2(Q^2)$ are:

$$A_{a,\mu} = Z_3^{1/2}(Q^2) A_{a,\mu}^R(Q^2), \quad \psi = Z_2^{1/2}(Q^2) \psi^R(Q^2),$$

the renormalization constants for gluon and quark fields respectively. The superscript R indicates the renormalized field. The renormalization factors in dimensional regularization are given by:

$$Z_1(Q^2) = 1 - \frac{\alpha_s(Q^2)}{4\pi} (N_c + C_F) \frac{1}{\varepsilon} \quad (2.2)$$

$$Z_2(Q^2) = 1 - \frac{\alpha_s(Q^2)}{4\pi} C_F \frac{1}{\varepsilon} \quad (2.3)$$

$$Z_3(Q^2) = 1 + \frac{\alpha_s(Q^2)}{4\pi} \left(\frac{5}{3} N_c - \frac{2}{3} N_f \right) \frac{1}{\varepsilon} \quad (2.4)$$

where ε is the regulator parameter for the UV-ultraviolet singularities. By substitution, we have that the UV divergence :

$$Z_\alpha(Q^2) = 1 - \frac{\beta_0 \alpha_s(Q^2)}{4\pi\varepsilon}, \quad (2.5)$$

with

$$\beta_0 = 11 - \frac{2N_f}{3}. \quad (2.6)$$

The singularities related to the UV poles are subtracted out by a redefinition of the coupling. In the MS scheme, the renormalized strong coupling $\alpha_s(Q^2)$ is related to the bare coupling $\overline{\alpha}_s$ by:

$$\overline{\alpha}_s = Q^{2\varepsilon} Z_\alpha(Q^2) \alpha_s(Q^2). \quad (2.7)$$

In the minimal subtraction scheme (MS) only the pole $1/\varepsilon$ related to the UV singularity is subtracted out. A more suitable scheme is $\overline{\text{MS}}$ [45–47], where also the constant term $\ln(4\pi) - \gamma_E$ is subtracted out. Different schemes can also be related by scale redefinition, e.g. $\mu^2 \rightarrow 4\pi\mu^2 e^{-\gamma_E}$. Thus, the renormalization procedure depends both on the particular choice of the scheme and on the subtraction point μ .

Hence, even though there are no dimensionful parameters in the initial bare Lagrangian, a mass scale μ is acquired during the renormalization procedure. The emergence of μ from a Lagrangian without any explicit scale is called dimensional transmutation [48]. The value of μ is arbitrary and is the momentum at which the UV divergences are subtracted out. Hence μ is called the subtraction point or renormalization scale. Thus, the definition of the renormalized coupling $\alpha_s^{\overline{\text{MS}}}(\mu)$ depends at the same time on the chosen scheme, $\overline{\text{MS}}$ and on the renormalization scale μ .

However, different schemes and scales can be related according to the so-called extended renormalization group equations, which we will introduce in the following sections. Given the perturbative nature of the theory, these relations are known up to a certain level of accuracy and the truncated formulas are responsible for an important source of uncertainties: *the scheme and scale ambiguities*.

2.2 The running coupling constant $\alpha_s(\mu)$

In this section we will discuss the dependence of the strong coupling on the renormalization scheme (RS) and scale (μ) and we will show how this dependence can be

controlled by means of the renormalization group equations (RGE). The strong coupling α_s , is a fundamental parameter of the SM theory and determines the strength of the interactions among quarks and gluons in quantum chromodynamics (QCD). As shown in the previous section, its value depends on the renormalization scale μ (i.e. the subtraction point). In order to understand hadronic interactions, it is necessary to determine the magnitude of the coupling and its behavior over a wide range of values, from low to high energy scales. Long and short distances are related to low and high energies respectively. In the high energy region the strong coupling has an *asymptotic behavior* and QCD becomes perturbative, while in the region of low energies, e.g. at the proton mass scale, the dynamics of QCD is affected by processes such as quark confinement, soft radiation and hadronization. In the first case experimental results can be matched with theoretical calculations and a precise determination of the α_s depends both on experimental accuracy and on theoretical errors. In the latter case experimental results are difficult to achieve and theoretical predictions are affected by the confinement and hadronization mechanisms, which are rather model dependent. Various processes also involve a precise knowledge of the coupling in both the high and low momentum transfer regions and in some cases calculations must be improved with electroweak (EW) corrections. Thus, the determination of the QCD coupling over a wide range of energy scales is a crucial task in order to achieve results and to test QCD to the highest precision. Theoretical uncertainties in the value of $\alpha_s(Q^2)$ contribute to the total theoretical uncertainty in the physics investigated at the Large Hadron Collider (LHC), such as the Higgs sector, e.g. gluon fusion Higgs production [1]. The behavior of the perturbative coupling at low-momentum transfer is also fundamental for the scale of the proton mass, in order to understand hadronic structure, quark confinement and hadronization processes. IR effects such as soft radiation and renormalon factorial growth spoil the perturbative nature of the QCD in the low-energy domain. Higher-twist effects can also play an important role. Processes involving the production of heavy quarks near threshold require the knowledge of the QCD coupling at very low momentum

scales. Even reactions at high energies may involve the integration of the behavior of the strong coupling over a large domain of momentum scales including IR regions. Precision tests of the coupling are crucial also for other aspects of QCD that are still under continuous investigation, such as the hadron masses and their internal structure. In fact, the strong interaction is responsible for the mass of hadrons in the zero-mass limit of the u, d quarks.

The origin and phenomenology of the behavior of $\alpha_s(\mu)$ at small distances, where asymptotic freedom appears, is well understood and explained in many textbooks on Quantum Field Theory and Particle Physics.

Numerous reviews exist; see e.g. Refs. [49, 50]. However, standard explanations often create an apparent puzzle, as will be addressed in this thesis. Other questions remain even in this well understood regime: a significant issue is how to identify the scale Q that controls a given hadronic process, especially if it depends on many physical scales. A fundamental requirement, called “renormalization group invariance”, is that physical observables cannot depend on the choice of the renormalization scale and scheme.

In the perturbative regime theoretical predictions are affected by several sources of errors, e.g. the top and Higgs mass uncertainty, the strong coupling uncertainty and the main source of errors is given by the renormalization scale and scheme ambiguity. In this section we discuss the scale and scheme dependence of the effective coupling $\alpha_s(\mu)$ in QCD.

2.3 The evolution of $\alpha_s(\mu)$ in perturbative QCD

As shown in the previous section the renormalization procedure is not void of ambiguities. The subtraction of the singularities depends on the subtraction point or renormalization scale μ and on the renormalization scheme (RS). Observables in physics cannot depend on the particular scheme or scale, given that the theory stems from a conformal Lagrangian. This implies that scale invariance must be recovered

imposing the invariance of the renormalized theory under the renormalization group equation (RGE). We discuss in this section the dependence of the renormalized coupling $\alpha_s(Q^2)$ on the scale Q^2 . As shown in QED by Gell-Mann and Low, this dependence can be described introducing the β -function given by:

$$\frac{1}{4\pi} \frac{d\alpha_s(Q^2)}{d \log Q^2} = \beta(\alpha_s), \quad (2.8)$$

and

$$\beta(\alpha_s) = - \left(\frac{\alpha_s}{4\pi} \right)^2 \sum_{n=0} \left(\frac{\alpha_s}{4\pi} \right)^n \beta_n. \quad (2.9)$$

Neglecting quark masses, the first two β -terms are RS independent and they have been calculated in Refs. [51–55] for the $\overline{\text{MS}}$ scheme:

$$\begin{aligned} \beta_0 &= \frac{11}{3} C_A - \frac{4}{3} T_R N_f, \\ \beta_1 &= \frac{34}{3} C_A^2 - 4 \left(\frac{5}{3} C_A + C_F \right) T_R N_f \end{aligned}$$

where $C_F = \frac{(N_c^2-1)}{2N_c}$, $C_A = N_c$ and $T_R = 1/2$ are the color factors for the SU(3) gauge group [56].

At higher loops we have that β_i , $i \geq 2$ are scheme dependent and results for $\overline{\text{MS}}$ are calculated in Ref. [57]:

$$\beta_2 = \frac{2857}{2} - \frac{5033}{18} N_f + \frac{325}{54} N_f^2;$$

in Ref. [58]:

$$\begin{aligned} \beta_3 &= \left(\frac{149753}{6} + 3564\zeta_3 \right) - \left(\frac{1078361}{162} + \frac{6508}{27}\zeta_3 \right) N_f \\ &+ \left(\frac{50065}{162} + \frac{6472}{81}\zeta_3 \right) N_f^2 + \frac{1093}{729} N_f^3; \end{aligned} \quad (2.10)$$

and in Ref. [59]:

$$\begin{aligned} \beta_4 &= \left\{ \frac{8157455}{16} + \frac{621885}{2}\zeta_3 - \frac{88209}{2}\zeta_4 - 288090\zeta_5 \right. \\ &+ N_f \left[-\frac{336460813}{1944} - \frac{4811164}{81}\zeta_3 + \frac{33935}{6}\zeta_4 + \frac{1358995}{27}\zeta_5 \right] \\ &+ N_f^2 \left[\frac{25960913}{1944} + \frac{698531}{81}\zeta_3 - \frac{10526}{9}\zeta_4 - \frac{381760}{81}\zeta_5 \right] \end{aligned}$$

$$\begin{aligned}
& + N_f^3 \left[-\frac{630559}{5832} - \frac{48722}{243} \zeta_3 + \frac{1618}{27} \zeta_4 + \frac{460}{9} \zeta_5 \right] \\
& + N_f^4 \left[\frac{1205}{2916} - \frac{152}{81} \zeta_3 \right] \Big\}, \tag{2.11}
\end{aligned}$$

with $\zeta_3 \simeq 1.20206$, $\zeta_4 \simeq 1.08232$ and $\zeta_5 \simeq 1.03693$, the Riemann zeta function. Given the renormalizability of QCD, new UV singularities arising at higher orders can be cancelled by redefinition of the same parameter, i.e. the strong coupling. This procedure leads to the renormalization factor:

$$\begin{aligned}
Z_a(\mu) &= 1 - \frac{\beta_0}{\epsilon} a + \left(\frac{\beta_0^2}{\epsilon^2} - \frac{\beta_1}{2\epsilon} \right) a^2 \\
&\quad - \left(\frac{\beta_0^3}{\epsilon^3} - \frac{7\beta_0\beta_1}{6\epsilon^2} + \frac{\beta_2}{3\epsilon} \right) a^3 \\
&\quad + \left(\frac{\beta_0^4}{\epsilon^4} - \frac{23\beta_1\beta_0^2}{12\epsilon^3} + \frac{5\beta_2\beta_0}{6\epsilon^2} + \frac{3\beta_1^2}{8\epsilon^2} - \frac{\beta_3}{4\epsilon} \right) a^4 + \dots, \tag{2.12}
\end{aligned}$$

where $a = \alpha_s(\mu)/(4\pi)$ in the $\overline{\text{MS}}$ scheme. Given the arbitrariness of the subtraction procedure of including also part of the finite contributions (e.g. the constant $[\ln(4\pi) - \gamma_E]$ for the $\overline{\text{MS}}$), there is an inherent ambiguity for these terms which translates into the RS dependence. In order to solve any truncated Eq. 2.8, this being a first order differential equation, we need an initial value of α_s at a given energy scale $\alpha_s(\mu_0)$. For this purpose we set the initial scale $\mu_0 = M_Z$ the Z^0 mass and the value $\alpha_s(M_Z)$ is determined phenomenologically. In QCD the number of colors N_c is set to 3, while N_f , i.e. the number of active flavors, varies with energy scale across quark thresholds.

2.4 One-loop result and asymptotic freedom

When all quark masses are set to zero two physical parameters dictate the dynamics of the theory and these are the numbers of flavors N_f and colors N_c . We determine in this section the exact analytical solution to the truncated Eq. 2.8. Considering the formula :

$$\int_{\alpha_s(\mu_0^2)}^{\alpha_s(\mu^2)} \frac{1}{4\pi} \frac{d\alpha_s}{\beta(\alpha_s)} = - \int_{\mu_0^2}^{\mu^2} \frac{dQ^2}{Q^2}, \tag{2.13}$$

and retaining only the first term:

$$\frac{Q^2}{\alpha_s^2} \frac{\partial \alpha_s}{\partial Q^2} = -\frac{1}{4\pi} \beta_0 \quad (2.14)$$

we achieve the solution for the coupling:

$$\frac{4\pi}{\alpha_s(\mu_0^2)} - \frac{4\pi}{\alpha_s(Q^2)} = \beta_0 \ln\left(\frac{\mu_0^2}{Q^2}\right). \quad (2.15)$$

This solution can be given in the explicit form:

$$\alpha_s(Q^2) = \frac{\alpha_s(\mu_0^2)}{1 + \beta_0 \frac{\alpha_s(\mu_0^2)}{4\pi} \ln(Q^2/\mu_0^2)}. \quad (2.16)$$

This solution relates one known (measured value) of the coupling at a given scale μ_0 with an unknown value $\alpha_s(Q^2)$. More conveniently, the solution can be given introducing the QCD scale parameter Λ . At β_0 order, this is defined as:

$$\Lambda^2 \equiv \mu^2 e^{-\frac{4\pi}{\beta_0 \alpha_s(\mu^2)}} \quad (2.17)$$

which yields the familiar one-loop solution:

$$\alpha_s(Q^2) = \frac{4\pi}{\beta_0 \ln(Q^2/\Lambda^2)}.$$

Already at the one loop level one can distinguish two regimes of the theory. For the number of flavors larger than $11N_c/2$ (i.e. the zero of the β_0 coefficient) the theory possesses an infrared non-interacting fixed point and at low energies the theory is known as non-abelian quantum electrodynamics (non-abelian QED). The high energy behavior of the theory is uncertain, it depends on the number of active flavors and there is the possibility that it could develop a critical number of flavors above which the theory reaches an UV fixed point [60] and therefore becomes safe. When the number of flavors is below $11N_c/2$ the non-interacting fixed point becomes UV in nature and then we say that the theory is *asymptotically free*.

It is straightforward to check the asymptotic limit of the coupling in the deep UV region:

$$\lim_{s \rightarrow \infty} \alpha_s(s) = 0. \quad (2.18)$$

This result is known as *asymptotic freedom* and it is the outstanding result that has justified QCD as the most accredited candidate for the theory of strong interactions. On the other hand, we have that the perturbative coupling diverges at the $\Lambda \sim (200 - 300)\text{MeV}$ scale. This is sometimes referred to as the *Landau ghost pole* to indicate the presence of a singularity in the coupling that is actually unphysical and indicates the breakdown of the perturbative regime. This itself is not an explanation for confinement, though it might indicate its presence. When the coupling becomes too large the use of a nonperturbative approach to QCD is mandatory in order to obtain reliable results. We remark that the scale parameter Λ is RS dependent and its definition depends on the order of accuracy of the coupling $\alpha_s(Q^2)$. Considering that the solution α_s at order β_0 or β_1 is universal, the definition of Λ at the first two orders is usually preferred, i.e. the Λ given at 1-loop by Eq. 2.17 or at 2-loops (see later) by Eq. 2.23 .

2.5 Two-loop solution and the perturbative conformal window

In order to determine the solution for the strong coupling α_s at NNLO, it is convenient to introduce the following notation: $x(\mu) \equiv \frac{\alpha_s(\mu)}{2\pi}$, $t = \log(\mu^2/\mu_0^2)$, $B = \frac{1}{2}\beta_0$ and $C = \frac{1}{2}\frac{\beta_1}{\beta_0}$, $x^* \equiv -\frac{1}{C}$. The truncated NNLO approximation of the Eq. 2.8 leads to the differential equation:

$$\frac{dx}{dt} = -Bx^2(1 + Cx) \quad (2.19)$$

An implicit solution of Eq. 2.19 is given by the Lambert $W(z)$ function:

$$We^W = z \quad (2.20)$$

with: $W = \left(\frac{x^*}{x} - 1\right)$. The general solution for the coupling is:

$$x = \frac{x^*}{1 + W}, \quad (2.21)$$

$$z = e^{\frac{x^*}{x_0}-1} \left(\frac{x^*}{x_0} - 1 \right) \left(\frac{\mu^2}{\mu_0^2} \right)^{x^* B}. \quad (2.22)$$

We will discuss here the solutions to Eq. 2.19 with respect to the particular initial phenomenological value $x_0 \equiv \alpha_s(M_Z)/(2\pi) = 0.01876 \pm 0.00016$ given by the coupling determined at the Z^0 mass scale [34].

The signs of β_0, β_1 and consequently of B, x^* , depends on the values of the N_c, N_f , since the number N_c is set by the theory $SU(N_c)$, we discuss the possible regions varying only the number of flavors N_f . We point out that different regions are defined by the signs of the β_0, β_1 , that have zeros in $\bar{N}_f^0 = \frac{11}{2}N_c$, $\bar{N}_f^1 = \frac{34N_c^3}{13N_c^2-3}$ respectively with $\bar{N}_f^0 > \bar{N}_f^1$.

In the range $N_f < \bar{N}_f^1$ and $N_f > \bar{N}_f^0$ we have $B > 0, C > 0$ and the physical solution is given by the W_{-1} branch, while for $\bar{N}_f^1 < N_f < \bar{N}_f^0$ the solution for the strong coupling is given by the W_0 branch. By introducing the phenomenological value x_0 , we define a restricted range for the IR fixed point discussed by Banks and Zaks [61]. Given the value $\bar{N}_f = x^{*-1}(x_0) = 15.222 \pm 0.009$, we have that in the range $\frac{34N_c^3}{13N_c^2-3} < N_f < \bar{N}_f$ the β -function has both a UV and an IR fixed point, while for $N_f > \bar{N}_f$ we no longer have the asymptotically free UV behavior. The two-dimensional region in the number of flavors and colors where asymptotically free QCD develops an IR interacting fixed point is colloquially known as the *conformal window of pQCD*.

Thus, the actual physical range of a conformal window for pQCD is given by $\frac{34N_c^3}{13N_c^2-3} < N_f < \bar{N}_f$. The behavior of the coupling is shown in Fig. 2.1. In the IR region the strong coupling approaches the IR finite limit, x^* , in the case of values of N_f within the conformal window (e.g. black dashed curve of Fig. 2.1), while it diverges at

$$\Lambda = \mu_0 \left(1 + \frac{|x^*|}{x_0} \right)^{\frac{1}{2B|x^*|}} e^{-\frac{1}{2Bx_0}} \quad (2.23)$$

outside the conformal window given the solution for the coupling with W_{-1} (e.g. the solid red curve of Fig. 2.1). The solution of the NNLO equation for the case $B > 0, C > 0$, i.e. $N_f < \frac{34N_c^3}{13N_c^2-3}$, can also be given using the standard QCD scale

parameter Λ of Eq. 2.23,

$$x = \frac{x^*}{1 + W_{-1}}, \quad (2.24)$$

$$z = -\frac{1}{e} \left(\frac{\mu^2}{\Lambda^2} \right)^{x^* B}. \quad (2.25)$$

Different solutions can be achieved using different schemes, i.e. different definitions of the Λ scale parameter [62]. We underline that the presence of a Landau “ghost” pole in the strong coupling is only an effect of the breaking of the perturbative regime, including non-perturbative contributions, or using non-perturbative QCD, a finite limit is expected at any N_f [22]. Both solutions have the correct UV asymptotic free behavior. In particular, for the case $\bar{N}_f < N_f < \frac{11}{2}N_c$, we have a negative z , a negative C and a multi-valued solution, one real and the other imaginary, actually only one (the real) is acceptable given the initial conditions, but this solution is not asymptotically free. Thus we restrict our analysis to the range $N_f < \bar{N}_f$ where we have the correct UV behavior. In general IR and UV fixed points of the β -function can also be determined at different values of the number of colors N_c (different gauge group $SU(N)$) and N_f extending this analysis also to other gauge theories [63].

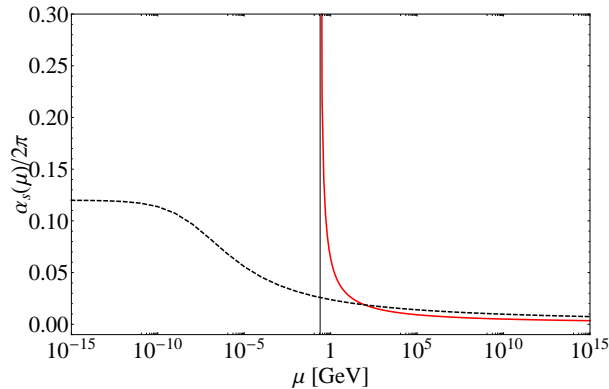


Figure 2.1: The strong running coupling $\alpha_s(\mu)$ for $N_f = 12$ (black dashed) and for $N_f = 5$ (solid red). [64]

2.6 α_s at higher loops

The 3-loop truncated RG equation 2.8, written using the same normalization of Eq. 2.19 is given by:

$$\beta(x) = \frac{dx}{dt} = -Bx^2 (1 + Cx + C_2x^2) \quad (2.26)$$

with $C_2 = \frac{\beta_2}{4\beta_0}$.

A straightforward integration of this equation would be hard to invert, as shown in Ref. [62] it is more convenient to extend the approach of the previous section by using the Padé Approximant (PA). The Padé Approximant of a given quantity calculated perturbatively in QCD up to the order n , i.e. of the series:

$$S(x) = x (1 + r_1x + r_2x^2 + \dots + r_nx^n) \quad (2.27)$$

is defined as the rational function:

$$x[N/M] = x \frac{1 + a_1x + \dots + a_Nx^N}{1 + b_1x + \dots + b_Mx^M} : \quad x[N/M] = S + x\mathcal{O}(x^{N+M+1}) \quad (2.28)$$

whose Taylor expansion up to the $N + M = n$ order is identical to the original truncated series. The use of the PA makes the integration of Eq. 2.26 straightforward. PA's may be also used either to predict the next term of a given perturbative expansion, called a Padé Approximant prediction (PAP), or to estimate the sum of the entire series, called Padé Summation. Features of the PA are shown in Ref. [65].

The Padé Approximant ($x^2[1/1]$) of the 3-loop β is given by the:

$$\beta_{\text{PA}}(x) = -Bx^2 \frac{1 + [C - (C_2/C)]x}{1 - (C_2/C)x} \quad (2.29)$$

that leads to the solution:

$$B \ln(Q^2/\Lambda^2) = \frac{1}{x} - C \ln \left[\frac{1}{x} + C - \frac{C_2}{C} \right] \quad (2.30)$$

and finally,

$$x(Q^2) = -\frac{1}{C} \frac{1}{1 - (C_2/C^2) + W(z)} \quad (2.31)$$

$$z = -\frac{1}{C} \exp \left[-1 + (C_2/C^2) - Bt/C \right], \quad (2.32)$$

the sign of C determines the sign of z and also the physically relevant branches of the Lambert function $W(z)$: for $C > 0, z < 0$ and the physical branch is $W_{-1}(z)$, taking real values in the range $(-\infty, -1)$, while for $C < 0, z > 0$ and the physical branch is given by the $W_0(z)$, taking real values in the range $(0, \infty)$.

We notice that the only significant difference between the 3-loop solution and the 2-loop solution 2.22 is in the solution $x(Q^2)$. This is because the difference in the definition of z can be reabsorbed into an appropriate redefinition of the scale parameter:

$$\Lambda^2 \longrightarrow \tilde{\Lambda}^2 = \Lambda^2 e^{C_2/(BC)}.$$

For orders up to β_4 , an approximate analytical solution is obtained integrating Eq. 2.8 :

$$\begin{aligned} \ln \frac{\mu^2}{\Lambda^2} &= \int \frac{da}{\beta(a)} = \frac{1}{\beta_0} \left[\frac{1}{a} + b_1 \ln a + a(-b_1^2 + b_2) \right. \\ &\quad + a^2 \left(\frac{b_1^3}{2} - b_1 b_2 + \frac{b_3}{2} \right) + a^3 \left(-\frac{b_1^4}{3} + b_1^2 b_2 - \frac{b_2^2}{3} \right. \\ &\quad \left. \left. - \frac{2}{3} b_1 b_3 + \frac{b_4}{3} \right) + O(a^4) \right] + C \end{aligned} \quad (2.33)$$

where $a = \alpha_s(\mu)/(4\pi)$ and $b_N \equiv \beta_N/\beta_0$, ($N = 1, \dots, 4$) and performing the inversion of the last formula by iteration as shown in Ref. [66], achieving the final result of the coupling at five-loop accuracy :

$$\begin{aligned} a &= \frac{1}{\beta_0 L} - \frac{b_1 \ln L}{(\beta_0 L)^2} + \frac{1}{(\beta_0 L)^3} \left[b_1^2 (\ln^2 L - \ln L - 1) + b_2 \right] \\ &\quad + \frac{1}{(\beta_0 L)^4} \left[b_1^3 \left(-\ln^3 L + \frac{5}{2} \ln^2 L + 2 \ln L - \frac{1}{2} \right) \right. \\ &\quad \left. - 3b_1 b_2 \ln L + \frac{b_3}{2} \right] + \frac{1}{(\beta_0 L)^5} \left[b_1^4 \left(\ln^4 L - \frac{13}{3} \ln^3 L \right) \right. \end{aligned}$$

$$\begin{aligned}
& -\frac{3}{2}\ln^2 L + 4\ln L + \frac{7}{6}) + 3b_1^2 b_2 (2\ln^2 L - \ln L - 1) \\
& - b_1 b_3 \left(2\ln L + \frac{1}{6} \right) + \frac{5}{3}b_2^2 + \frac{b_4}{3} \Big] + O\left(\frac{1}{L^6}\right). \tag{2.34}
\end{aligned}$$

where $L = \ln(\mu^2/\Lambda^2)$. The same definition of Λ scale given in Eq. 2.23 has been used for the $\overline{\text{MS}}$ scheme which leads to set the constant $C = (b_1/\beta_0) \ln(\beta_0)$.

2.7 The β coefficients in different schemes

The β_i are the coefficients of the β -function arising in the loop expansion, i.e. in orders of \hbar . Although the first two coefficients β_0, β_1 are universal scheme independent coefficients depending only on the number of colors N_c and flavors N_f , the higher-order terms are in contrast scheme dependent. In particular, for the 't Hooft scheme [19] the higher $\beta_i, i \geq 2$ terms are set to zero, leading to the solution of Eq. 2.5 for the β -function valid at all orders. Moreover, in all MS-like schemes all the β_i coefficients are gauge independent, while other schemes like the momentum space subtraction (MOM) scheme [8] depend on the particular gauge. Using the Landau gauge, the β terms for the MOM scheme are given by [67]:

$$\beta_2 = 3040.48 - 625.387N_f + 19.3833N_f^2$$

and

$$\beta_3 = 100541 - 24423.3N_f + 1625.4N_f^2 - 27.493N_f^3.$$

Results for the minimal MOM scheme and Landau gauge are shown in Ref. [68]. The renormalization condition for the MOM scheme sets the virtual quark propagator to the same form as a free massless propagator. Different MOM schemes exist and the above values of β_2 and β_3 are determined with the MOM scheme defined by subtracting the 3-gluon vertex to a point with one null external momentum. This leads to a coupling which is not only RS dependent but also gauge-dependent. The values of β_2 and β_3 given here are only valid in the Landau gauge. Values in the V-scheme defined by the static heavy quark potential [69–75] can be found in Ref. [76].

They result in: $\beta_2 = 4224.18 - 746.01N_f + 20.88N_f^2$ and $\beta_3 = 43175 - 12952N_f + 707.0N_f^2$ respectively. We recall that the sign of the β_i controls the running of α_s . We have $\beta_0 > 0$ for $N_f \leq 16$, $\beta_1 > 0$ for $N_f \leq 8$, $\beta_2 > 0$ for $N_f \leq 5$, and β_3 is always positive. Consequently, α_s decreases at high momentum transfer, leading to the asymptotic freedom of pQCD. Note that, β_i are sometimes defined with an additional multiplying factor $1/(4\pi)^{i+1}$. Different schemes are characterized by different $\beta_i, i \geq 2$ and lead to different definitions for the effective coupling.

2.8 The Λ parameter and quark thresholds

The Λ parameter represents the Landau ghost pole in the perturbative coupling in QCD. We recall that the Landau pole was initially identified in the context of Abelian QED. However, the presence of this pole does not affect QED. Given its value, $\Lambda \sim 10^{30-40}\text{GeV}$, above the Planck scale [77], at which new physics is expected to occur in order to suppress the unphysical divergence. The QCD Λ parameter in contrast is at low energies, its value depends on the RS, on the order of the β -series, β_i , on the approximation of the coupling $\alpha_s(\mu)$ at orders higher than β_1 and on the number of flavors N_f . Although mass corrections due to light quarks at higher order in perturbative calculations introduce negligible terms, they actually indirectly affect α_s through N_f . In fact, the number of active quark flavors runs with the scale Q^2 and a quark q is considered active in loop integration if the scale $Q^2 \geq m_q^2$. Thus, in general, light quarks can be considered massless regardless of whether they are active or not, while α_s varies smoothly when passing a quark threshold, rather than in discrete steps. The matching of the values of α_s below and above a quark threshold makes Λ depend on N_f . Matching requirements at leading order β_0 , imply that:

$$\alpha_s^{N_f-1} (Q^2 = m_q^2) = \alpha_s^{N_f} (Q^2 = m_q^2)$$

The numerical values of Λ in different schemes, MeV				
N_f	the order of approximation ν	$\Lambda_{\overline{\text{MS}}}^{(N_f)}$	$\Lambda_{\text{V}}^{(N_f)}$	$\Lambda_{\text{mMOM}}^{(N_f)}$
4	2	350	500	625
4	3	335	475	600
4	4	330	470	590
5	2	250	340	435
5	3	245	335	430
5	4	240	330	420

Table 2.1: Results for the Λ parameter in different schemes, at different values of the number of active flavor, N_f , and at different orders of accuracy ν [76].

and therefore that:

$$\Lambda^{N_f} = \Lambda^{N_f-1} \left(\frac{\Lambda^{N_f-1}}{m_q} \right)^{2/(33-2N_f)}$$

The formula with β_1 , can be found in [78] and the four-loop matching in the $\overline{\text{MS}}$ RS is given in [79].

As shown in the previous section at the lowest order β_0 , the Landau singularity is a simple pole on the positive real axis of the Q^2 -plane, whereas at higher order it acquires a more complicated structure. This pole is unphysical and is located on the positive real axis of the complex Q^2 -plane. This singularity of the coupling indicates that the perturbative regime of QCD breaks down and it may also suggest that a new mechanism takes over, such as the confinement. Thus, the value of Λ is often associated with the confinement scale, or equivalently to the hadronic mass scale. An explicit relation between hadron masses and the Λ scale has been obtained in the framework of holographic QCD [80]. Landau poles on the other hand, usually do not appear in nonperturbative approaches such as AdS/QCD. Approximate values of Λ in different schemes are given in Table 2.1:

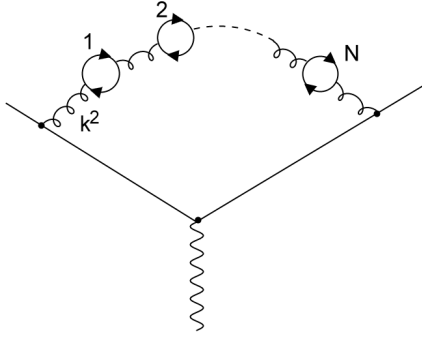


Figure 2.2: Example of a diagram with the “bubble-chain” insertion.

Different schemes are related perturbatively by:

$$\alpha_s^{(2)}(Q^2) = \alpha_s^{(1)}(Q^2) \left[1 + v_1 \alpha_s^{(1)}(Q^2) / (4\pi) \right] + \mathcal{O}(\alpha_s^2) \quad (2.35)$$

where v_1 is the leading order difference between $\alpha_s(Q^2)$ in the two schemes. In the case of the V-scheme and $\overline{\text{MS}}$ scheme we have : $v_1^{\overline{\text{MS}}} = \frac{31}{9}C_A - \frac{20}{9}T_F n_l$.

Thus, the relation between Λ_1 in a scheme 1 and Λ_2 in a scheme 2 is, at the one-loop order, given by:

$$\Lambda_2 = \Lambda_1 e^{\frac{v_1}{2\beta_0}}.$$

For example, the $\overline{\text{MS}}$ and V-scheme scale parameters are related by:

$$\Lambda_V = \Lambda_{\overline{\text{MS}}} e^{\frac{93-10N_f}{2(99-6N_f)}}$$

The relation is valid at each threshold translating all values for the scale from one scheme to the other.

In general, one may think that lower values of the scale parameter lead to slower increasing couplings in the IR. Unfortunately other effects can occur spoiling this criterion. In fact the nature of the perturbative expansion is affected by the renormalon growth [19] of the coefficients. The renormalons affect renormalizable gauge theories only, they stem from particular diagrams known as “bubble-chain” diagrams and shown in Fig. 2.2.

In loop integration these terms introduce a factorial growth, using Eq. 2.15 and considering $k^2 \geq \mu^2$ we obtain:

$$\int d^4k k^{-2n} \alpha_s(k^2) = \alpha_s(\mu) \sum_N \int d^4k k^{-2n} (\beta_0 \alpha_s(\mu) \ln(k^2/\mu^2))^N \sim \sum_N N! \left(\frac{\beta_0}{n-2}\right)^N \alpha_s(\mu)^{N+1},$$

with $n \geq 3$. Performing the Borel transform of the last series one obtains a geometric series,

$$B(z) = \sum_N \left(\frac{\beta_0}{n-2}\right)^N z^N = \frac{1}{1 - \left(\frac{\beta_0}{n-2}\right)z} \quad (2.36)$$

which has poles on the real positive axis:

$$z_n = \frac{n-2}{\beta_0}, \quad n = 3, 4, 5, \dots \quad (2.37)$$

These singularities introduce an ambiguity in the inverse Borel transform:

$$F(\alpha_s(\mu)) = \int_0^\infty dt e^{-t/\alpha_s(\mu)} B(t), \quad (2.38)$$

since they lie on the path of integration and lead to non-zero residue contributions of the type:

$$\Delta = \left(\frac{\Lambda}{\mu}\right)^{2\beta_0 z_n}. \quad (2.39)$$

IR and UV renormalons arise as singularities on the real negative and positive axis of the complex z plane of the Borel transform, (analogously to instanton poles, this explains the name given by 't Hooft), and are related to the Λ scale and thus to the Landau pole of the strong coupling. These terms affect the coefficients of the perturbative QCD series and its convergence. It has been shown in several applications of resummed quantities (i.e. applying the technique of resummation of large IR logarithms) renormalons do not affect the final result if one uses an appropriate prescription (e.g. the minimal prescription (MP) formula [81, 82]). Reviews on renormalons exist in the literature, e.g. Refs. [83, 84].

Thus, different growths of the coefficients in different renormalization schemes can balance the differences in values of the corresponding scales $\Lambda_{1,2}$. However, the growth of the coefficients is not only due to renormalons, in some cases the

coefficients have inherently fast rising behavior as shown in Ref. [85]. For further insights, relations among different RS and their associated Λ are discussed in Ref. [8].

2.9 The Renormalization Group Equations

The scale dependence of the coupling can be determined considering that the bare coupling $\overline{\alpha}_s$ and renormalized couplings, α_s , at different scales are related by:

$$\overline{\alpha}_s = Q^{2\varepsilon} Z_\alpha(Q^2) \alpha_s(Q^2) = \mu^{2\varepsilon} Z_\alpha(\mu^2) \alpha_s(\mu^2), \quad (2.40)$$

where ε is the regularization parameter, integrals are carried out in $4-2\varepsilon$ dimensions and the UV divergences are regularized to $1/\varepsilon$ poles. The Z_i are constructed as functions of $1/\varepsilon$, such that they cancel all $1/\varepsilon$ poles. From Eq. 2.40 we can obtain the relation from two different couplings at two different scales:

$$\alpha_s(Q^2) = \mathcal{Z}_\alpha(Q^2, \mu^2) \alpha_s(\mu^2), \quad (2.41)$$

with $\mathcal{Z}_\alpha(Q^2, \mu^2) \equiv (\mu^{2\varepsilon}/Q^{2\varepsilon}) [Z_\alpha(Q^2)/Z_\alpha(\mu^2)]$.

The \mathcal{Z}_α form a group with a composition law:

$$\mathcal{Z}_\alpha(Q^2, \mu^2) = \mathcal{Z}_\alpha(Q^2, \mu_0^2) \mathcal{Z}_\alpha(\mu_0^2, \mu^2), \quad (2.42)$$

a unity element: $\mathcal{Z}_\alpha(Q^2, Q^2) = 1$ and an inversion law: $\mathcal{Z}_\alpha(Q^2, \mu^2) = \mathcal{Z}_\alpha^{-1}(\mu^2, Q^2)$. Fundamental properties of the Renormalization group are: *reflexivity, symmetry and transitivity*. Thus the scale invariance of a given perturbatively calculated quantity is recovered by the invariance of the theory under the Renormalization Group Equations (RGE). As previously discussed, the QCD Lagrangian has only one dimensionless coupling constant g_s and in the case of a massless theory the Lagrangian has no particular mass scale, but is completely conformal. The only energy scale, μ , is introduced by the subtraction point with the renormalization procedure. Thus, all phenomena involving strong interactions can be described by only one parameter,

the strong coupling $\alpha_s(Q^2)$, and the same parameter is responsible for the interaction at low and high energy scales. As shown in the previous section, the strong coupling has a running behavior, it evolves and increases with the energy of the probe, Q^2 , from high to low values of the momentum transfer. Thus if we consider the case of the physical observable at an energy $s \geq m_f^2$, in order to neglect masses, for example the ratio:

$$R_{e^+e^-}(s) = \frac{\sigma(e^+e^- \rightarrow \text{hadrons})}{\sigma(e^+e^- \rightarrow \mu^+\mu^-)} \quad (2.43)$$

where the cross sections are given at the lowest order by:

$$\sigma(e^+e^- \rightarrow \mu^+\mu^-) = \frac{4\pi\alpha^2}{3s}, \quad (2.44)$$

and

$$\sigma(e^+e^- \rightarrow \text{hadrons}) = \frac{4\pi\alpha^2}{3s} N_c \sum_f Q_f^2, \quad (2.45)$$

with $\alpha \equiv e^2/4\pi$ the fine structure constant of QED. As shown in the formula the single cross sections depend on the center-of-mass energy $s = Q^2$, but this dependence cancels in the $R_{e^+e^-}$ at lowest order. Also by dimensional analysis, a constant value of the observable $R_{e^+e^-}$ would be predicted independently of any energy scale s , the ratio being a dimensionless quantity. However, higher order loop integrations and the renormalization procedure of the coupling constant introduce a scale dependence. Since R is dimensionless and since there is no mass scale in the QCD Lagrangian, scale dependence can be introduced only via the μ scale dependence of the coupling $\alpha_s(\mu)$ and via a ratio (Q^2/μ^2) -like dependence of the perturbative coefficients. In fact, except for the first two terms r_0, r_1 , which are scale independent, the coefficients r_n are polynomials of $\ln(Q^2/\mu^2)$ with highest power $n-1$. By means of the RGE all these logarithms can be reabsorbed into the running coupling. The purpose of taking α_s scale-dependent is to transfer to α_s all terms involving μ in the perturbative series of $R(s)$. The independence of R with respect to μ is given by the Callan-Symanzik relation for QCD [6, 7]:

$$R_{e^+e^-}(s; \mu) = N_c \sum_f Q_f^2 [1 + R(s; \mu)]. \quad (2.46)$$

where Q_f are quark charges summed over the flavor index f and

$$R(s; \mu) = \sum_{n=1}^{\tilde{n}} r_n(s; \mu) (\alpha_s(\mu)/\pi)^n \quad (2.47)$$

$$\mu^2 \frac{d}{d\mu^2} R_{e^+e^-}(s, \mu) = 0, \quad (2.48)$$

equivalently:

$$\left[\mu^2 \frac{\partial}{\partial \mu^2} + \beta(\alpha_s) \frac{\partial}{\partial \alpha_s} \right] R_{e^+e^-}(s; \mu) = 0, \quad (2.49)$$

where

$$\beta(\alpha_s) = \mu^2 \frac{\partial \alpha_s}{\partial \mu^2}, \quad (2.50)$$

setting the renormalization scale μ equal to the physical scale Q would remove the $\ln(Q^2/\mu^2)$ in the coefficients r_n and fold the μ -dependence into α_s ($\mu^2 = s$). Thus the option of choosing $\mu^2 = s$ yields the simplest form for the perturbative expansions of given observable.

2.10 The Extended Renormalization Group Equations

Given that physical predictions cannot depend on the choice of the renormalization scale nor on the scheme, the same approach used for the renormalization scale based on the invariance under RGE is extended to scheme transformations. This approach leads to the Extended Renormalization Group Equations, which were introduced first by Stückelberg and Peterman [3], then discussed by Stevenson [10–13] and also improved by Lu and Brodsky [86]. A physical quantity, R , calculated at the N -th order of accuracy is expressed as a truncated expansion in terms of a coupling

constant $\alpha_S(\mu)$ defined in the scheme S and at the scale μ , such as:

$$R_N = r_0 \alpha_S^p(\mu) + r_1(\mu) \alpha_S^{p+1}(\mu) + \dots + r_N(\mu) \alpha_S^{p+N}(\mu). \quad (2.51)$$

At any finite order, the scale and scheme dependencies of the coupling constant $\alpha_S(\mu)$ and of the coefficient functions $r_i(\mu)$ do not totally cancel, this leads to a residual dependence in the finite series and to the scale and scheme ambiguities.

In order to generalize the RGE approach it is convenient to improve the notation by introducing the universal coupling function as the extension of an ordinary coupling constant to include the dependence on the scheme parameters $\{c_i\}$:

$$\alpha = \alpha(\mu/\Lambda, \{c_i\}). \quad (2.52)$$

where Λ is the standard two-loop $\overline{\text{MS}}$ scale parameter. The subtraction prescription is now characterized by an infinite set of continuous *scheme parameters* $\{c_i\}$ and by the renormalization scale μ . Stevenson [11] has shown that one can identify the beta-function coefficients of a given renormalization scheme with the scheme parameters. Considering that the first two coefficients of the β -function are scheme independent, each scheme is identified by its $\{\beta_i, \quad i = 2, 3, \dots\}$ parameters.

More conveniently, let us define the rescaled coupling constant and the rescaled scale parameter as

$$a = \frac{\beta_1}{\beta_0} \frac{\alpha}{4\pi}, \quad \tau = \frac{2\beta_0^2}{\beta_1} \log(\mu/\Lambda). \quad (2.53)$$

Then, the rescaled β -function takes the canonical form:

$$\beta(a) = \frac{da}{d\tau} = -a^2 \left(1 + a + c_2 a^2 + c_3 a^3 + \dots \right) \quad (2.54)$$

with $c_n = \beta_n \beta_0^{n-1} / \beta_1^n$ for $n = 2, 3, \dots$.

The scheme and scale invariance of a given observable R , can be expressed as:

$$\begin{aligned} \frac{\delta R}{\delta \tau} &= \beta \frac{\partial R}{\partial a} + \frac{\partial R}{\partial \tau} = 0 \\ \frac{\delta R}{\delta c_n} &= \beta^{(n)} \frac{\partial R}{\partial a} + \frac{\partial R}{\partial c_n} = 0. \end{aligned} \quad (2.55)$$

The fundamental beta function that appears in Eqs. 2.55 reads:

$$\beta(a, \{c_i\}) \equiv \frac{\delta a}{\delta \tau} = -a^2 (1 + a + c_2 a^2 + c_3 a^3 + \dots) \quad (2.56)$$

and the extended or scheme-parameter beta functions are defined as:

$$\beta_{(n)}(a, \{c_i\}) \equiv \frac{\delta a}{\delta c_n}. \quad (2.57)$$

The extended beta functions can be expressed in terms of the fundamental beta function. Since the $(\tau, \{c_i\})$ are independent variables, second partial derivatives respect the commutativity relation:

$$\frac{\delta^2 a}{\delta \tau \delta c_n} = \frac{\delta^2 a}{\delta c_n \delta \tau}, \quad (2.58)$$

which implies

$$\frac{\delta \beta_{(n)}}{\delta \tau} = \frac{\delta \beta}{\delta c_n}, \quad (2.59)$$

$$\beta \beta'_{(n)} = \beta_{(n)} \beta' - a^{n+2}, \quad (2.60)$$

where $\beta'_{(n)} = \partial \beta_{(n)} / \partial a$ and $\beta' = \partial \beta / \partial a$. From here

$$\beta^{-2} \left(\frac{\beta_{(n)}}{\beta} \right)' = -a^{n+2}, \quad (2.61)$$

$$\beta_{(n)}(a, \{c_i\}) = -\beta(a, \{c_i\}) \int_0^a dx \frac{x^{n+2}}{\beta^2(x, \{c_i\})}, \quad (2.62)$$

where the lower limit of the integral has been set to satisfy the boundary condition

$$\beta_{(n)} \sim O(a^{n+1}).$$

That is, a change in the scheme parameter c_n can only affect terms of order a^{n+1} or higher in the evolution of the universal coupling function.

The extended renormalization group equations Eqs. 2.55 can be written in the form:

$$\begin{aligned} \frac{\partial R}{\partial \tau} &= -\beta \frac{\partial R}{\partial a} \\ \frac{\partial R}{\partial c_n} &= -\beta_{(n)} \frac{\partial R}{\partial a}. \end{aligned} \quad (2.63)$$

Thus, provided we know the extended beta functions, we can determine any variation of the expansion coefficients of R under scale-scheme transformations. In particular, we can evolve a given perturbative series into another determining the expansion coefficients of the latter and vice versa.

Chapter 3

Renormalization Scale Setting in QCD

The scale-scheme ambiguities are an important source of uncertainties in many processes in perturbative QCD preventing precise theoretical predictions for both SM and BSM physics. In principle, an infinite perturbative series is void of this issue, given the scheme and scale invariance of the entire physical quantities [3–7], in practice perturbative corrections are known up to a certain order of accuracy and scale invariance is only approximated in truncated series, leading to the scheme and scale ambiguities [8–18, 87, 88]. If on one hand, according to the conventional practice, or conventional scale setting (CSS), this problem cannot be avoided and is responsible for part of the theoretical errors, on the other hand some strategies for the optimization of the truncated expansion have been proposed, such as the Principle of Minimal Sensitivity proposed by Stevenson [11], the Fastest Apparent Convergence criterion introduced by Grunberg [14] and the Brodsky-Lepage-Mackenzie (BLM) method [17]. These are procedures commonly in use for scale setting in perturbative QCD. In general, a scale-setting procedure is considered reliable if it preserves important self consistency requirements. All Renormalization Group properties such as: *uniqueness*, *reflexivity*, *symmetry*, and *transitivity* should be preserved also by

the scale-setting procedure in order to be generally applied [24].

In fact, once the optimal scale is set, by means of the RG properties is possible to relate results in different schemes and different observables. Other requirements are also suggested by tested theories, by the convergence behavior of the series and also for phenomenological reasons or scheme independence. We discuss in this chapter the different optimization procedures and their properties. An introduction to these methods can also be found in Refs. [21, 22].

3.1 Conventional scale setting - CSS

According to common practice a first evaluation of the physical observable is obtained by calculating perturbative corrections in a given scheme (commonly used are MS or $\overline{\text{MS}}$) and at an initial renormalization scale $\mu_r = \mu_r^{\text{init}}$, obtaining the truncated expansion:

$$\rho_n = \mathcal{C}_0 \alpha_s^p(\mu_r) + \sum_{i=1}^n \mathcal{C}_i(\mu_r) \alpha_s^{p+i}(\mu_r), \quad (p \geq 0), \quad (3.1)$$

where \mathcal{C}_0 is the tree-level term, while $\mathcal{C}_1, \mathcal{C}_2, \dots, \mathcal{C}_n$ are the one-loop, two-loop, n-loop corrections respectively and p is the power of the coupling at tree-level.

In order to improve the pQCD estimate of the observable, after the initial renormalization a change of scale using the RGE and a chosen scale-setting method is performed in Eq. 3.1, which leads to:

$$\rho_n = \mathcal{C}_0 \alpha_s^p(\tilde{\mu}_r^0) + \sum_{i=1}^n \bar{\mathcal{C}}_i(\tilde{\mu}_r^i) \alpha_s^{p+i}(\bar{\mu}_r^i), \quad (p \geq 0) \quad (3.2)$$

where the new leading-order (LO) and higher-order scales $\tilde{\mu}_r^0$ and $\tilde{\mu}_r^i$ are functions of the initial renormalization scale μ_r^{init} , and they depend the particular choice of the scale-setting method. At the same time, the new coefficients $\bar{\mathcal{C}}_i(\bar{\mu}_r^i)$ are changed accordingly in order to obtain a consistent result.

The simple CSS procedure starts from the scale and scheme invariance of a given observable, which translates into complete freedom for the choice of the renormal-

ization scale. In practice in this approach, the initial scale is directly fixed to the typical momentum transfer of the process, Q , or to a value which minimizes the contributions of the loop diagrams and the errors are evaluated varying the value of Q in the range of $2, [Q/2, 2Q]$.

It is often claimed that this simple scale setting method estimates contributions from higher-order terms and that, due to the perturbative nature of the expansion, the introduction of higher order corrections would reduce the scheme and scale ambiguities order by order.

No doubt that the higher the loop corrections are calculated, the greater is the precision of the theoretical estimations in comparison with the experimental data, but we cannot know *a priori* the level of accuracy necessary for the CSS to achieve the desired precision and at present in the majority of cases only the NNLO corrections are available. Besides this, the divergent nature of the asymptotic perturbative series and the presence of factorial growing terms (i.e. renormalons) severely compromise the theoretical predictions.

However, even though this procedure may give an indication on the level of conformality and convergence reached by the truncated expansion, it leads to a numerical evaluation of theoretical errors that is quite unsatisfactory and dependent strictly on the value of the chosen scale. Different choices of the renormalization scale may lead to very different results when including higher order corrections. For example, the NLO correction in $W+3\text{jets}$ with the BlackHat code [20] can be either negligible or extremely severe depending on the choice of the particular renormalization scale. One may argue that the proper renormalization scale for a fixed-order prediction can be judged by comparing theoretical results with experimental data, but this method would be strictly process dependent and would compromise the predictivity of the pQCD approach.

Besides the complexity of the higher order calculations and the slow convergence of the perturbative series, there are many critical points in the CSS method:

- In general, no one knows the proper renormalization scale value, Q , and the correct range where the scale and scheme parameters should be varied in order to have the correct error estimate. In fact, in some processes there can be more than one typical momentum scale that can be taken as the renormalization scale according to the CSS procedure, for example in processes involving heavy quarks, typical scales are either the center-of-mass energy \sqrt{s} or also the heavy quark mass. Moreover, the idea of the typical momentum transfer as the renormalization scale only sets the order of magnitude of the scale, but does not indicate the optimal scale;
- No distinction is made among different sources of errors and their relative contributions, e.g. in addition to the errors due to scale-scheme uncertainties there are also the errors from missing higher-order uncalculated terms. In such an approach, theoretical uncertainties can become quite arbitrary and unreliable;
- The convergence of the perturbative series in QCD is affected by uncanceled large logarithms as well as by “renormalon” terms that diverge as $(n!\beta_i^n \alpha_s^{n+1})$ at higher orders [89,90], this is known as the *renormalon problem* [84]. These renormalon terms can give sizable contributions to the theoretical estimates, as shown in e^+e^- annihilation, τ decay, deep inelastic scattering, hard processes involving heavy quarks. These terms are responsible for important corrections at higher orders also in the perturbative region, leading to different predictions according to different choices of the scale (as shown in Ref. [20]). Large logarithms on the other hand can be resummed using the resummation technique [82,91–96] and results are IR renormalon free. This does not help for the renormalization scale and scheme ambiguities, which still affect theoretical predictions with or without resummed large logarithms. In fact, as recently shown in Ref. [2] for the $b\bar{b}$ production cross section at NNLO order of accuracy at hadron colliders, the CSS scale setting leads to theoretical uncertainties

that are of the same order of the NNLO corrections $\sim 20 - 30\%$ taking as the typical momentum scale the b-quark mass $m_b \sim 4.92\text{GeV}$.

- In the Abelian limit $N_c \rightarrow 0$ at fixed $\alpha_{em} = C_F \alpha_s$ with $C_F = (N_c^2 - 1)/2N_c$, a QCD case approaches effectively the QED analogous case [32, 97]. Thus, in order to be self-consistent any QCD scale-setting method should be also extendable to QED and results should be in agreement with the Gell-Mann and Low (GM-L) scheme. This is an important requirement also for the perspective of a grand unified theory (GUT), where only one method for setting the renormalization scale can be applied and then it can be considered as a good criterion for verifying if a scale setting is correct or not. CSS leads to incorrect results when applied to QED processes. In the GM-L scheme, the renormalization scale is set with no ambiguity to the virtuality of the exchanged photon/photons, that naturally sums an infinite set of vacuum polarization contributions into the running coupling. Thus the CSS approach of varying the scale of a factor of 2 does not apply to QED since the scale is already optimized.
- The forthcoming large amount of high-precision experimental data arising especially from the running of the high collision energy and high luminosity Large Hadronic Collider (LHC), will require more accurate and refined theoretical estimates. The CSS appears to be more a “lucky guess”; its results are affected by large errors and the perturbative series poorly converges with or without large-logarithm resummation or renormalon contributions. Moreover, within this background, it is nearly impossible to distinguish among SM and BSM signals and in many cases, improved higher-order calculations are not expected to be available in the short term.

To sum up, the conventional scale-setting method assigns an arbitrary range and an arbitrary systematic error to fixed-order perturbative calculations that greatly affects the predictions of pQCD.

3.2 The Principle of Minimal Sensitivity: PMS Scale-Setting

The Principle of Minimal Sensitivity [11,12] derives from the assumption that, since observables should be independent of the particular RS and scale, their optimal perturbative approximations should be stable under small RS variations. The RS scheme parameters β_2, β_3, \dots and the scale parameter Λ (or the subtraction point μ_r), are considered as “unphysical” and independent variables, and then their values are set in order to minimize the sensitivity of the estimate to their small variations. This is essentially the core of the Optimized Perturbation Theory (OPT) [11], based on the PMS procedure. The convergence of the perturbative expansion, Eq. 3.1, truncated to a given order ρ_n , is improved by requiring its independence from the choice of RS and μ . The optimization is implemented by identifying the RS-dependent parameters in the ρ_n -truncated series (the β_i for $2 \leq i \leq n$ and Λ), with the request that the partial derivative of the perturbative expansion of the observable with respect to the RS-dependent and scale parameters vanishes. In practice the PMS scale setting is designed to eliminate the remaining renormalization and scheme dependence in the truncated expansions of the perturbative series.

More explicitly, the PMS requires the truncated series, i.e. the approximant of a physical observable defined in Eq. 3.1, to satisfy the RG invariance given by the 2.63, with the substitution of the proper $\beta_{(n)}$ function:

$$\frac{\partial \alpha_s}{\partial \beta_j} = -\beta(\alpha_s) \int_0^{\alpha_s} d\alpha' \frac{\alpha'^{j+2}}{[\beta(\alpha')]^2} = \frac{\alpha_s^{j+1}}{\beta_0} \left(\frac{1}{j-1} - \frac{\beta_1}{\beta_0} \frac{j-2}{j(j-1)} \alpha_s + \dots \right), \quad (3.3)$$

it follows that:

$$\frac{\partial \rho_n}{\partial \tau} = \left(\frac{\partial}{\partial \tau} + \beta(\alpha_s) \frac{\partial}{\partial \alpha_s} \right) \rho_n \equiv 0 \quad (3.4)$$

$$\frac{\partial \rho_n}{\partial \beta_j} = \left(\frac{\partial}{\partial \beta_j} - \beta(\alpha_s) \int_0^{\alpha_s} d\alpha' \frac{\alpha'^{j+2}}{[\beta(\alpha')]^2} \frac{\partial}{\partial \alpha_s} \right) \rho_n \equiv 0 \quad (3.5)$$

where $\tau = \ln(\mu_r^2/\Lambda_{\text{QCD}}^2)$ and $j \geq 2$. Scheme labels have been omitted. The request of RS-independence modifies the series coefficients \mathcal{C}_i ($1 \leq i \leq n$) and the coupling α_s to the PMS “optimized” values $\tilde{\mathcal{C}}_i$ and $\tilde{\alpha}_s$. At first order the requirement of RS independence implies that Eq. 3.1 satisfies the Callan-Symanzik equation 2.50 with β truncated at order n . This implies that the scale dependence is not removed from the perturbative coefficients: $\mathcal{C}_n(Q^2, \mu^2)$. We can argue that this approach is more based on convergence rather than physical criteria. In particular, the PMS is a procedure that can be extended to higher order and it can be generally applied to calculations obtained in arbitrary initial renormalization schemes. Though this procedure leads to results that are suggested to be unique and scheme independent, unfortunately it violates important properties of the renormalization group as shown in Ref. [21], such as reflexivity, symmetry, transitivity and also the *existence and uniqueness* of the optimal PMS renormalization scheme are not guaranteed since they are strictly related to the presence of maxima and minima. Other phenomenological implications will be shown in section 3.5.

3.3 The Fastest Apparent Convergence principle - FAC scale setting

The Fastest Apparent Convergence (FAC) principle is based on the idea of *effective charges*. As pointed out by Grunberg [14–16], any perturbatively calculable physical quantity can be used to define an effective coupling, or “effective charge”, by entirely incorporating the radiative corrections into its definition. Effective charges can be defined from an observable starting from the assumption that the infinite series of a given quantity is scheme and scale invariant. Given the perturbative series $R = \mathcal{C}_0\alpha_s^p + \dots$, the relative effective charge α_R is given by

$$\alpha_R \equiv \left(\frac{R}{\mathcal{C}_0}\right)^{1/p}. \quad (3.6)$$

Since R, \mathcal{C}_0 and p are all renormalization scale and scheme invariant, the effective charge α_R is scale and scheme invariant.

The effective charge satisfies the same renormalization group equations as the usual coupling. Thus, the running behavior for both the effective coupling and the usual coupling are the same if their RG equations are calculated in the same renormalization scheme. This idea has been discussed in more detail in Refs. [98,99].

Using the effective charge α_R , the ratio $R_{e^+e^-}$ becomes [100]:

$$R_{e^+e^-}(Q^2) \equiv R_{e^+e^-}^0(Q^2) \left[1 + \frac{\alpha_R(Q)}{\pi} \right] \quad (3.7)$$

where $R_{e^+e^-}^0(Q^2)$ is the Born result and $s = Q^2$ is the center-of-mass energy squared.

An important suggestion is that all effective couplings defined in the same scheme satisfy the same RG equations. While different schemes or effective couplings, will differ through the third and higher coefficients of the $\{\beta_i^{\mathcal{R}}\}$ -functions, which are scheme \mathcal{R} dependent. Hence, any effective coupling can be used as a reference to define the renormalization procedure.

Given that expansions of the effective charges are known only up to a certain order, $\alpha_R \simeq \left(\frac{R_n}{\mathcal{C}_0}\right)^{1/p}$, an optimization procedure is used to improve the perturbative calculations, namely the FAC scale setting. The basic idea of the FAC scale setting method is to set to zero all the higher order perturbative coefficients, i.e. $\mathcal{C}_{i(\geq 1)}(\mu_r^{\text{FAC}}) \equiv 0$, including all fixed order corrections into the FAC renormalization scale of the leading term by means of the RG equations in order to provide a reliable estimate [101].

In practice given a physical observable in an arbitrary renormalization scheme written as:

$$\sigma = A + B [\alpha_s(\mu_r)]^d \left[1 + \sigma_1(\mu_r) \alpha_s(\mu_r) + \mathcal{O}(\alpha_s^2) \right],$$

the effective coupling $\bar{\alpha}_s(\mu_r)$ is defined by the identity

$$\sigma = A + B [\bar{\alpha}_s(\mu_r)]^d,$$

where A and B are general perturbative or non-perturbative quantities predicted in

principle by QCD, d is the α_s -order at the Born level and $\sigma_1(\mu_r)$ is the NLO coefficient. Consequently, $\bar{\alpha}_s(\mu_r)$ is the object effectively extracted from a LO analysis of the experimental data on σ .

In general this method can be applied to any observable calculated in any RS also in processes with large higher order corrections. The FAC scale setting, as has been shown in Ref. [21], preserves the RG self-consistency requirements, although the FAC method can be considered more an optimization approach rather than a proper scale-setting procedure to extend order by order. FAC results depend sensitively on the quantity to which the method is applied. In general, when the NLO correction is large, the FAC results to be a resummation of the most important higher order corrections and then a RG improved perturbation theory is achieved. Unfortunately phenomenological studies (see Fig. 3.1) with FAC show that this strategy is acceptable only in a particular range of values of a given variable related to the virtuality of the physical observable.

3.4 The BLM Scale-Setting

The Brodsky-Lepage-Mackenzie (BLM) [17] method was designed to improve the pQCD estimate by absorbing the $\{\beta_i\}$ -terms arising in the perturbative calculation into the running coupling using the RG equations. In the BLM approach and subsequently in its generalization and extension to all orders the Principle of Maximum Conformality (PMC), the BLM/PMC-scales are identified with the running N_f -terms related to UV divergent loops. In order to improve the discussion, we will use the following notation: n_f for the general number of active flavors, N_f for the number of active flavors related to the UV divergent diagrams and N_F for the number of active flavors related to UV finite diagrams. We underline that only terms related to the β -function, or equivalently to N_f , must be included into the BLM/PMC scales. The N_F terms may arise in a calculation but are not responsible for the running of the effective coupling α_s and thus they do not determine the BLM/PMC scales.

The BLM shows a way to resolve the renormalization scheme-scale ambiguities, by identifying the coefficients of the β terms. Once these coefficients are reabsorbed into the scale the perturbative expansion no longer suffers of the renormalon growth associated with the $n!\beta_0^n\alpha_s^{n+1}$, which are eliminated. This improves the convergence of the perturbative expansions in QED/QCD. More importantly, the renormalization scale can be determined without computing all higher-order corrections and in a unambiguous way. Thus, the lower-order or even the LO analysis can be meaningfully compared with experiments. BLM scale setting is greatly inspired by QED. The standard Gell-Mann-Low scheme determines the correct renormalization scale identifying the scale with the virtuality of the exchanged photon [4]. For example, in electron-muon elastic scattering, the renormalization scale is given by the virtuality of the exchanged photon, i.e. the spacelike momentum transfer squared $\mu_R^2 = q^2 = t$. Thus

$$\alpha(t) = \frac{\alpha(t_0)}{1 - \Pi(t, t_0)} \quad (3.8)$$

where

$$\Pi(t, t_0) = \frac{\Pi(t) - \Pi(t_0)}{1 - \Pi(t_0)}$$

is the vacuum polarization (VP) function. From Eq. 3.8 it follows that the renormalization scale $\mu_R^2 = t$ can be determined by the β_0 -term at the lowest order. This scale is sufficient to sum all the vacuum polarization contributions into the dressed photon propagator, both proper and improper to all orders.

Following the GM-L scheme in QED, the BLM scales can be determined at LO order in perturbation theory by writing explicit contributions coming from the different N_f terms of the NLO coefficient in a physical observable as [17]:

$$\begin{aligned} \rho &= C_0 \alpha_{s,\overline{\text{MS}}}^p(\mu_r) \left[1 + (AN_f + B) \frac{\alpha_{s,\overline{\text{MS}}}(\mu_r)}{\pi} \right] \\ &= C_0 \alpha_{s,\overline{\text{MS}}}^p(\mu_r) \left[1 + \left(-\frac{3}{2}A\beta_0 + \frac{33}{2}A + B \right) \frac{\alpha_{s,\overline{\text{MS}}}(\mu_r)}{\pi} \right] \end{aligned} \quad (3.9)$$

where $\mu_r = \mu_r^{\text{init}}$ stands for an initial renormalization scale, which practically can

be taken as the typical momentum transfer of the process. The N_f term is due to the quark vacuum polarization. Calculations are in the $\overline{\text{MS}}$ -scheme.

At the NLO level, all N_f terms should be resummed into the coupling. Using the NLO α_s -running formula:

$$\alpha_{s,\overline{\text{MS}}}(\mu_r^*) = \frac{\alpha_{s,\overline{\text{MS}}}(\mu_r)}{1 + \frac{\beta_0}{4\pi} \alpha_{s,\overline{\text{MS}}}(\mu_r) \ln\left(\frac{\mu_r^*}{\mu_r}\right)}, \quad (3.10)$$

we obtain

$$\rho = C_0 \alpha_{s,\overline{\text{MS}}}^p(\mu_r^*) \left[1 + C_1^* \frac{\alpha_{s,\overline{\text{MS}}}(\mu_r^*)}{\pi} \right] \quad (3.11)$$

where

$$\mu_r^* = \mu_r \exp\left(\frac{3A}{p}\right)$$

is the BLM scale and

$$C_1^* = \frac{33}{2}A + B,$$

is the *conformal* coefficient, i.e. the NLO coefficient not depending on the RS and scale μ . Both the effective BLM scale μ_r^* and the coefficient C_1^* are N_f independent and conformal at LO. By including the term $33A/2$ into the scale we eliminate the β_0 term of the NLO coefficient C_1 which is responsible for the running of the coupling constant, and the observable in the final results can be written in its *maximal conformal form*. Eq.3.11.

The BLM method can be extended to higher orders in a systematic way by including the n_f terms arising at higher order into the BLM scales consistently. In order to extend the BLM beyond the NLO, the following points are considered essential:

1. All n_f -terms associated with the β -function (i.e. N_f terms) and then with the renormalization of the coupling constant, must be absorbed into the effective coupling, while those n_f -terms that have no relation with UV divergent diagrams (i.e. N_F -terms) should be identified and considered as part of the conformal coefficients. After BLM scale setting, the perturbative series for

the physical observable becomes a conformal series, all non-conformal terms should be absorbed into the effective coupling in a consistent manner;

2. New N_f -terms (corresponding to new β_0 coefficients) arise at each perturbative order, thus a new BLM scale that sums these terms consistently into the running coupling, should be introduced at each calculated perturbative order. In fact there is no reason to use a unified effective scale for the whole perturbative series as shown in Refs. [102, 103].
3. The BLM scales themselves should be a RG-improved perturbative series [26]. The length of the perturbative series for each BLM scale depends on how many new N_f -terms (or β_i -terms) we have from the higher-order calculation and to what perturbative order we have performed.

Actually the last point is not mandatory and needs clarification. In order to apply the BLM/PMC using perturbative scales, the argument of the coupling in the expansion of the BLM/PMC scale should be the physical scale of the process Q , that can be either the center-of-mass energy \sqrt{s} or also another variable such as \sqrt{t} , \sqrt{u} , M_H , ..., depending on the process. Setting the initial scale to the physical scale would greatly simplify the BLM/PMC procedure, preserving the original scale invariance of the observable and eliminating the initial scale dependence from the BLM/PMC scales. In case the BLM/PMC scales are not perturbatively calculated, as it will be shown in section 5.1, the initial scale can be treated as an arbitrary parameter.

In agreement with these indications, it is possible to achieve a scale setting method extendible iteratively to all orders, which leads to the correct coefficients $\mathcal{C}_i(\mu_{BLM}^*)$ for the final “maximally conformal” series:

$$\rho_n = \mathcal{C}_0 \alpha_s^p(\mu_{BLM}^*) + \mathcal{C}_1(\mu_{BLM}^{**}) \alpha_s^{p+1}(\mu_{BLM}^{**}) + \mathcal{C}_2(\mu_{BLM}^{***}) \alpha_s^{p+2}(\mu_{BLM}^{***}) + \dots \quad (3.12)$$

where the BLM scales μ_{BLM}^* , μ_{BLM}^{**} , ... are set by a recursive use of the RG equations in

order to cancel all the N_f terms from the series. We remark that since the coefficients $\mathcal{C}_i(\mu_{BLM}^*)$ have been obtained cancelling all β terms related to running of the coupling they actually are free from any scale and scheme dependence left. In other words the $\mathcal{C}_i(\mu_{BLM}^*) \equiv \tilde{\mathcal{C}}_i$ where the $\tilde{\mathcal{C}}_i$ are conformal coefficients not depending on the renormalization scale. Hence the BLM approach leads to an observable maximally conformal, i.e. where all the renormalization scale and scheme dependence has been confined to the effective coupling and to its renormalization scale $\alpha_s(\mu_{BLM})$.

Fundamental features of the BLM method:

- A) BLM scales at LO , are set simply by identifying the coefficient A of the N_f term;
- B) since all n_f -terms related to the running of the coupling are reabsorbed, scheme differences do not affect the results and the perturbative expansions in $\alpha_s(\mu_r^*)$ in two different schemes, e.g. $\overline{\text{MS}}$ and $\overline{\text{MS}}$, are identical. We notice that n_f -terms related to the UV finite diagrams, may arise at every order in perturbation theory. These terms might be related either to the particular kinematics of the initial state or even to finite loop diagrams arising at higher orders, thus in both cases are insensitive to the UV cutoff or to the RS and cannot be considered as β -terms. We label these terms as N_F -terms and they do not give contributions to the BLM scales;
- C) Using BLM scale setting, the perturbative expansion does not change across quark threshold, given that all vacuum-polarization effects due to a new quark are automatically absorbed into the effective coupling. This implies that in a process with fixed kinematic variables (e.g. a total cross section), we can use a naive LO/NLO $\alpha_s(\mu_r^{\text{BLM}})$ -running with the number of active flavor N_f fixed to the value determined by the BLM scale, to perform the calculation [104];
- D) The BLM method preserves all the RG properties of *existence and uniqueness, reflexivity, symmetry, and transitivity*. As shown in Refs. [105–108],

the RG invariance of the BLM leads to scheme independent transformations that relate couplings in different schemes. These are known as *commensurate scale relations* (CSRs), and it has been shown that even though the expansion coefficients under different renormalization schemes can be different, after a proper scale setting, one can determine a relation between the effective couplings leading to an invariant result for the calculated quantity. Using this approach it is also possible to extend conformal properties to renormalizable gauge theories, such as the generalized Crewther relation [109–112];

- E) The BLM approach reduces to the GM-L scheme for QED in the Abelian limit $N_c \rightarrow 0$ [32], the results are in perfect agreement;
- F) The elimination of the N_f term related with the β_0 coefficient, from the perturbative series eliminates the renormalon terms $n!\beta_0^n \alpha_s^{n+1}$ over the entire range of the accessible physical energies and not only in the low-energy domain. The convergence of the resulting series is then greatly improved.

3.5 Phenomenological comparison

Though results should be invariant with respect to the particular method used for scale-setting, at a low level of accuracy (NLO, NNLO,..) they can be different and even incorrect or unphysical. Since the scale setting methods, such as FAC, PMS and BLM/PMC, are designed from different fundamental principles, they can give strikingly different results in practical applications. In fact, as shown by Kramer and Lampe [23], the resulting PMS and FAC scales can be unphysical, Fig.3.1; this is the case of the prediction of jet production fractions in $e^+e^- \rightarrow q\bar{q}g$ annihilation, the PMS and the FAC scale grow without bound when the gluon virtuality becomes soft.

Usually, jets are defined by clustering particles in narrow cones with invariant mass less than \sqrt{ys} , where y stands for the resolution parameter and \sqrt{s} is the

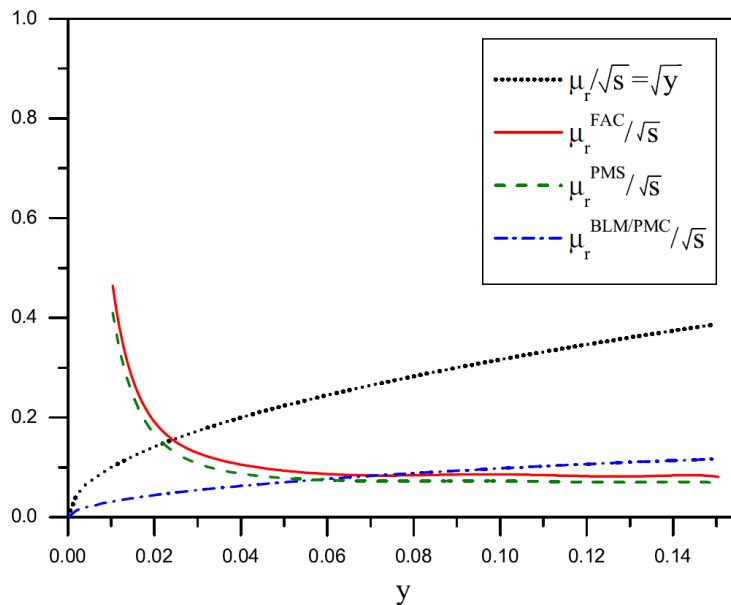


Figure 3.1: Comparison of the results for the renormalization scale μ_r/\sqrt{s} for the three-jet rate in e^+e^- annihilation, under the BLM/PMC, PMS, FAC scale settings, according to the usual \sqrt{y} , i.e. the jet virtuality, as computed by Kramer and Lampe [23]. (Figure from Ref. [21])

total center-of-mass energy. Physically, one expects the renormalization scale μ_r to reflect the invariant mass of the jet. For example, in the analogous problem in QED, the maximum virtuality of the photon jet which sets the argument of the running coupling α_s cannot be larger than \sqrt{ys} . Thus one expects μ_r to decrease as $y \rightarrow 0$. However, as shown in the Fig. 3.1, the scales chosen by the FAC and PMS methods do not reproduce this physical behavior: The predicted scales μ_r^{PMS} and μ_r^{FAC} rise at small values of the invariant mass y . This shows that the FAC and PMS cannot get the right physical behavior in this limit, since they have included also physics into the running coupling not associated with renormalization. On the other hand, the BLM/PMC scale has the correct physical behavior approaching low values, $y \rightarrow 0$, which indicates the breaking of standard pQCD [113], while in contrast, the scales chosen by PMS and FAC show no indications of non-perturbative effects.

Chapter 4

The Principle of Maximum Conformality - PMC scale setting

The Principle of Maximum Conformality (PMC) [25–29] is the principle underlying BLM and it generalizes the BLM method to all possible applications and to all orders.

Several extended versions of the BLM approach beyond the NLO have been proposed in the literature such as the dressed skeleton expansion, the large β_0 -expansion, the BLM expansion with an overall renormalization scale, the sequential BLM (seBLM), an extension to the sequential BLM (xBLM) in Refs. [102, 108, 112, 114–118]. These different extensions of the BLM are mostly partial or *ad hoc* improvements of the first LO-BLM [17] in some cases up to NNLO, in other cases using a rather effective approach, i.e. by introducing an overall effective BLM scale for the entire perturbative expansion. Results obtained with these approaches did not respect also the basic points (1-3) explained in section 3.4. Most important, these methods lead to results that are still dependent on the initial renormalization scale. The fundamental feature of the BLM is to obtain results free from scale ambiguities and thus independent of the choice of initial renormalization scale. The first aim of the BLM scale is to eliminate the renormalization scale and scheme

uncertainties; thus any extension of the BLM not respecting this basic requirement does not represent a real improvement of the standard conventional scale setting CSS method.

The reasons for the different extensions of the BLM method to higher order were mainly two: first it was not clear how to generalize this approach to all possible quantities, which translates into the question: what is the principle underlying the BLM method? And second, what is the correct procedure to identify and reabsorb the N_f -terms unambiguously order-by-order? A practical reason that makes the extension to higher orders not straightforward is the presence of UV finite corrections given by the three and four-gluon vertices of the additional N_F -terms that are unrelated to the running of α_s .

In its first formulation in Ref. [25] it was suggested to use a unique PMC scale at LO to reabsorb all β contributions related to different skeleton graphs scale by properly weighting the two contributions, such as that of the t-channel and s-channel. This approach was more oriented towards a single PMC scale that reabsorbs all β terms related to the running coupling. A multi-scale approach was later developed considering different scales arising at each order of accuracy including different β coefficients according to the perturbative expansion. We remark that the PMC method has all the (A,B,C,D,E,F) properties of the BLM procedure (Sec. 3.4) and it extends these properties to all orders eliminating the renormalization scale and scheme ambiguities. The PMC also generalizes this approach to all gauge theories. First this is crucial in order to apply the same method to all SM sectors. Secondly, in the perspective of a *grand unified theory* (GUT), only one scale setting method can be applied for consistency, and this method must agree with the GM-L scheme and with the QED results.

In order to apply the PMC is convenient to follow the flowchart shown in Fig. 4.1 and to write the observable of Eq. 3.1 with the explicit contributions of the n_f terms in the coefficients calculated at each order of accuracy:

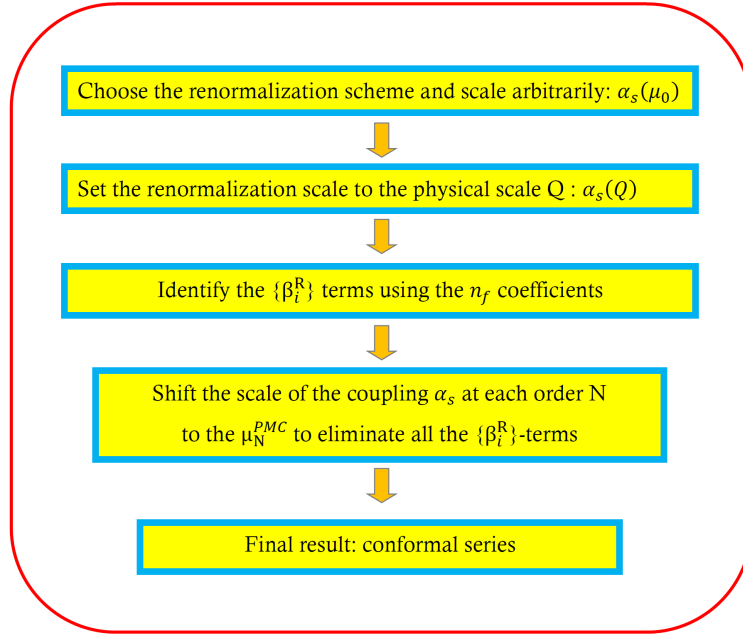


Figure 4.1: Flowchart for the PMC procedure.

$$\rho(Q) = \sum_{i=1}^n \left(\sum_{j=0}^{i-1} c_{i,j}(\mu_r, Q) n_f^j \right) \alpha_s^{p+i-1}(\mu_r), \quad (4.1)$$

where Q represents the kinematic scale or the physical scale of the measured observable and p is the power of α_s associated with the tree-level terms. In general, this procedure is always possible either for analytic or numerical (e.g. MonteCarlo) calculations, given that both strategies keep track of terms related to different color factors. The core of the PMC method, as was for BLM, is that all N_f terms related to the β -function arising in a perturbative calculation must be summed, by proper definition of the renormalization scale μ_{PMC} , into the effective coupling α_s by recursive use of the RGE. Essentially the difference between the two procedures is that while in BLM the scales are set iteratively order by order to remove all n_f terms, in PMC the n_f terms are written first as β terms and then reabsorbed into the effective coupling. The two procedures are related by the *correspondence principle* [26].

4.1 The multi-scale Principle of Maximum Conformality: PMCm

The PMCm method is based on a multi-scale application of the PMC. We show in this section how to implement this method at any order of accuracy. First, as shown in the flowchart in Fig. 4.1, for the pQCD approximant (4.1), it is convenient to transform the $\{n_f\}$ series at each order into the $\{\beta_i\}$ series. The QCD degeneracy relations [119] ensure the realizability of such transformation. For example, Eq. 4.1 can be rewritten as [28, 29]

$$\begin{aligned}
\rho(Q) &= r_{1,0}a_s(\mu_r) + \left(r_{2,0} + \beta_0 r_{2,1}\right)a_s^2(\mu_r) \\
&+ \left(r_{3,0} + \beta_1 r_{2,1} + 2\beta_0 r_{3,1} + \beta_0^2 r_{3,2}\right)a_s^3(\mu_r) \\
&+ \left(r_{4,0} + \beta_2 r_{2,1} + 2\beta_1 r_{3,1} + \frac{5}{2}\beta_1\beta_0 r_{3,2} \right. \\
&\left. + 3\beta_0 r_{4,1} + 3\beta_0^2 r_{4,2} + \beta_0^3 r_{4,3}\right)a_s^4(\mu_r) + \dots, \tag{4.2}
\end{aligned}$$

where $r_{i,j}$ can be derived from $c_{i,j}$; $r_{i,0}$ are conformal coefficients, and $r_{i,j}$ ($j \neq 0$) are nonconformal. For definiteness and without loss of generality, we have set $p = 1$ and $n = 4$ for illustrating the PMC procedures. Different types of $\{\beta_i\}$ -terms can be absorbed into α_s in an order-by-order manner by using the RGE, which leads to distinct PMC scales at each order:

$$\begin{aligned}
a_s^k(Q_k) &\leftarrow a_s^k(\mu_r) \left\{ 1 + k\beta_0 \frac{r_{k+1,1}}{r_{k,0}} a_s(\mu_r) \right. \\
&+ k \left(\beta_1 \frac{r_{k+1,1}}{r_{k,0}} + \frac{k+1}{2} \beta_0^2 \frac{r_{k+2,2}}{r_{k,0}} \right) a_s^2(\mu_r) \\
&+ k \left(\beta_2 \frac{r_{k+1,1}}{r_{k,0}} + \frac{2k+3}{2} \beta_0 \beta_1 \frac{r_{k+2,2}}{r_{k,0}} \right. \\
&\left. + \frac{(k+1)(k+2)}{3!} \beta_0^3 \frac{r_{k+3,3}}{r_{k,0}} \right) a_s^3(\mu_r) + \dots \left. \right\}. \tag{4.3}
\end{aligned}$$

The coefficients $r_{i,j}$ are generally functions of μ_r , which can be redefined as

$$r_{i,j} = \sum_{k=0}^j C_j^k \hat{r}_{i-k,j-k} \ln^k(\mu_r^2/Q^2), \tag{4.4}$$

where the reduced coefficients $\hat{r}_{i,j} = r_{i,j}|_{\mu_r=Q}$ (specifically, we have $\hat{r}_{i,0} = r_{i,0}$), and the combinatorial coefficients $C_j^k = j!/(k!(j-k)!)$. As discussed in section 3.4, we set the renormalization scale μ_r to the physical scale of the process Q :

$$\begin{aligned} \ln \frac{Q^2}{Q_1^2} &= \frac{\hat{r}_{2,1}}{\hat{r}_{1,0}} + \beta_0 \left(\frac{\hat{r}_{1,0}\hat{r}_{3,2} - \hat{r}_{2,1}^2}{\hat{r}_{1,0}^2} \right) a_s(Q) \\ &\quad + \left[\beta_1 \left(\frac{3\hat{r}_{3,2}}{2r_{1,0}} - \frac{3\hat{r}_{2,1}^2}{2\hat{r}_{1,0}^2} \right) + \beta_0^2 \left(\frac{\hat{r}_{4,3}}{\hat{r}_{1,0}} - \frac{2\hat{r}_{3,2}\hat{r}_{2,1}}{\hat{r}_{1,0}^2} + \frac{\hat{r}_{2,1}^3}{\hat{r}_{1,0}^3} \right) \right] a_s^2(Q) + \dots, \end{aligned} \quad (4.5)$$

$$\ln \frac{Q^2}{Q_2^2} = \frac{\hat{r}_{3,1}}{\hat{r}_{2,0}} + 3\beta_0 \frac{\hat{r}_{2,0}\hat{r}_{4,2} - \hat{r}_{3,1}^2}{2\hat{r}_{2,0}^2} a_s(Q) + \dots, \quad (4.6)$$

$$\ln \frac{Q^2}{Q_3^2} = \frac{\hat{r}_{4,1}}{\hat{r}_{3,0}} + \dots. \quad (4.7)$$

Note that the PMC scales are of a perturbative nature, which is also a kind of resummation and we need to know more loop terms to achieve more accurate predictions. The PMC resums all the known same type of $\{\beta_i\}$ -terms to form precise PMC scales for each order. Thus, the precision of the PMC scale for the high-order terms decreases at the higher-and-higher orders due to the less known $\{\beta_i\}$ -terms in those higher-order terms. For example, Q_1 is determined up to next-to-next-to-leading log (N²LL)-accuracy, Q_2 is determined up to NLL-accuracy and Q_3 is determined at the LL-accuracy. Thus the PMC scales at higher-orders are of less accuracy due to more of its perturbative terms being unknown. This perturbative property of the PMC scale causes the *first kind of residual scale dependence*.

After fixing the magnitude of $a_s(Q_k)$, we achieve a conformal series

$$\rho(Q) = \sum_{i=1}^4 \hat{r}_{i,0} a_s^i(Q_i) + \dots. \quad (4.8)$$

The PMC scale for the highest-order term, e.g. Q_4 for the present case, is unfixed, since there is no $\{\beta_i\}$ -terms to determine its magnitude. This renders the last perturbative term unfixed and causes the *second kind of residual scale dependence*. Usually, the PMCM suggests setting Q_4 as the last determined scale Q_3 , which ensures the scheme independence of the prediction due to commensurate scale relations among the predictions under different renormalization schemes [108, 120]. The

pQCD series (4.8) is renormalization scheme and scale independent, and becomes more convergent due to the elimination of the β terms including those related to the renormalon divergence. Thus a more accurate pQCD prediction can be achieved by applying the PMCm. Two residual scale dependences are due to perturbative nature of either the pQCD approximant or the PMC scale, which is in principle different from the conventional arbitrary scale dependence. In practice, we have found that those two residual scale dependences are quite small even at low orders. This is due to a generally faster pQCD convergence after applying the PMCm. Some examples can be found in Ref. [121].

4.2 The single-scale Principle of Maximum Conformality: PMCs

In some cases, the perturbative series might have a weak convergence and the PMC scales might retain a comparatively larger residual scale dependence. In order to overcome this a single scale approach has been proposed, namely the PMCs, in order to suppress the residual scale dependence by directly fixing a single effective α_s . Following the standard procedures of PMCs [122], the pQCD approximant (4.2) changes to the following conformal series,

$$\rho(Q) = \sum_{i=1}^4 \hat{r}_{i,0} a_s^i(Q_*) + \dots \quad (4.9)$$

As in the previous section, we have set $p = 1$ and $n = 4$ for illustrating the procedure. The PMC scale Q_* can be determined by requiring all the nonconformal terms vanish, which can be fixed up to N²LL-accuracy for $p = 1$ and $n = 4$, i.e. $\ln Q_*^2/Q^2$ can be expanded as a power series over $a_s(Q)$,

$$\ln \frac{Q_*^2}{Q^2} = T_0 + T_1 a_s(Q) + T_2 a_s^2(Q) + \dots, \quad (4.10)$$

where the coefficients T_i ($i = 0, 1, 2$) are

$$T_0 = -\frac{\hat{r}_{2,1}}{\hat{r}_{1,0}}, \quad (4.11)$$

$$T_1 = \frac{\beta_0(\hat{r}_{2,1}^2 - \hat{r}_{1,0}\hat{r}_{3,2})}{\hat{r}_{1,0}^2} + \frac{2(\hat{r}_{2,0}\hat{r}_{2,1} - \hat{r}_{1,0}\hat{r}_{3,1})}{\hat{r}_{1,0}^2}, \quad (4.12)$$

and

$$\begin{aligned} T_2 &= \frac{3\beta_1(\hat{r}_{2,1}^2 - \hat{r}_{1,0}\hat{r}_{3,2})}{2\hat{r}_{1,0}^2} \\ &+ \frac{4(\hat{r}_{1,0}\hat{r}_{2,0}\hat{r}_{3,1} - \hat{r}_{2,0}^2\hat{r}_{2,1}) + 3(\hat{r}_{1,0}\hat{r}_{2,1}\hat{r}_{3,0} - \hat{r}_{1,0}^2\hat{r}_{4,1})}{\hat{r}_{1,0}^3} \\ &+ \frac{\beta_0(4\hat{r}_{2,1}\hat{r}_{3,1}\hat{r}_{1,0} - 3\hat{r}_{4,2}\hat{r}_{1,0}^2 + 2\hat{r}_{2,0}\hat{r}_{3,2}\hat{r}_{1,0} - 3\hat{r}_{2,0}\hat{r}_{2,1}^2)}{\hat{r}_{1,0}^3} \\ &+ \frac{\beta_0^2(2\hat{r}_{1,0}\hat{r}_{3,2}\hat{r}_{2,1} - \hat{r}_{2,1}^3 - \hat{r}_{1,0}^2\hat{r}_{4,3})}{\hat{r}_{1,0}^3}. \end{aligned} \quad (4.13)$$

Eq. 4.10 shows that the PMC scale Q_* is also a power series over α_s , which resums all the known $\{\beta_i\}$ -terms and is explicitly independent of μ_r at any fixed order, but depends only on the physical scale Q . It represents the correct momentum flow of the process, and determines an overall effective α_s value. Together with the μ_r -independent conformal coefficients, the resultant PMC pQCD series is scheme and scale independent [123]. By using a single PMC scale determined with the highest accuracy from the known pQCD series, both the *first* and the *second kind of residual scale dependence* are suppressed.

Chapter 5

Infinite-Order Scale-Setting using the Principle of Maximum Conformality: PMC_∞

We introduce in this chapter a parametrization of the observables that stems directly from the analysis of the perturbative QCD corrections and which reveals interesting properties like scale invariance independently of the process or of the kinematics. We point out that this parametrization can be an intrinsic general property of gauge theories and we define this property as *intrinsic conformality* (iCF¹). We also show how this property directly indicates the correct renormalization scale μ_R at each order of calculation and we define this new method PMC_∞ : *Infinite-Order Scale-Setting using the Principle of Maximum Conformality*. We apply the iCF property and the PMC_∞ to the case of the thrust and C-parameter distributions in $e^+e^- \rightarrow 3jets$ and we show the results.

¹Here the conformality has to be understood as RG invariance only.

5.1 Intrinsic conformality (iCF)

In order to introduce intrinsic conformality (iCF), we consider the case of a normalized IR-safe single-variable distribution and write the explicit sum of pQCD contributions calculated up to NNLO at the initial renormalization scale μ_0 :

$$\frac{1}{\sigma_0} \frac{Od\sigma(\mu_0)}{dO} = \left\{ \frac{\alpha_s(\mu_0)}{2\pi} \frac{OdA_O(\mu_0)}{dO} + \left(\frac{\alpha_s(\mu_0)}{2\pi} \right)^2 \frac{OdB_O(\mu_0)}{dO} + \left(\frac{\alpha_s(\mu_0)}{2\pi} \right)^3 \frac{OdC_O(\mu_0)}{dO} + \mathcal{O}(\alpha_s^4) \right\}, \quad (5.1)$$

where the σ_0 is tree-level hadronic cross section, the A_O, B_O, C_O are respectively the LO, NLO and NNLO coefficients, O is the selected non-integrated variable. For the sake of simplicity we will refer to the perturbatively calculated differential coefficients as *implicit coefficients* and we drop the derivative symbol, i.e.

$$\begin{aligned} A_O(\mu_0) &\equiv \frac{OdA_O(\mu_0)}{dO}, \quad B_O(\mu_0) \equiv \frac{OdB_O(\mu_0)}{dO}, \\ C_O(\mu_0) &\equiv \frac{OdC_O(\mu_0)}{dO}. \end{aligned} \quad (5.2)$$

We define here the *intrinsic conformality* as the property of a renormalizable SU(N)/U(1) gauge theory, like QCD, which yields a particular structure of the perturbative corrections that can be made explicit representing the perturbative coefficients using the following parametrization²:

$$\begin{aligned} A_O(\mu_0) &= A_{Conf}, \\ B_O(\mu_0) &= B_{Conf} + \frac{1}{2}\beta_0 \ln \left(\frac{\mu_0^2}{\mu_1^2} \right) A_{Conf}, \\ C_O(\mu_0) &= C_{Conf} + \beta_0 \ln \left(\frac{\mu_0^2}{\mu_{II}^2} \right) B_{Conf} + \\ &\quad + \frac{1}{4} \left[\beta_1 + \beta_0^2 \ln \left(\frac{\mu_0^2}{\mu_1^2} \right) \right] \ln \left(\frac{\mu_0^2}{\mu_1^2} \right) A_{Conf}, \end{aligned} \quad (5.3)$$

where the $A_{Conf}, B_{Conf}, C_{Conf}$ are the scale invariant *Conformal Coefficients* (i.e. the coefficients of each perturbative order not depending on the scale μ_0) while we

²We are neglecting here other running parameters such as the mass terms.

define the μ_N as *Intrinsic Conformal Scales* and β_0, β_1 are the first two coefficients of the β -function. We recall that the implicit coefficients are defined at the scale μ_0 and that they change according to the standard RG equations under a change of the renormalization scale according to :

$$\begin{aligned}
A_O(\mu_R) &= A_O(\mu_0), \\
B_O(\mu_R) &= B_O(\mu_0) + \frac{1}{2}\beta_0 \ln\left(\frac{\mu_R^2}{\mu_0^2}\right) A_O(\mu_0), \\
C_O(\mu_R) &= C_O(\mu_0) + \beta_0 \ln\left(\frac{\mu_R^2}{\mu_0^2}\right) B_O(\mu_0) + \\
&\quad + \frac{1}{4} \left[\beta_1 + \beta_0^2 \ln\left(\frac{\mu_R^2}{\mu_0^2}\right) \right] \ln\left(\frac{\mu_R^2}{\mu_0^2}\right) A_O(\mu_0)
\end{aligned} \tag{5.4}$$

It can be shown that the form of Eq. 5.3 is scale invariant and it is preserved under a change of the renormalization scale from μ_0 to μ_R by standard RG equations Eq. 5.4, i.e.:

$$\begin{aligned}
A_O(\mu_R) &= A_{Conf}, \\
B_O(\mu_R) &= B_{Conf} + \frac{1}{2}\beta_0 \ln\left(\frac{\mu_R^2}{\mu_I^2}\right) A_{Conf}, \\
C_O(\mu_R) &= C_{Conf} + \beta_0 \ln\left(\frac{\mu_R^2}{\mu_{II}^2}\right) B_{Conf} + \\
&\quad + \frac{1}{4} \left[\beta_1 + \beta_0^2 \ln\left(\frac{\mu_R^2}{\mu_I^2}\right) \right] \ln\left(\frac{\mu_R^2}{\mu_I^2}\right) A_{Conf}
\end{aligned} \tag{5.5}$$

We note that the form of Eq. 5.3 is invariant and that the initial scale dependence is exactly removed by μ_R . Extending this parametrization to all orders we achieve a scale invariant quantity: *the iCF-parametrization is a sufficient condition in order to obtain a scale invariant observable.*

In order to show this property we collect together the terms identified by the same *conformal coefficient*, we name each set as a *conformal subset* and we extend the property to order n :

$$\begin{aligned}
\sigma_{\text{I}} &= \left\{ \left(\frac{\alpha_s(\mu_0)}{2\pi} \right) + \frac{1}{2} \beta_0 \ln \left(\frac{\mu_0^2}{\mu_{\text{I}}^2} \right) \left(\frac{\alpha_s(\mu_0)}{2\pi} \right)^2 \right. \\
&\quad \left. + \frac{1}{4} \left[\beta_1 + \beta_0^2 \ln \left(\frac{\mu_0^2}{\mu_{\text{I}}^2} \right) \right] \ln \left(\frac{\mu_0^2}{\mu_{\text{I}}^2} \right) \left(\frac{\alpha_s(\mu_0)}{2\pi} \right)^3 + \dots \right\} A_{\text{Conf}} \\
\sigma_{\text{II}} &= \left\{ \left(\frac{\alpha_s(\mu_0)}{2\pi} \right)^2 + \beta_0 \ln \left(\frac{\mu_0^2}{\mu_{\text{II}}^2} \right) \left(\frac{\alpha_s(\mu_0)}{2\pi} \right)^3 + \dots \right\} B_{\text{Conf}} \\
\sigma_{\text{III}} &= \left\{ \left(\frac{\alpha_s(\mu_0)}{2\pi} \right)^3 + \dots \right\} C_{\text{Conf}}, \\
&\vdots \\
\sigma_n &= \left\{ \left(\frac{\alpha_s(\mu_0)}{2\pi} \right)^n \right\} \mathcal{L}_{n\text{Conf}}, \tag{5.6}
\end{aligned}$$

in each subset we have only one intrinsic scale and only one conformal coefficient and the subsets are disjoint; thus no mixing terms among the scales or the coefficients are introduced in this parametrization. Moreover, the structure of the subsets remains invariant under a global change of the renormalization scale, as shown from Eq. 5.5. The structure of each conformal set $\sigma_{\text{I}}, \sigma_{\text{II}}, \sigma_{\text{III}}, \dots$ and consequently the iCF are preserved also if we fix a different renormalization scale for each conformal subset, i.e.

$$\left(\mu^2 \frac{\partial}{\partial \mu^2} + \beta(\alpha_s) \frac{\partial}{\partial \alpha_s} \right) \sigma_n = 0. \tag{5.7}$$

We define here this property of Eq. 5.6 of separating an observable in the union of ordered scale invariant disjoint subsets $\sigma_{\text{I}}, \sigma_{\text{II}}, \sigma_{\text{III}}, \dots$ an *ordered scale invariance*.

In order to extend the iCF to all orders, we perform the $n \rightarrow \infty$ limit using the following strategy: we first perform a partial limit $J_{/n} \rightarrow \infty$ including the higher order corrections relative only to those $\beta_0, \beta_1, \beta_2, \dots, \beta_{n-2}$ terms that have been determined already at order n for each subset, and then we perform the complementary \bar{n} limit, which consists in including all the remaining higher order terms. For the $J_{/n}$ limit we have:

$$\begin{aligned}
\lim_{J/n \rightarrow \infty} \sigma_{\text{I}} &\rightarrow \left(\frac{\alpha_s(\mu_{\text{I}})|_{n-2}}{2\pi} \right) A_{\text{Conf}} \\
\lim_{J/n \rightarrow \infty} \sigma_{\text{II}} &\rightarrow \left(\frac{\alpha_s(\mu_{\text{II}})|_{n-3}}{2\pi} \right)^2 B_{\text{Conf}} \\
\lim_{J/n \rightarrow \infty} \sigma_{\text{III}} &\rightarrow \left(\frac{\alpha_s(\mu_{\text{III}})|_{n-4}}{2\pi} \right)^3 C_{\text{Conf}} \\
&\vdots \\
\lim_{J/n \rightarrow \infty} \sigma_n &\equiv \left(\frac{\alpha_s(\mu_0)}{2\pi} \right)^n \mathcal{L}_{n\text{Conf}}
\end{aligned} \tag{5.8}$$

where $\alpha_s(\mu_{\text{I}})|_{n-2}$ is the coupling calculated up to β_{n-2} at the intrinsic scale μ_{I} . Given the particular ordering of the powers of the coupling, in each conformal subset we have the coefficients of the $\beta_0, \dots, \beta_{n-k-1}$ terms, where k is the order of the conformal subset and the n is the order of the highest subset with no β -terms. We note that the limit of each conformal subset is finite and scale invariant up to σ_{n-1} . The remaining scale dependence is confined in the coupling of the n^{th} term. Any combination of the $\sigma_{\text{I}}, \dots, \sigma_{n-1}$ subsets is finite and scale invariant. We can now extend the iCF to all orders performing the \bar{n} limit. In this limit we include all the remaining higher order corrections. For the calculated conformal subsets this leads to define the coupling at the same scales but including all the missing β terms. Thus each conformal subset remains scale invariant. We point out that we are not making any assumption on the convergence of the series for this limit. Thus, we have:

$$\begin{aligned}
\lim_{\bar{n} \rightarrow \infty} \sigma_{\text{I}} &\rightarrow \left(\frac{\alpha_s(\mu_{\text{I}})}{2\pi} \right) A_{\text{Conf}} \\
\lim_{\bar{n} \rightarrow \infty} \sigma_{\text{II}} &\rightarrow \left(\frac{\alpha_s(\mu_{\text{II}})}{2\pi} \right)^2 B_{\text{Conf}} \\
\lim_{\bar{n} \rightarrow \infty} \sigma_{\text{III}} &\rightarrow \left(\frac{\alpha_s(\mu_{\text{III}})}{2\pi} \right)^3 C_{\text{Conf}} \\
&\vdots \\
\lim_{\bar{n} \rightarrow \infty} \sigma_n &\equiv \lim_{n \rightarrow \infty} \left(\frac{\alpha_s(\mu_0)}{2\pi} \right)^n \mathcal{L}_{n\text{Conf}} \rightarrow \text{Conformal Limit}
\end{aligned}$$

(5.9)

where here now $\alpha_s(\mu_I)$ is the complete coupling determined at the same scale μ_I . Eq. 5.9 shows that the whole renormalization scale dependence has been completely removed. In fact, neither the intrinsic scales μ_N nor the conformal coefficients $A_{Conf}, B_{Conf}, C_{Conf}, \dots, \mathcal{L}_{nConf}, \dots$ depend on the particular choice of the initial scale. The only term with a residual μ_0 dependence is the n-term, but this dependence cancels in the limit $n \rightarrow \infty$. The scale dependence is totally confined to the coupling $\alpha_s(\mu_0)$ and its behavior does not depend on the particular choice of any scale μ_0 in the perturbative region, i.e. $\lim_{n \rightarrow \infty} \alpha_s(\mu_0)^n \sim a^n$ with $a < 1$. Hence the limit of $\lim_{n \rightarrow \infty} \sigma_n$ depends only on the properties of the theory and not on the scale of the coupling in the perturbative regime. The proof given here shows that the iCF is *sufficient* to have a scale invariant observable and it does not depend on the particular convergence of the series. In order to show the *necessary* condition we separate the two cases of a convergent series and an asymptotic expansion. For the first case the *necessary* condition stems directly from the uniqueness of the iCF form, since given a finite limit and the scale invariance any other parametrization can be reduced to the iCF by means of appropriate transformations in agreement with the RG equations. For the second case, we have that an asymptotic expansion though not convergent, can be truncated at a certain order n , which is the case of Eq. 5.6. Given the particular structure of the iCF we can perform the first partial limit $J_{/n}$ and we would achieve a finite and scale invariant prediction, $\sigma_{N-1} = \sum_{i=1}^{n-1} \sigma_i$, for a truncated asymptotic expansion, as shown in Eq. 5.8. Given the truncation of the series in the region of maximum of convergence the n-th term would be reduced to the lowest value and so the scale dependence of the observable would reach its minimum. Given the finite and scale invariant limit σ_{N-1} we conclude that the iCF is unique and thus *necessary* for an *ordered* scale invariant truncated asymptotic expansion up to the n^{th} order. We point out that in general the iCF form is the most general and irreducible parametrization which leads to the scale invariance,

other parametrization are forbidden since if we introduce more scales ³ into the logarithms of one subset we would spoil the invariance under the RG transformation and we could not achieve Eq. 5.5, while on the other hand no scale dependence can be introduced into the intrinsic scales since it would remain in the observable already in the first partial limit J/n and it could not be eliminated. The conformal coefficients are conformal by definition at each order, thus they do not depend on the renormalization scale and they do not have a perturbative expansion. Hence *the iCF is a necessary and sufficient condition for scale invariance.*

5.2 Comments on the iCF and the ordered scale invariance

The iCF-parametrization can stem either from an inner property of the theory, the iCF, or from direct parametrization of the scale-invariant observable. In both cases the iCF-parametrization makes the scale dependence of the observable explicit and it exactly preserves the scale invariance. The iCF parametrization is invariant with respect to the choice of initial scale μ_0 , this implies that the same calculation performed choosing different arbitrary initial scales, $\mu_0; \mu'_0$ leads to the same result in the limit J/n , a limit that is scale and scheme independent. The iCF is also strongly motivated by the renormalizability of QCD and by the uniqueness of the β function in a given scheme, i.e. two different β_i, β'_i do not occur in a perturbative calculation at any order in one RS and the UV divergencies are cancelled by redefinition of the same parameters at lowest and higher orders. We remark that the conservation of the iCF form in one observable is strongly related to the validity of the RG transformations, thus we expect the iCF to be well preserved in the deep Euclidean region.

³Here we refer to the form of Eq. 5.3. In principle it is possible to write other parametrizations preserving the scale invariance, but these can be reduced to the iCF by means of appropriate transformations in agreement with the RG equations.

Once we have defined an observable in the iCF-form, we have not only the scale invariance of the entire observable, but also the *ordered scale invariance* (i.e. the scale invariance of each subset σ_n or σ_{N-1}). The latter property is crucial in order to obtain scale invariant observables independently from the particular kinematic region and independently from the starting order of the observable or the order of the truncation of the series. Since in general, a theory is blind with respect to the particular observable/process that we might investigate, the theory should preserve the *ordered scale invariance* in order to define always scale invariant observables. Hence if the iCF is an inner property of the theory, it leads to implicit coefficients that are neither independent nor conformal. This is made explicit in Eq. 5.3, but it is hidden in the perturbative calculations in the case of the implicit coefficients. For instance, the presence of the iCF clearly reveals itself when a particular kinematic region is approached and the A_O becomes null. This would cause a breaking of the scale invariance since a residual initial scale dependence would remain in the observable in the higher order coefficients. The presence of the iCF solves this issue by leading to the correct redefinition of all the coefficients at each order preserving the correct scale invariance exactly. Thus, in the case of a scale-invariant observable O , defined according to the implicit form (Eq. 5.1), by the coefficients $\{A_O, B_O, C_O, \dots, O_O, \dots\}$, it cannot simply undergo the change $\rightarrow \{0, B_O, C_O, \dots, O_O, \dots\}$, since this would break the scale invariance. In order to preserve the scale invariance, we must redefine the coefficients $\{\tilde{A}_O = 0, \tilde{B}_O, \tilde{C}_O, \dots, \tilde{O}_O, \dots\}$ cancelling out all the initial scale dependence originating from the LO coefficient A_O at all orders. This is equivalent to subtracting out a whole invariant conformal subset σ_I related to the coefficient A_{Conf} from the scale invariant observable O . This mechanism is clear in the case of the explicit form of the iCF, Eq. 5.3, where if $A_{Conf} = 0$ then the whole conformal subset is null and the scale invariance is preserved. We underline that the conformal coefficients can acquire all possible values without breaking the scale invariance, they contain the essential information on the physics of the process, while all the correlation factors can be reabsorbed into the renormalization scales as shown by

the PMC method [26, 26–29]. Hence if a theory has the property of *ordered scale invariance*, it preserves exactly the scale invariance of observables independently of the process, the kinematics and the starting order of the observable. We underline that if a theory has the intrinsic conformality all the renormalized quantities, such as cross sections, can be parametrized with the iCF-form. This property should be preserved by the renormalization scheme or by the definition of IR safe quantities and it should be preserved also in observables defined in effective theories. The iCF shows that point (3) of the BLM/PMC approach (Section 3.4) can be improved by eliminating the perturbative expansion of the BLM/PMC scales, leading to a scale and scheme invariant result. Though we remark that the perturbative corrections in the BLM or PMCm scales are suppressed in the perturbative region.

5.3 The PMC_∞

We introduce here a new method to eliminate the scale-setting ambiguity in single variable scale invariant distributions, which we call PMC_∞ . This method is based on the original PMC principle and agrees with all the different PMC formulations for the PMC-scales at the lowest order. Essentially the core of the PMC_∞ is the same for all the BLM-PMC prescriptions, i.e. the effective running coupling value and hence its renormalization scale at each order is determined by the β_0 -term of the next higher order, or equivalently by the *intrinsic conformal scale* μ_N . The PMC_∞ preserves the iCF and thus the scale and scheme invariance, absorbing an infinite set of β -terms to all orders. This method differs from the other PMC prescriptions since, due to the presence of the intrinsic conformality, no perturbative correction in α_s needs to be introduced at higher orders in the PMC-scales. Given that all the β -terms of a single conformal subset are included in the renormalization scale already with the definition at lowest order, no initial scale or scheme dependence are left due to the unknown β -terms in each subset. The PMC_∞ -scale of each subset can be unambiguously determined by β_0 -term of each order, we underline that all

logarithms of each subset have the same argument and all the differences arising at higher orders have to be included only in the conformal coefficients. Reabsorbing all the β -terms into the scale also the $n!\beta_0^n\alpha_s^n$ terms (related to renormalons [84]) are eliminated, thus the precision is improved and the perturbative QCD predictions can be extended to a wider range of values. The initial scale dependence is totally confined in the unknown PMC_∞ scale of the last order of accuracy (i.e. up to NNLO case in the $\alpha_s(\mu_0)^3$). Thus if we fix the renormalization scale independently to the proper intrinsic scale for each subset μ_N , we end up with a perturbative sum of totally conformal contributions up to the order of accuracy:

$$\frac{1}{\sigma_0} \frac{Od\sigma(\mu_I, \mu_{II}, \mu_{III})}{dO} = \left\{ \frac{\alpha_s(\mu_I)}{2\pi} \frac{OdA_{Conf}}{dO} + \left(\frac{\alpha_s(\mu_{II})}{2\pi} \right)^2 \frac{OdB_{Conf}}{dO} + \left(\frac{\alpha_s(\mu_{III})}{2\pi} \right)^3 \frac{OdC_{Conf}}{dO} \right\} + \mathcal{O}(\alpha_s^4), \quad (5.10)$$

at this order, the last scale is set to the physical scale Q , i.e. $\mu_{III} = \mu_0 = Q$.

5.4 iCF coefficients and scales: a new “How-To” method

We describe here how all the coefficients of Eq. 5.3 can be identified from either a numerical or analytical perturbative calculation. This method applies in general to any perturbative calculation once results for the different color factors are kept separate, however we refer to the particular case of the NNLO thrust distribution results calculated in Refs. [124, 125] for the purpose. Since the leading order is already (A_{Conf}) void of β -terms we start with NLO coefficients. A general numerical/analytical calculation keeps tracks of all the color factors and the respective coefficients:

$$B_O(N_f) = C_F \left[C_A B_O^{N_c} + C_F B_O^{C_F} + T_F N_f B_O^{N_f} \right] \quad (5.11)$$

where $C_F = \frac{(N_c^2-1)}{2N_c}$, $C_A = N_c$ and $T_F = 1/2$. The dependence on N_f is made explicit here for sake of clarity. We can determine the conformal coefficient B_{Conf} of the NLO order straightforwardly, by fixing the number of flavors N_f in order to kill the β_0 term:

$$\begin{aligned} B_{Conf} &= B_O \left(N_f \equiv \frac{33}{2} \right), \\ B_{\beta_0} \equiv \log \frac{\mu_0^2}{\mu_1^2} &= 2 \frac{B_O - B_{Conf}}{\beta_0 A_{Conf}} \end{aligned} \quad (5.12)$$

we would achieve the same results in the usual PMC way, i.e. identifying the N_f coefficient with the β_0 term and then determining the conformal coefficient. Both methods are consistent and results for the intrinsic scales and the coefficients are in perfect agreement. At the NNLO a general coefficient is composed of the contribution of six different color factors:

$$\begin{aligned} C_O(N_f) &= \frac{C_F}{4} \left\{ N_c^2 C_O^{N_c^2} + C_O^{N_c^0} + \frac{1}{N_c^2} C_O^{\frac{1}{N_c^2}} \right. \\ &\quad \left. + N_f N_c \cdot C_O^{N_f N_c} + \frac{N_f}{N_c} C_O^{N_f/N_c} + N_f^2 C_O^{N_f^2} \right\}. \end{aligned} \quad (5.13)$$

In order to identify all the terms of Eq. 5.3 we notice first that the coefficients of the terms β_0^2 and β_1 are already given by the NLO coefficient B_{β_0} , thus we need to determine only the β_0 and the conformal C_{Conf} terms. In order to determine the latter coefficients we use the same procedure we used for the NLO; i.e. we set the number of flavors $N_f \equiv 33/2$ in order to drop off all the β_0 terms. We have then:

$$\begin{aligned} C_{Conf} &= C_O \left(N_f \equiv \frac{33}{2} \right) - \frac{1}{4} \bar{\beta}_1 B_{\beta_0} A_{Conf}, \\ C_{\beta_0} \equiv \log \left(\frac{\mu_0^2}{\mu_{II}^2} \right) &= \frac{1}{\beta_0 B_{Conf}} \left(C_O - C_{Conf} \right. \\ &\quad \left. - \frac{1}{4} \beta_0^2 B_{\beta_0}^2 A_{Conf} - \frac{1}{4} \beta_1 B_{\beta_0} A_{Conf} \right), \end{aligned} \quad (5.14)$$

with $\bar{\beta}_1 \equiv \beta_1(N_f = 33/2) = -107$. This procedure can be extended to every order and one may decide whether to cancel β_0 , β_1 or β_2 by fixing the appropriate

number of flavors. The results can be compared leading to determine exactly all the coefficients. We point out that extending the intrinsic conformality to all orders we can predict at this stage the coefficients of all the color factors of the higher orders related to the β -terms except those related to the higher order conformal coefficients and β_0 -terms (e.g. at NNNLO the D_{Conf} and D_{β_0}). The β -terms are coefficients that stem from UV-divergent diagrams connected with the running of the coupling constant and not from UV-finite diagrams. UV-finite N_F terms may arise but would not contribute to the β -terms. These terms can be easily identified by the kinematic constraint at lowest order or by checking deviations of the n_f coefficients from the iCF form. In fact, only the N_f terms coming from UV-divergent diagrams, depending dynamically on the virtuality of the underlying quark and gluon subprocesses have to be considered as β -terms and they would determine the intrinsic conformal scales. In general, each μ_N is an independent function of the physical scale of the process \sqrt{s} (or $\sqrt{t}, \sqrt{u}, \dots$), of the selected variable O and it varies with the number of colors N_c mainly due to ggg and $gggg$ vertices. The latter terms arise at higher orders only in a non-Abelian theory but they are not expected to spoil the iCF-form. We underline that iCF applies to scale-invariant single-variable distributions, in case one is interested in the renormalization of a particular diagram, e.g. the ggg vertex, contributions from different β -terms should be singled out in order to identify the respective intrinsic conformal scale consistently with the renormalization of the non-Abelian ggg vertex, as shown in [126].

5.5 PMC_∞ results for thrust and C-parameter

The thrust distribution and the event shape variables are a fundamental tool in order to probe the geometrical structure of a given process at colliders. Being observables that are exclusive enough with respect to the final state, they allow for a deeper geometrical analysis of the process and they are also particularly suitable for the measurement of the strong coupling α_s [127].

Given the high precision data collected at LEP and SLAC [128–132], refined calculations are crucial in order to extract information to the highest possible precision. Though extensive studies on these observables have been released during the last decades including higher order corrections from next-to-leading order (NLO) calculations [133–138] to the next-to-next-to-leading order (NNLO) [124, 125, 139–141] and including resummation of the large logarithms [95, 96], the theoretical predictions are still affected by significant theoretical uncertainties that are related to large renormalization scale ambiguities.

In the particular case of the three-jet event-shape distributions the conventional practice of CSS leads to results that do not match the experimental data and the extracted values of α_s deviate from the world average [34].

The thrust (T) and C-parameter (C) are defined as

$$T = \max_{\vec{n}} \left(\frac{\sum_i |\vec{p}_i \cdot \vec{n}|}{\sum_i |\vec{p}_i|} \right), \quad (5.15)$$

$$C = \frac{3 \sum_{i,j} |\vec{p}_i| |\vec{p}_j| \sin^2 \theta_{ij}}{2 (\sum_i |\vec{p}_i|)^2}, \quad (5.16)$$

where the sum runs over all particles in the hadronic final state, and \vec{p}_i denotes the three-momentum of particle i . The unit vector \vec{n} is varied to maximize thrust T , and the corresponding \vec{n} is called the thrust axis and denoted by \vec{n}_T . The variable $(1 - T)$ is often used, which for the LO of 3-jet production is restricted to the range $(0 < 1 - T < 1/3)$. We have a back-to-back or a spherically symmetric event respectively at $T = 1$ and at $T = 2/3$ respectively. For the C-parameter, θ_{ij} is the angle between \vec{p}_i and \vec{p}_j . At LO for the 3 jet production the C-parameter is restricted to the range: $0 \leq C \leq 0.75$ by kinematics.

In general a normalized IR-safe single-variable observable, such as the thrust distribution for the $e^+e^- \rightarrow 3jets$ [142, 143], is the sum of pQCD contributions calculated up to NNLO at the initial renormalization scale $\mu_0 = \sqrt{s} = M_Z$:

$$\frac{1}{\sigma_{tot}} \frac{d\sigma(\mu_0)}{dO} = \left\{ x_0 \cdot \frac{d\bar{A}_O(\mu_0)}{dO} + x_0^2 \cdot \frac{d\bar{B}_O(\mu_0)}{dO} \right.$$

$$+ x_0^3 \cdot \left. \frac{Od\bar{C}_O(\mu_0)}{dO} + \mathcal{O}(\alpha_s^4) \right\}, \quad (5.17)$$

where $x(\mu) \equiv \alpha_s(\mu)/(2\pi)$, O is the selected event shape variable, σ the cross section of the process,

$$\sigma_{tot} = \sigma_0 \left(1 + x_0 A_{tot} + x_0^2 B_{tot} + \mathcal{O}(\alpha_s^3) \right)$$

is the total hadronic cross section and $\bar{A}_O, \bar{B}_O, \bar{C}_O$ are respectively the normalized LO, NLO and NNLO coefficients:

$$\begin{aligned} \bar{A}_O &= A_O \\ \bar{B}_O &= B_O - A_{tot} A_O \\ \bar{C}_O &= C_O - A_{tot} B_O - (B_{tot} - A_{tot}^2) A_O, \end{aligned} \quad (5.18)$$

where A_O, B_O, C_O are the coefficients normalized to the tree-level cross section σ_0 calculated by MonteCarlo (see e.g. the EERAD and Event2 codes [124,125,139–141]) and A_{tot}, B_{tot} are:

$$\begin{aligned} A_{tot} &= \frac{3}{2} C_F; \\ B_{tot} &= \frac{C_F}{4} N_c + \frac{3}{4} C_F \frac{\beta_0}{2} (11 - 8\zeta(3)) - \frac{3}{8} C_F^2, \end{aligned} \quad (5.19)$$

where ζ is the Riemann zeta function.

In general according to CSS the renormalization scale is set to $\mu_0 = \sqrt{s} = M_Z$ and theoretical uncertainties are evaluated using standard criteria. In this case, we have used the definition given in Ref. [140] of the parameter δ , we define the average error for the event shape variable distributions as:

$$\bar{\delta} = \frac{1}{N} \sum_i^N \frac{\max_{\mu}(\sigma_i(\mu)) - \min_{\mu}(\sigma_i(\mu))}{2\sigma_i(\mu = M_Z)} \quad (5.20)$$

where i is the index of the bin and N is the total number of bins, the renormalization scale is varied in the range: $\mu \in [M_Z/2; 2M_Z]$.

5.6 The PMC_∞ scales at LO and NLO

According to the PMC_∞ prescription we fix the renormalization scale to μ_N at each order absorbing all the β terms into the coupling. We notice a small mismatch between the zeroes of the conformal coefficient B_{Conf} and those of the remaining β_0 term in the numerator (the formula is shown in Eq. 5.14). Due to our limited knowledge of the strong coupling at low energies, in order to avoid singularities in the NLO-scale μ_{II} , we introduce a regularization that leads to a finite scale $\tilde{\mu}_{\text{II}}$ in the whole range of values of the variable $(1 - T)$. These singularities might be due either to the presence of UV finite N_F terms or to the logarithmic behavior of the conformal coefficients when low values of the variable $1 - T$ are approached. Large logarithms arise from the IR-divergence cancellation procedure and they can be resummed in order to restore a predictive perturbative regime [91–96, 144]. We point out that IR cancellation should not spoil the iCF property. Whether this is an actual deviation from the iCF-form has to be further investigated. However, since the discrepancies between the coefficients are rather small, we introduce a regularization method based on redefinition of the norm of the coefficient B_{Conf} in order to cancel out these singularities in the μ_{II} -scale. This regularization is consistent with the PMC principle and up to the accuracy of the calculation it does not introduce any bias effect in the results or any ambiguity in the NLO- PMC_∞ scale. All the differences introduced by the regularization would start at the N^3LO order of accuracy and they can be reabsorbed after in the higher order PMC_∞ scales. Thus we obtain for the PMC_∞ scales, μ_N :

$$\mu_{\text{I}} = \sqrt{s} \cdot e^{f_{sc} - \frac{1}{2}B\beta_0}, \quad (1-T) < 0.33 \quad (5.21)$$

$$\tilde{\mu}_{\text{II}} = \begin{cases} \sqrt{s} \cdot e^{f_{sc} - \frac{1}{2}C\beta_0} \cdot \frac{B_{\text{Conf}}}{B_{\text{Conf}} + \eta \cdot A_{\text{tot}} A_{\text{Conf}}}, & (1-T) < 0.33 \\ \sqrt{s} \cdot e^{f_{sc} - \frac{1}{2}C\beta_0}, & (1-T) > 0.33 \end{cases} \quad (5.22)$$

where $\sqrt{s} = M_Z$ and the third scale is set to $\mu_{\text{III}} = \mu_0 = \sqrt{s}$. The renormalization scheme factor for the QCD results is set to $f_{sc} \equiv 0$. This scheme factor reabsorbs also the scheme difference into the renormalization scale and is related to the particular choice of the scale parameter Λ as discussed in section 2.8. The coefficients B_{β_0}, C_{β_0} are the coefficients related to the β_0 -terms of the NLO and NNLO perturbative order of the thrust distribution respectively. They are determined from the calculated A_O, B_O, C_O coefficients.

The η parameter is a regularization term to cancel the singularities of the NLO scale, μ_{II} , in the range $(1 - T) < 0.33$, depending on non-matching zeroes between numerator and denominator in the C_{β_0} . In general this term is not mandatory for applying the PMC_∞ , it is necessary only in case one is interested in applying the method all over the entire range covered by the thrust, or any other observable. Its value has been determined as $\eta = 3.51$ for the thrust distribution and it introduces no bias effects up to the accuracy of the calculations and the related errors are totally negligible up to this stage.

We point out that in the region $(1 - T) > 0.33$ we have a clear example of intrinsic conformality-iCF where the kinematic constraints set the $A_{\text{Conf}} = 0$. According to Eq. 5.5 setting the $A_{\text{Conf}} = 0$ the whole conformal subset σ_{I} becomes null. In this case all the β terms at NLO and NNLO disappear except the β_0 -term at NNLO which determines the μ_{II} scale. The surviving n_f terms at NLO or the n_f^2 at NNLO are related to the finite N_F -term at NLO and to the mixed $N_f \cdot N_F$ term arising from $B_O \cdot \beta_0$ at NNLO. Using the parametrization with explicit n_f terms we have for $(1 - T) > 0.33$:

$$\begin{aligned}
A_O &= 0, \\
B_O &= B_0 + B_1 \cdot N_F, \\
C_O &= C_0 + C_1 \cdot n_f + C_2 \cdot N_f \cdot N_F.
\end{aligned} \tag{5.23}$$

we can determine the $\tilde{\mu}_{\text{II}}$ for the region $(1 - T) > 0.33$ as shown in Eq. 5.22:

$$C_{\beta_0} = \left(\frac{C_1}{\frac{11}{3}C_A B_1 - \frac{2}{3}B_0} \right) \quad (5.24)$$

by identifying the β_0 -term at NNLO. The LO and NLO PMC_∞ scales are shown in Fig. 5.1. We notice that the two PMC_∞ scale have similar behaviors in the

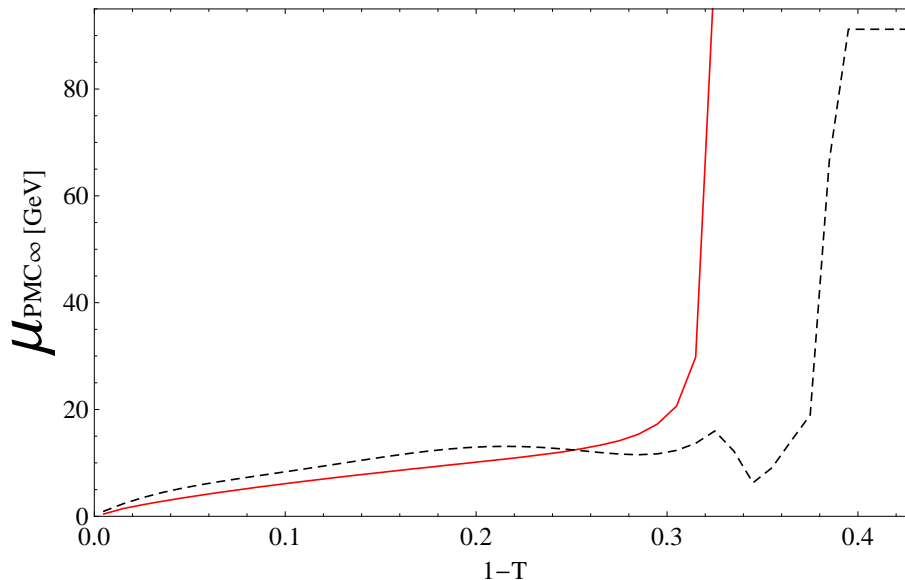


Figure 5.1: The LO- PMC_∞ (solid red) and the NLO- PMC_∞ (dashed black) scales for thrust. [145]

range $(1 - T) < 0.33$ and the LO- PMC_∞ scale agrees with the PMC scale used in Ref. [146]. This method totally eliminates both the ambiguity in the choice of the renormalization scale and the scheme dependence at all orders in QCD.

5.7 NNLO Thrust distribution results

We use here the results of Ref. [124,125] and for the running coupling $\alpha_s(Q)$ we use the RunDec program [147]. In order to normalize consistently the thrust distribution we expand the denominator in $\alpha_0 \equiv \alpha_s(\mu_0)$ while the numerator has the couplings renormalized at different PMC_∞ scales $\alpha_I \equiv \alpha_s(\mu_I)$, $\alpha_{II} \equiv \alpha_s(\tilde{\mu}_{II})$. We point out here that the proper normalization would be given by the integration of the total

cross section after renormalization with the PMC_∞ scales, nonetheless since the PMC_∞ prescription involves only absorption of higher order terms into the scales, the difference would be within the accuracy of the calculations, i.e. $\sim \mathcal{O}(\alpha_s^4(\mu_0))$. Eq. 5.17 becomes:

$$\frac{1}{\sigma_{tot}} \frac{d\sigma(\mu_I, \tilde{\mu}_{II}, \mu_0)}{dO} = \left\{ \bar{\sigma}_I + \bar{\sigma}_{II} + \bar{\sigma}_{III} + \mathcal{O}(\alpha_s^4) \right\}, \quad (5.25)$$

where the $\bar{\sigma}_N$ are normalized subsets that are given by:

$$\begin{aligned} \bar{\sigma}_I &= A_{Conf} \cdot x_I \\ \bar{\sigma}_{II} &= (B_{Conf} + \eta A_{tot} A_{Conf}) \cdot x_{II}^2 - \eta A_{tot} A_{Conf} \cdot x_0^2 \\ &\quad - A_{tot} A_{Conf} \cdot x_0 x_I \\ \bar{\sigma}_{III} &= (C_{Conf} - A_{tot} B_{Conf} - (B_{tot} - A_{tot}^2) A_{Conf}) \cdot x_0^3, \end{aligned} \quad (5.26)$$

$A_{Conf}, B_{Conf}, C_{Conf}$ are the scale-invariant conformal coefficients (i.e. the coefficients of each perturbative order not depending on the scale μ_R) while x_I, x_{II}, x_0 are the couplings determined at the $\mu_I, \tilde{\mu}_{II}, \mu_0$ scales respectively.

Normalized subsets for the region $(1-T) > 0.33$ can be achieved simply by setting $A_{Conf} \equiv 0$ in the Eq. 5.26. Within the numerical precision of these calculations there is no evidence of the presence of spurious terms, such as any further UV-finite N_F term up to NNLO [148] besides the kinematic term at lowest order in the multi-jet region. These terms, if there are any, must remain rather small all over the range of the thrust variable in comparison with the β term or even be compatible with numerical fluctuations. Moreover, we notice a small rather constant difference between the iCF-predicted and the calculated coefficient for the N_f^2 -color factor of Ref. [124] which might be due to a n_f^2 UV-finite coefficient or possibly to statistics. This small difference must be included in the conformal coefficient but it has a completely negligible impact on the total thrust distribution. In Fig. 5.2 we show the thrust distribution at NLO and at NNLO with the use of the PMC_∞ method. Theoretical errors for the thrust distribution at NLO and at NNLO are

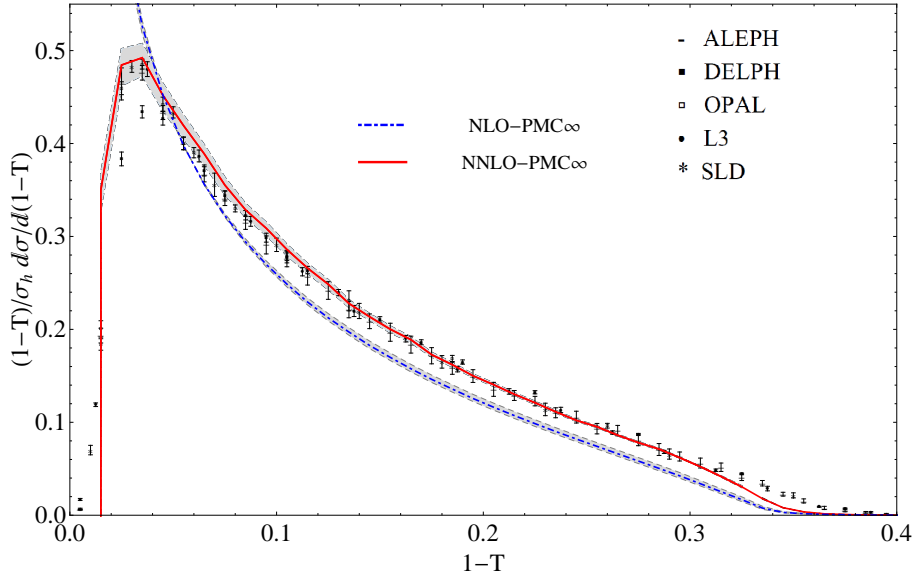


Figure 5.2: The thrust distribution under the PMC_∞ at NLO (dotdashed blue) and at NNLO (solid red) [145]. The experimental data points are taken from the ALEPH, DELPHI, OPAL, L3, SLD experiments [128–132]. The shaded area shows theoretical errors for the PMC_∞ predictions at NLO and at NNLO.

also shown (the shaded area). Conformal quantities are not affected by a change of renormalization scale. Thus the errors shown give an evaluation of the level of conformality achieved up to the order of accuracy and they have been calculated using standard criteria, i.e. varying the remaining initial scale value in the range $\sqrt{s}/2 \leq \mu_0 \leq 2\sqrt{s}$. Using the same definition of the parameter $\bar{\delta}$ given in Eq. 5.20, we have in the interval $0 < (1 - T) < 0.33$ an average error of $\bar{\delta} \simeq 3.54\%$ and 1.77% for the thrust at NLO and at NNLO respectively. A larger improvement has been obtained in the entire range of reliable results for thrust distribution, i.e. $0 < (1 - T) < 0.42$, from $\bar{\delta} \simeq 7.36\%$ to 1.95% from NLO to the NNLO accuracy with the PMC_∞ .

In Fig. 5.3 a direct comparison of the PMC_∞ with the CSS results (obtained in [124] and [140,141]) is shown. In addition, we have shown also the results of the first PMC approach used in [146], which we indicate as $\text{PMC}(\mu_{\text{LO}})$ extended to NNLO

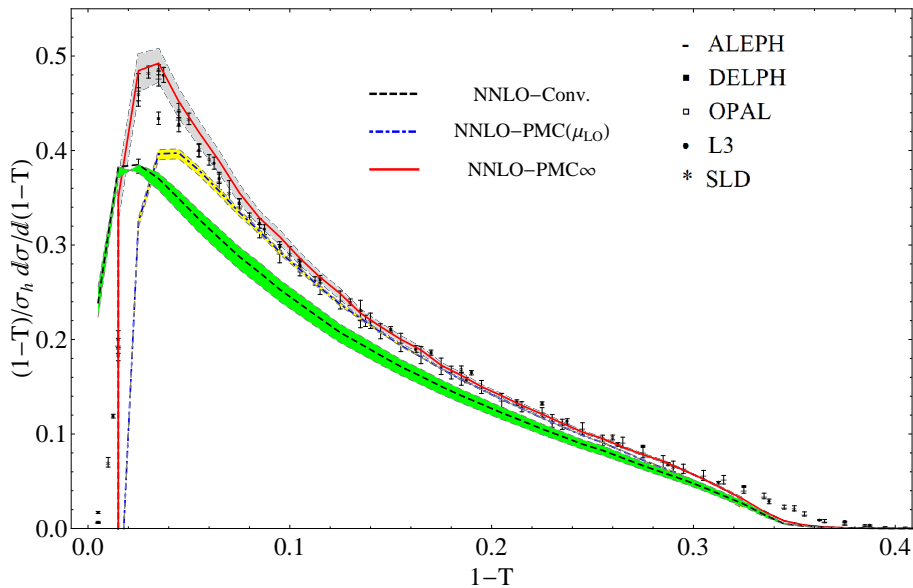


Figure 5.3: The thrust distribution at NNLO under the Conventional (dashed black), the PMC(μ_{LO}) (dotted blue) and the PMC $_{\infty}$ (solid red) [145]. The experimental data points are taken from the ALEPH, DELPHI, OPAL, L3, SLD experiments [128–132]. The shaded areas show theoretical error predictions at NNLO, which have been calculated varying the remaining initial scale value in the range $\sqrt{s}/2 \leq \mu_0 \leq 2\sqrt{s}$.

accuracy. In this approach the last unknown PMC scale μ_{NLO} of the NLO was set to the last known PMC scale μ_{LO} of the LO, while the NNLO scale $\mu_{NNLO} \equiv \mu_0$ was left unset and varied in the range $\sqrt{s}/2 \leq \mu_0 \leq 2\sqrt{s}$. This analysis was performed in order to show that the procedure of setting the last unknown scale to the last known one leads to stable and precise results and is consistent with the proper PMC method in a wide range of values of the $(1 - T)$ variable.

Average errors calculated in different regions of the spectrum are reported in Table 5.1. From the comparison with the CSS we notice that the PMC $_{\infty}$ prescription significantly improves the theoretical predictions. Moreover, results are in remarkable agreement with the experimental data in a wider range of values ($0.015 \leq 1 - T \leq 0.33$) and they show an improvement of the PMC(μ_{LO}) results when the two-jets and the multi-jets regions are approached, i.e. the region of the

$\bar{\delta}[\%]$	Conv.	PMC(μ_{LO})	PMC $_{\infty}$
$0.10 < (1 - T) < 0.33$	6.03	1.41	1.31
$0.21 < (1 - T) < 0.33$	6.97	2.19	0.98
$0.33 < (1 - T) < 0.42$	8.46	-	2.61
$0.00 < (1 - T) < 0.33$	5.34	1.33	1.77
$0.00 < (1 - T) < 0.42$	6.00	-	1.95

Table 5.1: Average error, $\bar{\delta}$, for NNLO Thrust distribution under Conventional, PMC(μ_{LO}) and PMC $_{\infty}$ scale settings calculated in different ranges of values of the $(1 - T)$ variable.

peak and the region $(1 - T) > 0.33$ respectively. The use of the PMC $_{\infty}$ approach in perturbative thrust QCD calculations restores the correct behavior of the thrust distribution in the region $(1 - T) > 0.33$ and this is a clear effect of the iCF property. Comparison with experimental data has been improved all over the spectrum and the introduction of the N³LO order correction would improve this comparison especially in the multi-jet $(1 - T) > 0.33$ region. In the PMC $_{\infty}$ method theoretical errors are given by the unknown intrinsic conformal scale of the last order of accuracy. We expect this scale not to be significantly different from that of the previous orders. In this particular case, as shown in Eq. 5.26, we have also a dependence on the initial scale $\alpha_s(\mu_0)$ left due to the normalization and to the regularization terms. These errors represent 12.5% and 1.5% respectively of the whole theoretical errors in the range $0 < (1 - T) < 0.42$ and they could be improved by means of a correct normalization.

5.8 NNLO C-parameter distribution results

The same analysis applies straightforwardly to the C-parameter distribution including the regularizing η parameter, which has been set to the same value 3.51. The same scales of Eq. 5.21 and Eq. 5.22 apply to the C-parameter distribution in the

region $0 < C < 0.75$ and in the region $0.75 < C < 1$. In fact, due to kinematic constraints that set the $A_{Conf} = 0$, we have the same iCF effect also for the C-parameter. Results for the C-parameter scales and distributions are shown in Fig. 5.4 and Fig. 5.5 respectively.

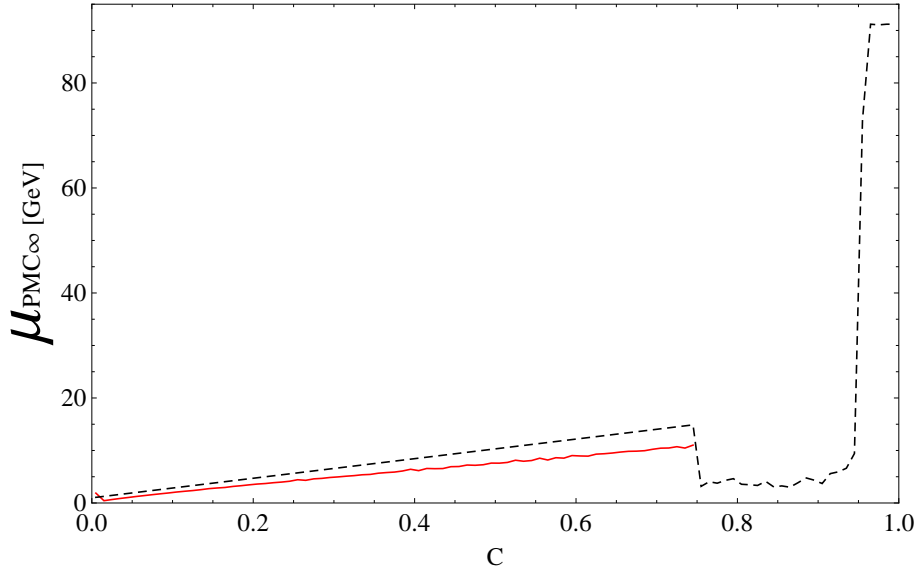


Figure 5.4: The LO- PMC_∞ (solid red) and the NLO- PMC_∞ (dashed black) scales for C-parameter. [145]

Theoretical errors have been calculated, as in the previous case, using standard criteria and results indicate an average error over the whole spectrum $0 < C < 1$ of the C-parameter distribution at NLO and at NNLO of $\bar{\delta} \simeq 7.26\%$ and 2.43% respectively.

A comparison of average errors according to the different methods is shown in Table 5.2. Results show that the PMC_∞ improves the NNLO QCD predictions for the C-parameter distribution over the entire spectrum.

A comparison of the distributions calculated with the CSS, the $\text{PMC}(\mu_{\text{LO}})$ [149] and the PMC_∞ is shown in Fig. 5.6. Results for the PMC_∞ show remarkable agreement with the experimental data away from the regions $C < 0.05$ and $C \simeq 0.75$. The errors due to the normalization and to the regularization terms (Eq. 5.26) are respec-

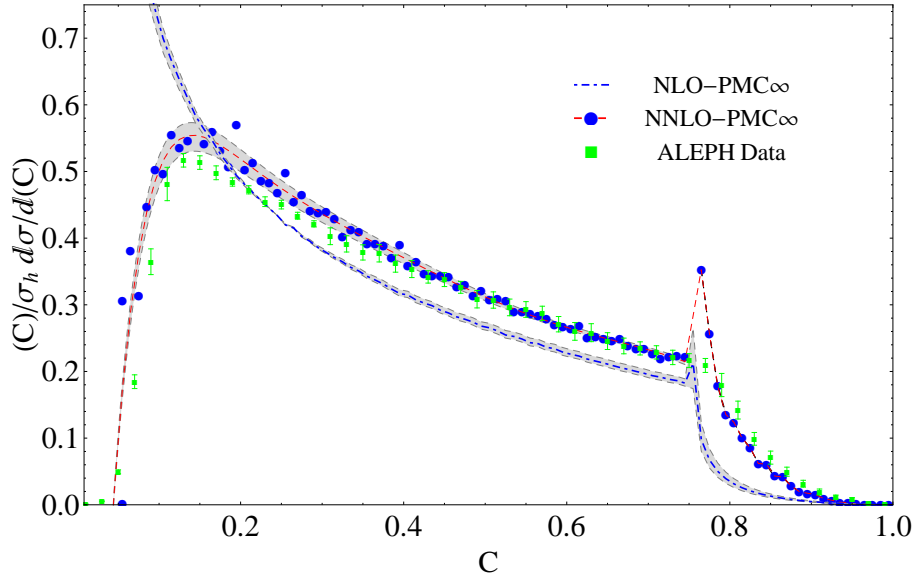


Figure 5.5: The C-parameter distribution under the PMC_∞ at NLO (dotted blue) and at NNLO (dashed red) [145]. Blue points indicate the NNLO- PMC_∞ thrust distribution obtained with $\mu_{\text{III}} = \mu_0 = M_Z$. The experimental data points (green) are taken from the ALEPH experiment [128]. The dashed lines of the NNLO distribution show fits of the theoretical calculations with interpolating functions for the values of the remaining initial scale $\mu_0 = 2M_Z$ and $M_Z/2$. The shaded area shows theoretical errors for the PMC_∞ predictions at NLO and at NNLO calculated varying the remaining initial scale value in the range $\sqrt{s}/2 \leq \mu_0 \leq 2\sqrt{s}$.

tively 8.8% and 0.7% of the whole theoretical errors. The perturbative calculations could be further improved using a correct normalization and also by introducing the large-logarithm resummation technique in order to extend the perturbative regime.

$\bar{\delta}[\%]$	Conv.	PMC(μ_{LO})	PMC $_{\infty}$
$0.00 < (C) < 0.75$	4.77	0.85	2.43
$0.75 < (C) < 1.00$	11.51	3.68	2.42
$0.00 < (C) < 1.00$	6.47	1.55	2.43

Table 5.2: Average error $\bar{\delta}$, for NNLO C-parameter distribution under Conventional, PMC(μ_{LO}) and PMC $_{\infty}$ scale settings calculated in different ranges of values of the (C) variable.

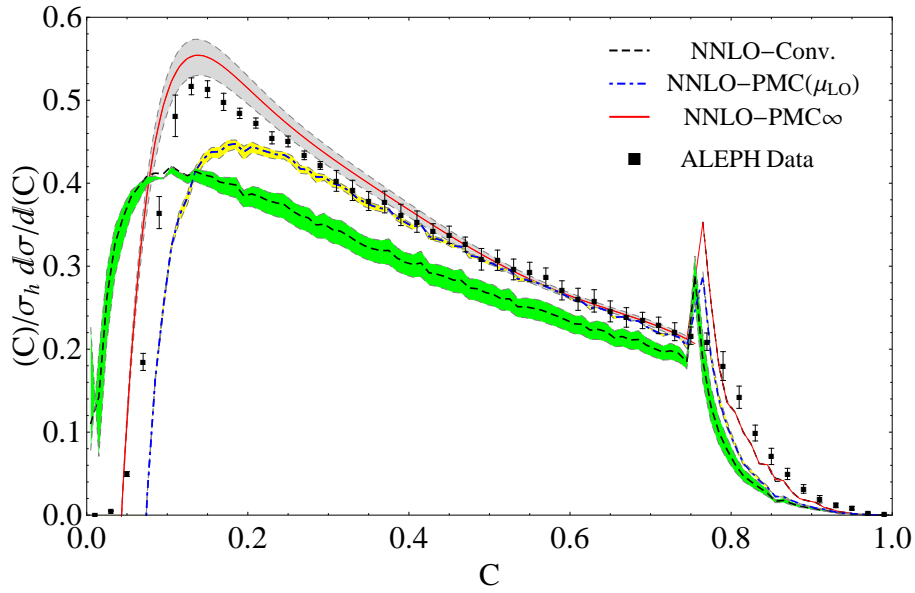


Figure 5.6: The NNLO C-parameter distribution under CSS (dashed black), the PMC(μ_{LO}) (dotdashed blue) and the PMC $_{\infty}$ (solid red) [145]. The experimental data points (Black) are taken from the ALEPH experiment [128]. The shaded area shows theoretical error predictions at NNLO calculated varying the remaining initial scale value in the range $\sqrt{s}/2 \leq \mu_0 \leq 2\sqrt{s}$.

Chapter 6

The thrust distribution in the QCD perturbative conformal window and in QED

We employ, for the first time, the perturbative regime of the quantum chromodynamics (pQCD) infrared conformal window as a laboratory to investigate in a controllable manner (near) conformal properties of physically relevant quantities such as the thrust distribution in electron-positron annihilation processes [64].

The conformal window of pQCD has a long and noble history conveniently summarized and generalized to arbitrary representations in Ref. [150]. Several lattice gauge theory applications and results have been summarized in a recent report on the subject in Ref. [151].

6.1 The thrust distribution according to N_f

It would be highly desirable to compare the PMC and CSS methods along the entire renormalization group flow from the highest energies down to zero energy. This is precluded in standard QCD with a number of active flavors less than six because the theory becomes strongly coupled at low energies. We therefore employ the

perturbative regime of the conformal window (Sec. 2.5) which allows us to arrive at arbitrary low energies and obtain the corresponding results for the SU(3) case at the cost of increasing the number of active flavors. Here we are able to deduce the full solution at NNLO in the strong coupling. In this chapter we will consider the region of flavors and colors near the upper bound of the conformal window, i.e. $N_f \sim 11/2N_c$, where the IR fixed point can be reliably accessed in perturbation theory and we compare the two renormalization scale setting methods, the CSS and the PMC_∞ .

Results for the thrust distribution calculated using the NNLO solution for the coupling $\alpha_s(\mu)$, at different values of the number of flavors, N_f , is shown in Fig. 6.1.

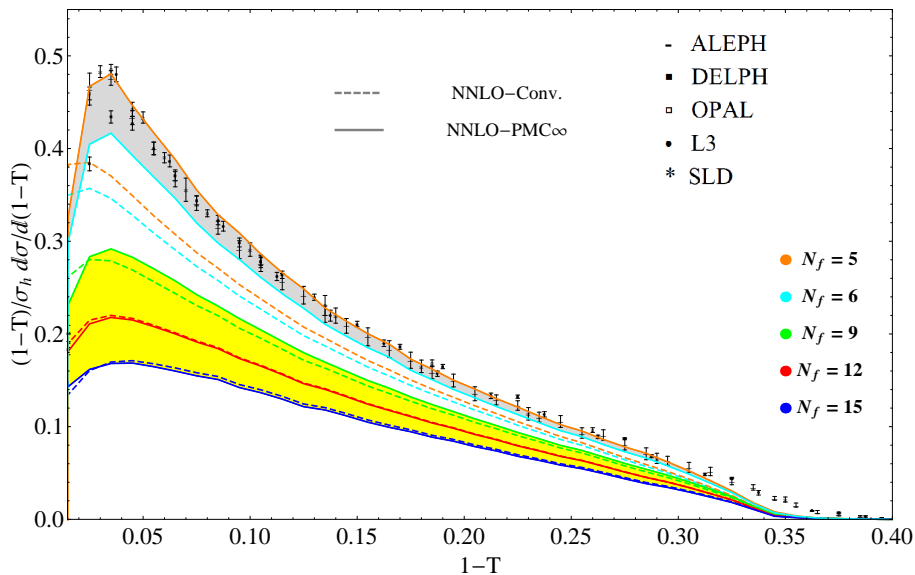


Figure 6.1: Thrust distributions for different values of N_f , using the PMC_∞ (solid line) and the CSS (dashed line) [64]. The Yellow shaded area is the results for the values of N_f taken in the conformal window. The experimental data points are taken from the ALEPH, DELPHI, OPAL, L3, SLD experiments [128–132].

A direct comparison between PMC_∞ (solid line) and CSS (dashed line) is shown at different values of the number of flavors. We notice that, despite the phase

transition (i.e. the transition from an infrared finite coupling to an infrared diverging coupling), the curves given by the PMC_∞ at different N_f , preserve with continuity the same characteristics of the conformal distribution setting N_f out of the conformal window of pQCD. In fact, the position of the peak of the thrust distribution is well preserved varying N_f in and out of the conformal window using the PMC_∞ , while there is constant shift towards lower values using the CSS. These trends are shown in Fig. 6.2. We notice that in the central range, $2 < N_f < 15$, the position of the peak is exactly preserved using the PMC_∞ and overlaps with the position of the peak shown by the experimental data. According to our analysis for the case PMC_∞ , in the range, $N_f < 2$ the number of bins is not enough to resolve the peak, though the behavior of the curve is consistent with the presence of a peak in the same position, while for $N_f \rightarrow 0$ the peak is no longer visible. Theoretical uncertainties on the position of the peak have been calculated using standard criteria, i.e. varying the remaining initial scale value in the range $M_Z/2 \leq \mu_0 \leq 2M_Z$, and considering the lowest uncertainty given by the half of the spacing between two adjacent bins.

Using the definition given in Eq. 5.20, we have determined the average error, $\bar{\delta}$, calculated in the interval $0.005 < (1 - T) < 0.4$ of thrust and results for CSS and PMC_∞ are shown in Fig. 6.3. We notice that the PMC_∞ in the perturbative and IR conformal window, i.e. $12 < N_f < \bar{N}_f$, which is the region where $\alpha_s(\mu) < 1$ in the whole range of the renormalization scale values, from 0 up to ∞ , the average error given by PMC_∞ tends to zero ($\sim 0.23 - 0.26\%$) while the error given by the CSS tends to remain constant ($0.85 - 0.89\%$). The comparison of the two methods shows that, out of the conformal window, $N_f < \frac{34N_c^3}{13N_c^2 - 3}$, the PMC_∞ leads to a higher precision.

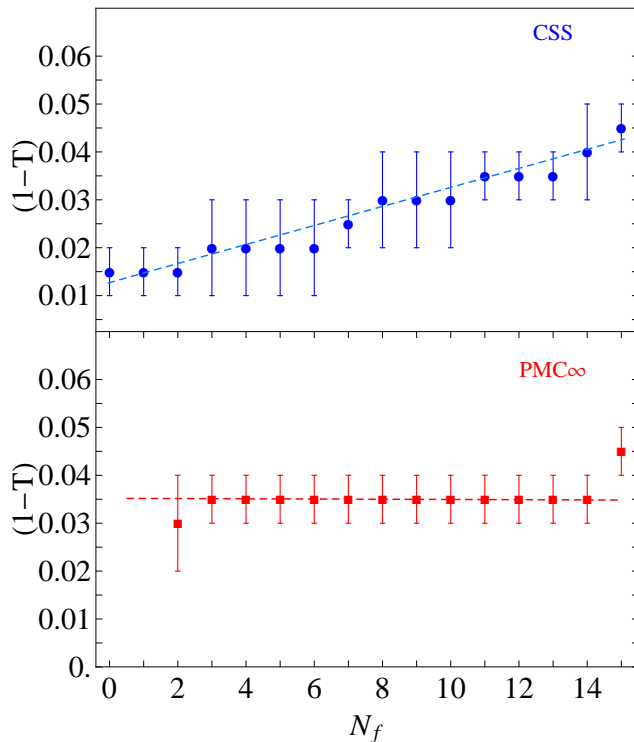


Figure 6.2: Comparison of the position of the peak for the thrust distribution using the CSS and the PMC_∞ vs the number of flavors, N_f . Dashed lines indicate the particular trend in each graph [64].

6.2 The thrust distribution in the Abelian limit

$$N_c \rightarrow 0$$

We consider now the thrust distribution in U(1) Abelian QED, which rather than being infrared interacting is infrared free. We obtain the QED thrust distribution performing the $N_c \rightarrow 0$ limit of the QCD thrust at NNLO according to [32, 76]. In the zero number of colors limit the gauge group color factors are fixed by $N_A = 1$, $C_F = 1$, $T_R = 1$, $C_A = 0$, $N_c = 0$, $N_f = N_l$, where N_l is the number of active leptons, while the β -terms and the coupling rescale as β_n/C_F^{n+1} and $\alpha_s \cdot C_F$ respectively. In particular $\beta_0 = -\frac{4}{3}N_l$ and $\beta_1 = -4N_l$ using the normalization of Eq. 2.8. According to this rescaling of the color factors we have determined the QED thrust and the

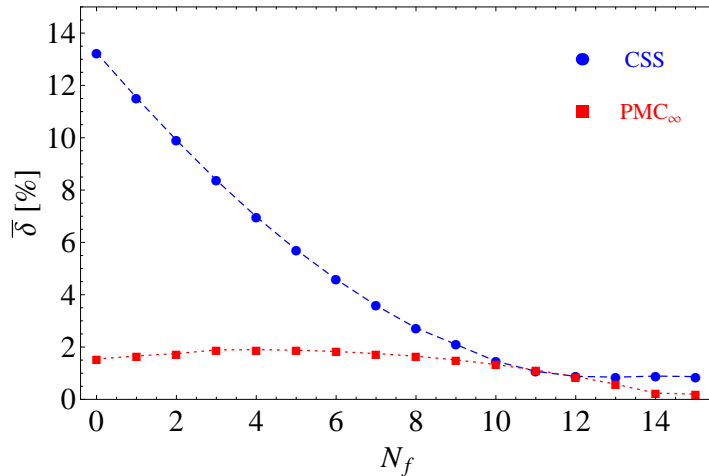


Figure 6.3: Comparison of the average theoretical error, $\bar{\delta}$, calculated using standard criteria in the range: $0.005 < (1 - T) < 0.4$, using the CSS and the PMC_∞ for the thrust distribution vs the number of flavors, N_f [64].

QED PMC_∞ scales. For the QED coupling, we have used the analytic formula for the effective fine structure constant in the $\overline{\text{MS}}$ -scheme:

$$\alpha(Q^2) = \frac{\alpha}{\left(1 - \Re e \Pi^{\overline{\text{MS}}}(Q^2)\right)}, \quad (6.1)$$

with $\alpha^{-1} \equiv \alpha(0)^{-1} = 137.036$ and the vacuum polarization function (Π) calculated perturbatively at two loops including contributions from leptons, quarks and W boson. The QED PMC_∞ scales have the same form of Eqs. 5.21 and 5.22 with the factor for the $\overline{\text{MS}}$ -scheme set to $f_{sc} \equiv 5/6$ and the η regularization parameter introduced to cancel singularities in the NLO PMC_∞ scale μ_{II} in the $N_c \rightarrow 0$ limit tends to the same QCD value, $\eta = 3.51$. A direct comparison between QED and QCD PMC_∞ scales is shown in Fig. 6.4.

We note that in the QED limit the PMC_∞ scales have analogous dynamical behavior as those calculated in QCD, differences arise mainly owing to the $\overline{\text{MS}}$ scheme factor reabsorption, the effects of the N_c number of colors at NLO are very small. Thus we notice that perfect consistency is shown from QCD to QED using

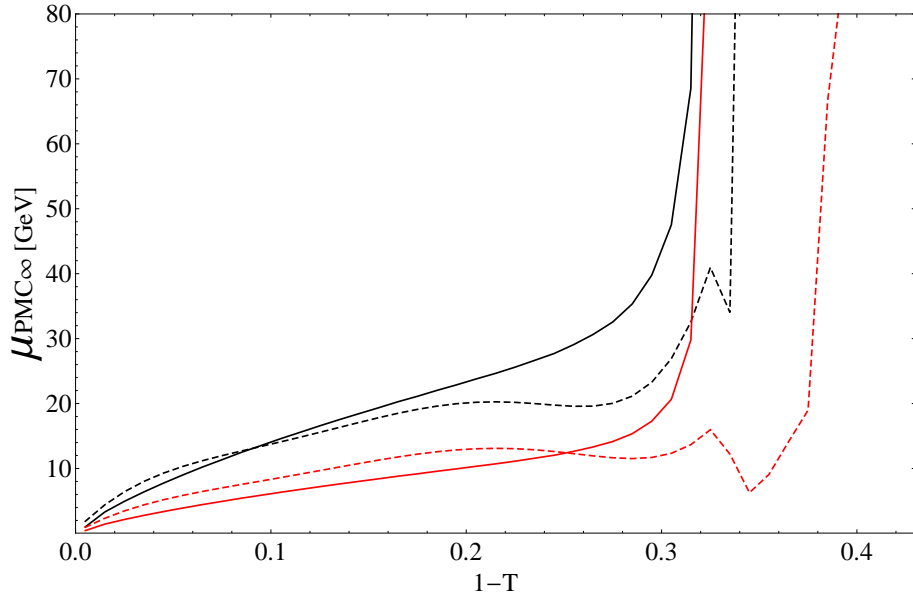


Figure 6.4: PMC_∞ scales for the thrust distribution: LO-QCD scale (solid red); LO-QED scale (solid black); NLO-QCD scale (dashed red); NLO-QED scale (dashed black) [64].

the PMC_∞ method. The normalized QED thrust distribution is shown in Fig. 6.5. We note that the curve is peaked at the origin, $T = 1$, which suggests that the three-jet event in QED occurs with a rather back-to-back symmetry. Results for the CSS and the PMC_∞ methods in QED are of the order of $O(\alpha)$ and show very small differences, given the good convergence of the theory.

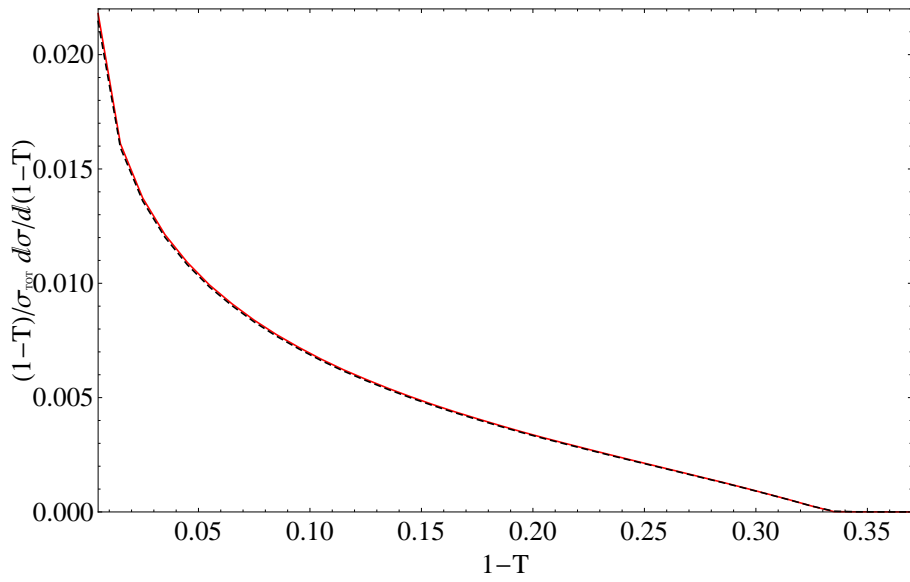


Figure 6.5: Thrust distributions in the QED limit at NNLO using the PMC_∞ (solid red) and the CSS (dashed black) [64].

Chapter 7

Precise determination of the strong coupling and its behavior from Event Shape variables using the PMC

In this section we present a novel method for precisely determining the running QCD coupling constant $\alpha_s(Q)$ over a wide range of Q from Event Shape variables for the electron-positron annihilation process measured at a single center-of-mass energy \sqrt{s} , based on PMC scale setting. In particular, we show results obtained in Refs. [146, 149] using the approach of a single PMC scale at LO and at NLO, i.e. the PMC(μ_{LO}) of the previous chapter.

The precise determination of the strong coupling $\alpha_s(Q)$ is one of the crucial tests of QCD. The dependence of $\alpha_s(Q)$ on the renormalization scale Q obtained from many different physical processes shows consistency with QCD predictions and asymptotic freedom. The Particle Data Group (PDG) currently gives the world average: $\alpha_s(M_Z) = 0.1181 \pm 0.0011$ [152] in the $\overline{\text{MS}}$ renormalization scheme.

Particularly suitable to the determination of the strong coupling is the pro-

cess $e^+e^- \rightarrow 3jets$ since its lowest order is $\mathcal{O}(\alpha_s)$ [127]. Currently, theoretical calculations for event shapes are based on CSS. By using conventional scale setting, only one value of α_s at the scale \sqrt{s} can be extracted and the main source of the uncertainty is given by the choice of the renormalization scale. Several values for the strong coupling have been extracted from several processes, e.g. $\alpha_s(M_Z) = 0.1224 \pm 0.0035$ [153] is obtained by using perturbative corrections and resummation of the large logarithms at the NNLO+NLL accuracy predictions. Other evaluations improving the resummation calculations up to N³LL give a result of $\alpha_s(M_Z^2) = 0.1135 \pm 0.0011$ [96] from thrust, and $\alpha_s(M_Z) = 0.1123 \pm 0.0015$ [154] from the C-parameter. Non-perturbative corrections for hadronization effects have also been included in Ref. [155], but as pointed out in Ref. [152], the systematics of the theoretical uncertainties given by hadronization effects are not well understood.

We show in this section that using the PMC is possible to eliminate the renormalization scale ambiguities and obtain consistent results for the strong coupling using the precise experimental data of Event Shape variable distributions. We notice that improved event shape distributions have been obtained in Refs. [23, 148, 156] using BLM and the soft and collinear effective theory (SCET) .

7.1 Running behavior

Given that the PMC scale ($\text{PMC}(\mu_{\text{LO}})$) is not a single-valued but rather a monotonically increasing function of \sqrt{s} and of the selected observable, (as shown in Figs. 5.1 and 5.4), it is possible to determine the strong coupling values at different scales from one single experiment at one single center-of-mass energy. The dependence of the scale on the observable reflects the dynamics of the underlying gluon and quark subprocess. This dynamics varies also the number of active flavors N_f . Considering that PMC scales for QCD and QED show the same behavior and their relation at LO is only given by a RS redefinition term: $Q_{\text{QCD}}^2/Q_{\text{QED}}^2 = e^{-5/3}$ this approach can also be extended to QED.

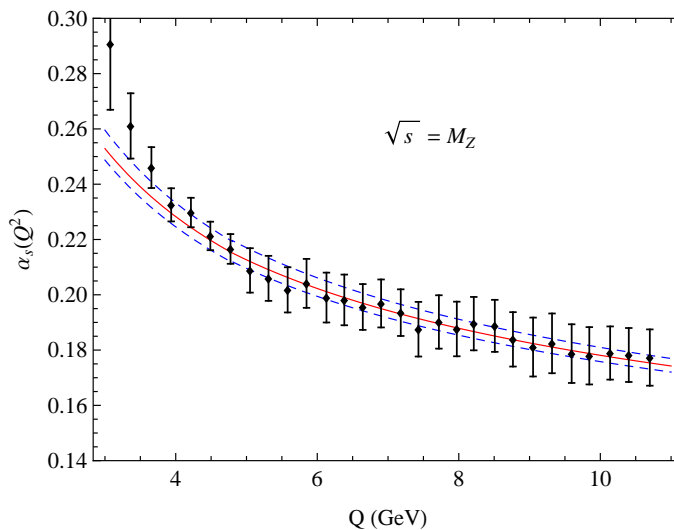


Figure 7.1: The coupling constant $\alpha_s(Q)$ extracted by comparing PMC predictions with the ALEPH data [128] at a single energy of $\sqrt{s} = M_Z$ from the C-parameter distributions in the $\overline{\text{MS}}$ scheme (from Ref. [149]). The error bars are the squared averages of the experimental and theoretical errors. The three lines are the world average evaluated from $\alpha_s(M_Z) = 0.1181 \pm 0.0011$ [152].

We extract α_s at different scales bin-by-bin from the comparison of PMC predictions for $(1 - T)$ and C differential distributions with measurements at $\sqrt{s} = M_Z$. The extracted α_s values from the C-parameter distribution are shown in Fig. 7.1. We note that the extracted α_s in the scale range of $3 \text{ GeV} < Q < 11 \text{ GeV}$ are in excellent agreement with the world average evaluated from $\alpha_s(M_Z)$ [152]. Given that the PMC scale setting eliminates the scale uncertainties, the corresponding extracted α_s values are not plagued by any ambiguity in the choice of μ_r . The extracted α_s values from the thrust observable using PMC are shown in Fig. 7.2. Also in this case there is good agreement in the range $3.5 \text{ GeV} < \mu_r < 16 \text{ GeV}$ (corresponding to the $(1 - T)$ range: $0.05 < (1 - T) < 0.29$). These extracted values of α_s are in good agreement also with the world average value of the PDG [152].

Thus, PMC scale setting provides a remarkable way to verify the running of $\alpha_s(Q)$ from event shapes measured at a single energy of \sqrt{s} . Analogously in QED,

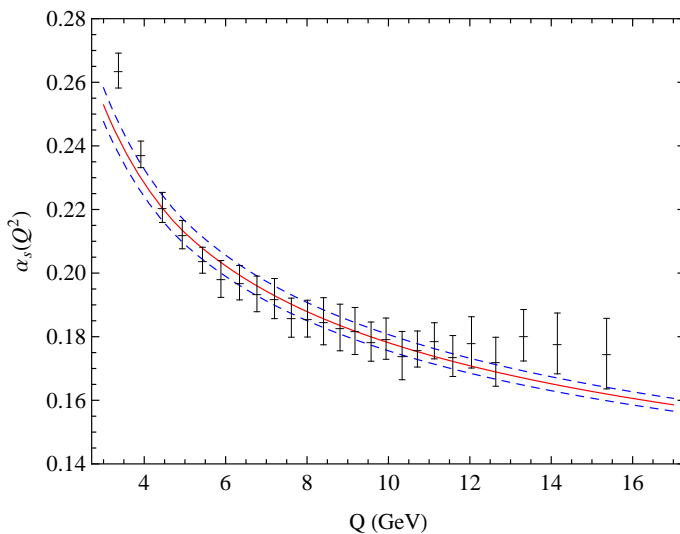


Figure 7.2: The extracted α_s from the comparison of PMC predictions with ALEPH data at $\sqrt{s} = M_Z$ (from Ref. [146]). The error bars are from the experimental data. The three lines are the world average evaluated from $\alpha_s(M_Z) = 0.1181 \pm 0.0011$ [152].

the running of QED coupling $\alpha(Q)$ can be measured at a single energy of \sqrt{s} (see e.g. [157]).

The differential distributions of event shapes are afflicted with large logarithms especially in the two-jet region. Thus, the comparison of QCD predictions with experimental data and thus the extracted α_s values are restricted to the region where the theory is able to describe the data well.

Choosing a different area of distributions leads to the different values of α_s .

7.2 $\alpha_s(Q)$ from mean values

The mean value of an event shape defined by:

$$\langle y \rangle = \int_0^{y_0} \frac{y}{\sigma_h} \frac{d\sigma}{dy} dy, \quad (7.1)$$

where y_0 is the kinematically allowed upper bound of the y variable, involves an integration over the full phase space, it thus provides an important platform to complement the differential distributions and to determinate α_s .

The mean values of event shapes have been extensively measured and studied. At the present moment, pQCD predictions including NNLO QCD corrections [158, 159] based on CSS substantially underestimate experimental data.

PMC scales for the mean values of the event shapes are respectively:

$$\mu_r^{\text{pmc}}|_{\langle 1-T \rangle} = 0.0695\sqrt{s}, \text{ and } \mu_r^{\text{pmc}}|_{\langle C \rangle} = 0.0656\sqrt{s},$$

for thrust and the C-parameter. Both PMC scales are $\mu_r^{\text{pmc}} \ll \sqrt{s}$.

When taking $\sqrt{s} = M_Z = 91.1876$ GeV, the PMC scales are $\mu_r^{\text{pmc}}|_{\langle 1-T \rangle} = 6.3$ GeV and $\mu_r^{\text{pmc}}|_{\langle C \rangle} = 6.0$ GeV for the thrust and the C-parameter, respectively. The PMC scales of the differential distributions for the thrust and the C-parameter are also very small. The average of the PMC scales $\langle \mu_r^{\text{pmc}} \rangle$ of the differential distributions for the thrust and the C-parameter are close to the PMC scales $\mu_r^{\text{pmc}}|_{\langle 1-T \rangle}$ and $\mu_r^{\text{pmc}}|_{\langle C \rangle}$, respectively. This shows that PMC scale setting is self-consistent from the differential distributions to the mean values.

The results for the mean values of thrust and the C-parameter versus the center-of-mass energy \sqrt{s} are shown in Fig. 7.3. We note that the results obtained with conventional scale setting substantially deviate from experimental data. In contrast, PMC scale setting leads to improved mean values results for both thrust and the C-parameter. PMC predictions are in excellent agreement with experimental data over a wide range of energies.

We point out that PMC predictions eliminate the scale μ_r uncertainty thus errors estimated with the standard criteria are almost negligible. A better estimate of the unknown higher-order terms can be obtained by analyzing the magnitude of the perturbative corrections and the convergence of the series.

The relative magnitude of corrections for the C-parameter distribution is $C_{\text{LO}} : C_{\text{NLO}} : C_{\text{NNLO}} \sim 1 : 0.5 : 0.2$ [141] in the intermediate region using CSS. Using the PMC, the relative magnitude at NLO is improved to be $C_{\text{LO}} : C_{\text{NLO}} \sim 1 : 0.2$. The error estimate of an n th-order calculation for the unknown C_{n+1} term can be characterized by the last known term, i.e., $\pm C_n$, where n stands for LO, NLO,

NNLO, \dots . The unknown C_{n+1} term can be reasonably estimated assuming the same rate of increment of the last known order, $C_{n+1}/C_n = C_n/C_{n-1}$. Hence, in this case, we have that error bars are given by: $\pm 0.2C_n$ (as shown in Fig. 7.3).

Given the high level of agreement of the PMC predictions with the measurements, we can extract α_s to a very high precision.

Results are shown in Fig. 7.4. We notice an excellent agreement of the α_s values with the world average in the scale range of $1\text{GeV} < Q < 15\text{GeV}$.

The extracted α_s are not plagued by the scale μ_r uncertainty. In addition, unlike the α_s extracted from the differential distributions, the extracted α_s from the mean values are not afflicted with the large logarithms nor the non-perturbative effects.

7.3 $\alpha_s(M_Z)$ from χ^2 -fit

In order to obtain a reliable α_s at the scale of the Z^0 mass, we determine $\alpha_s(M_Z)$ from the fit of the PMC predictions to measurements. In particular, we perform the fit by minimizing the χ^2 respect to the $\alpha_s(M_Z)$ parameter. The variable χ^2 is defined as:

$$\chi^2 = \sum_i \left((\langle y \rangle_i^{\text{expt}} - \langle y \rangle_i^{\text{th}}) / \sigma_i \right)^2,$$

where $\langle y \rangle_i^{\text{expt}}$ is the value of the experimental data, σ_i is the corresponding experimental uncertainty and $\langle y \rangle_i^{\text{th}}$ is the theoretical prediction. The fit for thrust and the C-parameter leads to the results:

$$\begin{aligned} \alpha_s(M_Z^2) &= 0.1185 \pm 0.0011(\text{expt}) \pm 0.0005(\text{th}) \\ &= 0.1185 \pm 0.0012, \end{aligned} \tag{7.2}$$

with $\chi^2/\text{d.o.f.} = 27.3/20$ for the thrust mean value, and

$$\begin{aligned} \alpha_s(M_Z^2) &= 0.1193_{-0.0010}^{+0.0009}(\text{expt})_{-0.0016}^{+0.0019}(\text{th}) \\ &= 0.1193_{-0.0019}^{+0.0021}, \end{aligned} \tag{7.3}$$

with $\chi^2/\text{d.o.f.} = 43.9/20$ for the C-parameter mean value, where the first error is the experimental uncertainty and the second error is the theoretical uncertainty. Both results are consistent with the world average of $\alpha_s(M_Z^2) = 0.1181 \pm 0.0011$ [152].

The precision of the extracted α_s has been greatly improved by using the PMC: the dominant scale μ_r uncertainties are eliminated and the convergence of pQCD series is greatly improved. In particular, a strikingly much faster pQCD convergence is obtained for the thrust mean value [146], theoretical uncertainties are even smaller than the experimental uncertainties. We remark that these results for $\alpha_s(M_Z)$ are one of the most precise determinations of strong coupling at the Z^0 mass from event shape variables.

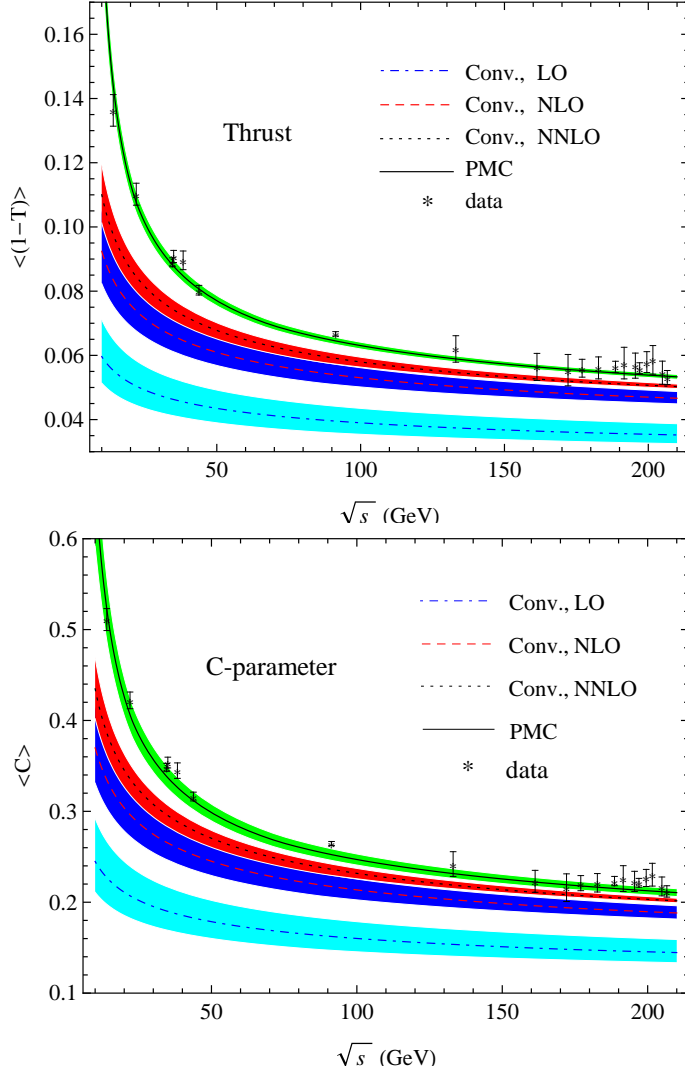


Figure 7.3: The mean values for the thrust and C-parameter versus the center-of-mass energy \sqrt{s} using CSS (Conv.) and PMC scale settings (from Ref. [149]). The dotdashed, dashed and dotted lines are the conventional results at LO, NLO and NNLO [158, 159], respectively, and the corresponding error bands are obtained by varying $\mu_r \in [M_Z/2, 2M_Z]$. The solid line is the PMC result and its error band is the squared average of the errors for $\alpha_s(M_Z) = 0.1181 \pm 0.0011$ [152] and for estimated unknown higher-order terms $\pm 0.2C_n$. The data are from the JADE and OPAL experiments, taken from [130, 160].

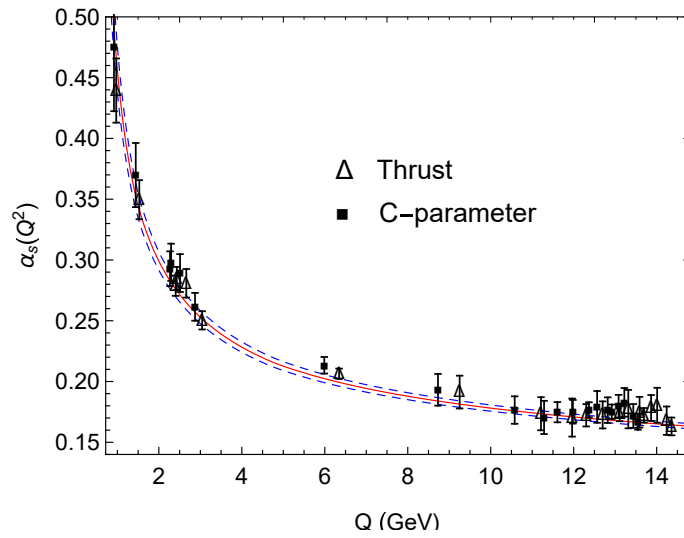


Figure 7.4: The coupling constant $\alpha_s(Q)$ extracted from the thrust and C-parameter mean values by comparing PMC predictions with the JADE and OPAL data [130, 160] in the $\overline{\text{MS}}$ scheme (from Ref. [149]). The error bars are the squared averages of the experimental and theoretical errors. The three lines are the world average evaluated from $\alpha_s(M_Z) = 0.1181 \pm 0.0011$ [152].

Chapter 8

Heavy-quark pair production near the threshold region

Heavy fermion pair production in e^+e^- annihilation near the threshold region is a fundamental process for the Standard Model and of considerable interest for various phenomena. The precise prediction of the production cross section for $e^+e^- \rightarrow \tau^+\tau^-$ at the threshold region is important in order to improve the measurement of the τ -lepton mass [161]. Precise theoretical predictions for the production cross section of $e^+e^- \rightarrow c\bar{c}/b\bar{b}$ at the thresholds are also crucial to determine the precise values of the c/b quark mass and of the coupling constant α_s determined by the sum rule method [162–164].

For the physics of the future high-energy electron-positron colliders, one of the most important goals is the precise measurement of top-quark properties, especially the top quark mass and width in the threshold region [165]; in order to reach the aimed precision, precise predictions for the top-quark pair production cross section are mandatory.

For heavy-fermion pair production in e^+e^- annihilation, it is well known that the Coulomb correction appears near the threshold region, and the fixed-order perturbative calculations are spoiled by the presence of singular terms. Physically, the

renormalization scale should become very soft in this region. However, the renormalization scale is usually set to the mass of the heavy fermion $\mu_r = m_f$ for the calculation of the production cross sections using standard CSS. Results are then affected by systematic errors, due to inherent scheme and scale uncertainties, and predictions are quite unreliable in this kinematic region. In this chapter, we apply the PMC to make a comprehensive analysis for heavy-fermion pair production in e^+e^- annihilation near the threshold region. We show that two distinctly different scales are determined for heavy fermion pair production near the threshold region and we show consistency of PMC scale setting with QED. For the purpose we show the results in both the modified minimal subtraction scheme ($\overline{\text{MS}}$ scheme) and the V-scheme and we compare the results with the QED GM-L scheme.

8.1 The QCD process of the quark pair production in the $\overline{\text{MS}}$ scheme

The interaction between two heavy quarks can be described at threshold by considering separate contributions arising from non-relativistic and hard processes dynamics. Non-relativistic contributions are determined by a non-relativistic potential that is essentially the result of the effects of a static Coulomb-like potential and of the linearly diverging confining term. While the hard contributions encompass virtual perturbative QCD corrections between heavy quarks in the final state. At the threshold, kinematic boundaries enhance the effects of the Coulomb non-relativistic terms that become large. Thus, we can distinguish two typologies of perturbative corrections for the heavy quark pair production cross section that we label as Coulomb and non-Coulomb corrections. The cross section for $e^+e^- \rightarrow \gamma^* \rightarrow Q\bar{Q}$ is known at two-loop level (Ref. [166]) and it is given by:

$$\sigma = \sigma^{(0)} \left[1 + \Delta^{(1)} a_s(\mu_r) + \Delta^{(2)}(\mu_r) a_s^2(\mu_r) + \mathcal{O}(a_s^3) \right], \quad (8.1)$$

where $a_s(\mu_r) = \alpha_s(\mu_r)/\pi$, μ_r is the renormalization scale. The LO cross section is

$$\sigma^{(0)} = \frac{4\pi\alpha^2}{3s} N_c e_Q^2 \frac{v(3-v^2)}{2}, \quad (8.2)$$

and the quark velocity v is

$$v = \sqrt{1 - \frac{4m_Q^2}{s}}. \quad (8.3)$$

Here, N_c is the number of colors, e_Q is the Q quark electric charge, s is the center-of-mass energy squared and m_Q is the mass of the heavy quark Q . The one-loop correction $\Delta^{(1)}$ near the threshold region can be written as

$$\Delta^{(1)} = C_F \left(\frac{\pi^2}{2v} - 4 \right). \quad (8.4)$$

The two-loop correction $\Delta^{(2)}$ can be conveniently split into terms proportional to various SU(3) color factors,

$$\begin{aligned} \Delta^{(2)} = & C_F^2 \Delta_A^{(2)} + C_F C_A \Delta_{NA}^{(2)} \\ & + C_F T_R n_f \Delta_L^{(2)} + C_F T_R \Delta_H^{(2)}. \end{aligned} \quad (8.5)$$

The terms $\Delta_A^{(2)}$, $\Delta_L^{(2)}$ and $\Delta_H^{(2)}$ are the same in either Abelian or non-Abelian theories; the term $\Delta_{NA}^{(2)}$ only arises in the non-Abelian theory. This process provides the opportunity to explore rigorously the scale-setting method in non-Abelian and Abelian theories.

The Coulomb corrections play an important role in the threshold region, since they are proportional to powers of $(\pi/v)^n$. This implies that the renormalization scale can be relatively soft in this region. Thus the PMC scales must be determined separately for the non-Coulomb and Coulomb corrections [27, 107]. When the quark velocity $v \rightarrow 0$, the Coulomb correction dominates the contribution of the production cross section, and the contribution of the non-Coulomb correction will be suppressed.

From general grounds, one expects threshold physics to be governed by the non-relativistic instantaneous potential.

The potential affects the cross section through final state interactions when the scale is above threshold; it leads to bound states when the scale is below threshold.

In order to apply the PMC, we write explicitly the n_f -dependent and n_f -independent parts in the Eq. 8.1, i.e.,

$$\begin{aligned}\sigma &= \sigma^{(0)} \left[1 + \Delta_h^{(1)} a_s(\mu_r) + \left(\Delta_{h,in}^{(2)}(\mu_r) + \Delta_{h,n_f}^{(2)}(\mu_r) n_f \right) a_s^2(\mu_r) \right. \\ &\quad + \left(\frac{\pi}{v} \right) \Delta_v^{(1)} a_s(\mu_r) + \left(\frac{\pi}{v} \right) \left(\Delta_{v,in}^{(2)}(\mu_r) + \Delta_{v,n_f}^{(2)}(\mu_r) n_f \right) a_s^2(\mu_r) \\ &\quad \left. + \left(\frac{\pi}{v} \right)^2 \Delta_{v^2}^{(2)} a_s^2(\mu_r) + \mathcal{O}(a_s^3) \right].\end{aligned}\quad (8.6)$$

The coefficients $\Delta_h^{(1)}$ and $\Delta_h^{(2)}$ are for the non-Coulomb corrections, and the coefficients $\Delta_v^{(1)}$, $\Delta_v^{(2)}$ and $\Delta_{v^2}^{(2)}$ are for the Coulomb corrections. These coefficients in the $\overline{\text{MS}}$ scheme are calculated in Refs. [166–168] and at the scale $\mu_r = m_Q$ they can be written as

$$\begin{aligned}\Delta_h^{(1)} &= -4 C_F, & \Delta_v^{(1)} &= \frac{C_F \pi}{2}, \\ \Delta_{h,in}^{(2)} &= -\frac{1}{72} C_F (C_A (302 + 468\zeta_3 + \pi^2(-179 + 192 \ln 2)) \\ &\quad - 2(-16(-11 + \pi^2) T_R + C_F (351 + 6\pi^4 - 36\zeta_3 \\ &\quad + \pi^2(-70 + 48 \ln 2))) + 24(3 C_A + 2 C_F) \pi^2 \ln v), \\ \Delta_{h,n_f}^{(2)} &= \frac{11 C_F T_R}{9}, \\ \Delta_{v,in}^{(2)} &= -\frac{1}{72} C_F \pi (-31 C_A + 144 C_F + 66 C_A \ln(2v)), \\ \Delta_{v,n_f}^{(2)} &= \frac{1}{18} C_F \pi T_R (-5 + 6 \ln(2v)), \\ \Delta_{v^2}^{(2)} &= \frac{C_F^2 \pi^2}{12}.\end{aligned}\quad (8.8)$$

After absorbing the nonconformal term $\beta_0 = 11/3 C_A - 4/3 T_R n_f$ into the coupling constant using the PMC, we achieve:

$$\begin{aligned}\sigma &= \sigma^{(0)} \left[1 + \Delta_h^{(1)} a_s(Q_h) + \Delta_{h,sc}^{(2)}(\mu_r) a_s^2(Q_h) \right. \\ &\quad \left. + \left(\frac{\pi}{v} \right) \Delta_v^{(1)} a_s(Q_v) + \left(\frac{\pi}{v} \right) \Delta_{v,sc}^{(2)}(\mu_r) a_s^2(Q_v) \right]\end{aligned}$$

$$+ \left(\frac{\pi}{v} \right)^2 \Delta_{v^2}^{(2)} a_s^2(Q_v) + \mathcal{O}(a_s^3) \Big]. \quad (8.9)$$

The PMC scales Q_i can be written as

$$Q_i = \mu_r \exp \left[\frac{3 \Delta_{i,n_f}^{(2)}(\mu_r)}{2 T_R \Delta_i^{(1)}} \right], \quad (8.10)$$

and the coefficients $\Delta_{i,\text{sc}}^{(2)}(\mu_r)$ are

$$\Delta_{i,\text{sc}}^{(2)}(\mu_r) = \frac{11 C_A \Delta_{i,n_f}^{(2)}(\mu_r)}{4 T_R} + \Delta_{i,\text{in}}^{(2)}(\mu_r), \quad (8.11)$$

where, $i = h$ and v stand for the non-Coulomb and Coulomb corrections, respectively. The nonconformal β_0 term is eliminated, and the resulting pQCD series matches the conformal series and thus only the conformal coefficients remain in the cross section. The conformal coefficients are independent of the renormalization scale μ_r . At the present two-loop level, the PMC scales are also independent of the renormalization scale μ_r . Thus, the resulting cross section in Eq. 8.9 eliminates the renormalization scale uncertainty.

Considering the color factors $C_A = 3$, $C_F = 4/3$ and $T_R = 1/2$ for QCD, the PMC scales in the $\overline{\text{MS}}$ scheme are

$$Q_h = e^{-11/24} m_Q \quad (8.12)$$

for the non-Coulomb correction, and

$$Q_v = 2 e^{-5/6} v m_Q \quad (8.13)$$

for the Coulomb correction. The scale Q_h stems from the hard gluon-virtual corrections, and thus it is determined from the short-distance process. The scale Q_v originates from the static Coulomb potential. As expected, the scale Q_h is of order m_Q , while the scale Q_v is of order $v m_Q$.

In the following, we take bottom-quark pair production as an example to make a detailed analysis near the threshold region. Taking $m_Q = 4.89$ GeV [170], we obtain

$$Q_h = 3.09 \text{ GeV}, \quad (8.14)$$

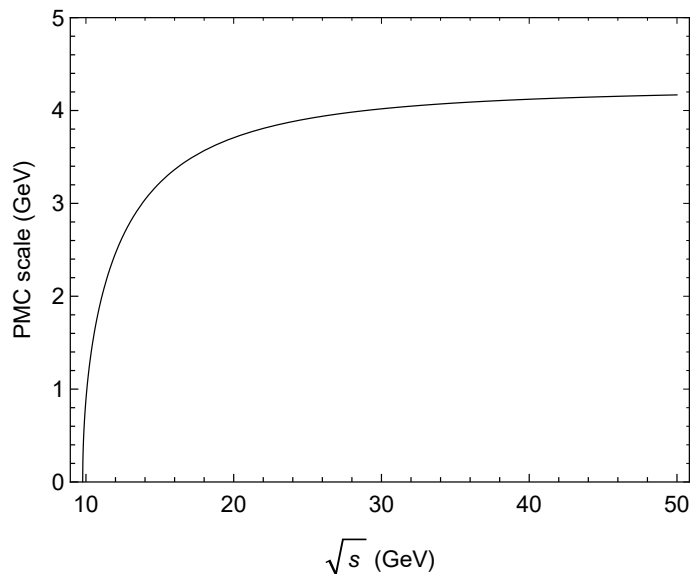


Figure 8.1: The PMC scale Q_v versus the center-of-mass energy \sqrt{s} for the b quark pair production in the $\overline{\text{MS}}$ scheme [169]. $m_Q = 4.89$ GeV.

which is smaller than m_Q in the $\overline{\text{MS}}$ scheme. For the Coulomb correction part, the scale Q_v is shown in Fig. 8.1. It shows that the scale Q_v depends continuously on the quark velocity v , and becomes soft for $v \rightarrow 0$, yielding the correct physical behavior of the scale and reflecting the virtuality of the QCD dynamics. Also the number of active flavors n_f changes with the quark velocity v according to the PMC scale.

When the quark velocity $v \rightarrow 0$, the small scale in the coupling constant shows that the perturbative QCD theory becomes unreliable and non-perturbative effects must be taken into account. One can adopt light-front holographic QCD [80] to evaluate α_s in the low-scale region.

In contrast, the renormalization scale is simply fixed to the typical scale $\mu_r = m_Q$ using CSS. Our calculations show that in the $\overline{\text{MS}}$ scheme, the scale should be $e^{-11/24} m_Q$, which is smaller than m_Q for the non-Coulomb correction. For the Coulomb correction, simply fixing the renormalization scale $\mu_r = m_Q$ obviously violates the physical behavior near the threshold region, since the scale becomes soft for $v \rightarrow 0$.

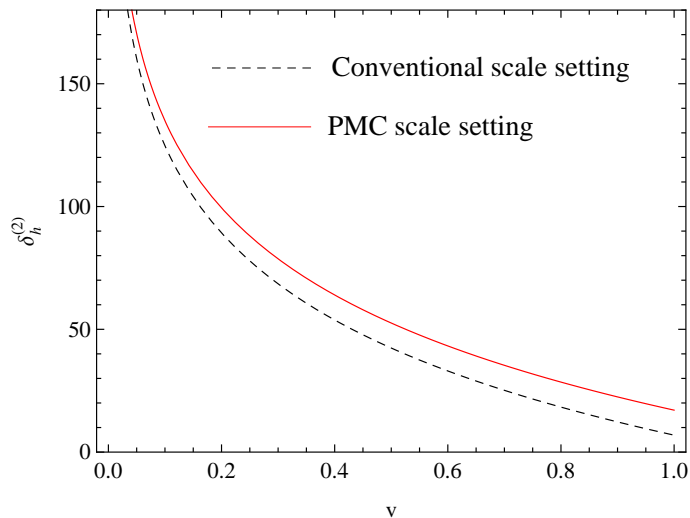


Figure 8.2: The two-loop coefficients $\Delta_h^{(2)}$ of the non-Coulomb correction in the $\overline{\text{MS}}$ scheme for the b quark pair production, where $\Delta_h^{(2)} = (\Delta_{h,in}^{(2)} + \Delta_{h,n_f}^{(2)} n_f)$ is for conventional scale setting while $\Delta_h^{(2)} = \Delta_{h,sc}^{(2)}$ is for PMC scale setting [169].

The two-loop coefficients $\Delta_h^{(2)}$ of the non-Coulomb correction in the $\overline{\text{MS}}$ scheme using conventional and PMC scale settings are shown in Fig. 8.2. We note that although the v -dependent behavior of the coefficients $\Delta_h^{(2)}$ is the same, their magnitudes are different using different scale settings. When the quark velocity $v \rightarrow 0$, both curves diverge $\Delta_h^{(2)} \rightarrow +\infty$ due to the presence of the term $-\ln v$. As expected, after multiplying this term by the v -factor in the LO cross section $\sigma^{(0)}$ given in Eq. 8.2, the contribution of the non-Coulomb corrections is finite and is suppressed near the threshold region, i.e. $(\sigma^{(0)} \Delta_h^{(2)} a_s^2) \rightarrow 0$ for the quark velocity $v \rightarrow 0$.

In the small relative velocity domain, i.e. ($v \ll 1$), the effect of multiple-photon exchange between charged particles becomes significant.

It was shown by Sommerfeld that the correction due to re-scattering of charged particles in the final state is proportional to the wave function at the origin squared, $|\Psi(0)|^2$. Thus, the annihilation process acquires some characteristics of the corresponding bound state. It was shown by Gamow-Sommerfeld-Sakharov [171–173] that the leading contributions α_s^n/v^n can be resummed using the so-called SGS

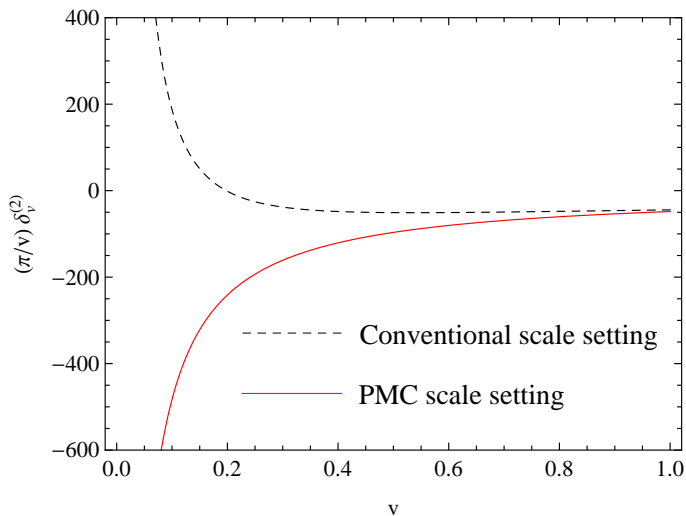


Figure 8.3: The two-loop coefficients $(\pi/v)\Delta_v^{(2)}$ of the Coulomb correction in the $\overline{\text{MS}}$ scheme for the b quark pair production, where $\Delta_v^{(2)} = (\Delta_{v,in}^{(2)} + \Delta_{v,n_f}^{(2)} n_f)$ is for conventional scale setting and $\Delta_v^{(2)} = \Delta_{v,sc}^{(2)}$ is for PMC scale setting [169].

factor:

$$T \equiv |\Psi(0)|^2 = \frac{z}{1 - \exp(-z)}, \quad (8.15)$$

with $z = \frac{C_F \alpha_s \pi}{v}$. Thus the Coulomb term of the form $(\pi/v)^2 \Delta_{v,2}^{(2)} a_s^2$ can be reabsorbed in the Sommerfeld rescattering formula [166].¹

For the Coulomb term of the form $(\pi/v) \Delta_v^{(2)} a_s^2$, we present the coefficients $(\pi/v)\Delta_v^{(2)}$ in the $\overline{\text{MS}}$ scheme using conventional and PMC scale settings in Fig. 8.3. It shows that when the quark velocity $v \rightarrow 0$, the v -dependent behavior of the coefficients $(\pi/v)\Delta_v^{(2)}$ is dramatically different using conventional and PMC scale settings. In the case of conventional scale setting, its behavior is $(\pi/v)\Delta_v^{(2)} \rightarrow +\infty$ for $v \rightarrow 0$ due to the presence of the term $-\ln v/v$. After multiplying this term by the v -factor in the LO cross section $\sigma^{(0)}$, the contribution of the Coulomb cor-

¹It is also believed that the subleading terms α_s^{n+1}/v can be resummed by adding a hard coefficient factor, such as:

$$\sigma = \sigma^{(0)} \left(1 - 4C_F \frac{\alpha_s}{\pi}\right) |\Psi(0)|^2.$$

rection using conventional scale setting is not finite, i.e., $(\sigma^{(0)} (\pi/v) \Delta_v^{(2)} a_s^2) \rightarrow +\infty$ for $v \rightarrow 0$. It should be stressed that the term $\ln v$ vanishes, and the term $-1/v$ remains in the conformal coefficient after applying PMC scale setting. Thus the v -dependent behavior is $(\pi/v) \Delta_v^{(2)} \rightarrow -\infty$ for $v \rightarrow 0$. This term $-1/v$ is cancelled by multiplying it by the v -factor in the LO cross section $\sigma^{(0)}$, and thus the contribution of the Coulomb correction using PMC scale setting is finite for $v \rightarrow 0$. For $v \rightarrow 1$, contributions of the Coulomb correction using conventional and PMC scale settings are both suppressed.

8.2 Quark-pair production in the V-scheme

In order to investigate possible scheme dependence effects, we perform the above analysis also in a different scheme. Particularly suitable for the purpose is the scheme defined by the effective charge $a_s^V = \alpha_V/\pi$ (V-scheme) given by the static potential between two heavy quarks [69–75],

$$V(Q^2) = -\frac{4\pi^2 C_F a_s^V(Q)}{Q^2}, \quad (8.16)$$

which provides a physically-based alternative to the usual $\overline{\text{MS}}$ scheme. Analogously to QED and the GM-L scheme, setting the scale to the virtuality of the exchanged gluon, all vacuum polarization corrections are resummed into the coupling a_s^V . By using the relation between a_s and a_s^V at the one-loop level, i.e.,

$$a_s^V(Q) = a_s(Q) + \left(\frac{31}{36} C_A - \frac{5}{9} T_R n_f \right) a_s^2(Q) + \mathcal{O}(a_s^3), \quad (8.17)$$

we can perform the change of scheme for Eq. 8.6, from the $\overline{\text{MS}}$ scheme to the V-scheme. Thus, the corresponding perturbative coefficients in the V-scheme are:

$$\sigma^{(0)}|_V = \sigma^{(0)}, \quad (8.18)$$

$$\Delta_h^{(1)}|_V = \Delta_h^{(1)}, \quad \Delta_v^{(1)}|_V = \Delta_v^{(1)}, \quad (8.19)$$

$$\begin{aligned}
\Delta_{h,in}^{(2)}|_V &= \Delta_{h,in}^{(2)} - \frac{31}{36} C_A \Delta_h^{(1)}, \\
\Delta_{h,n_f}^{(2)}|_V &= \Delta_{h,n_f}^{(2)} + \frac{5}{9} T_R \Delta_h^{(1)}, \\
\Delta_{v,in}^{(2)}|_V &= \Delta_{v,in}^{(2)} - \frac{31}{36} C_A \Delta_v^{(1)}, \\
\Delta_{v,n_f}^{(2)}|_V &= \Delta_{v,n_f}^{(2)} + \frac{5}{9} T_R \Delta_v^{(1)}, \\
\Delta_{v^2}^{(2)}|_V &= \Delta_{v^2}^{(2)}.
\end{aligned} \tag{8.20}$$

And the corresponding PMC scales in the V-scheme are:

$$Q_h = e^{3/8} m_Q \tag{8.21}$$

for the non-Coulomb correction, and

$$Q_v = 2v m_Q \tag{8.22}$$

for the Coulomb correction. Again, in the V-scheme, Q_h is of order m_Q , while Q_v is of order $v m_Q$, since the scale Q_h originates from the hard-gluon virtual corrections, and Q_v originates from Coulomb rescattering. The physical behavior of the scales does not change using different renormalization schemes. We notice that the difference between the PMC scales in the $\overline{\text{MS}}$ scheme and in the physically-based V-scheme is given by e^{δ_C} scheme factor. This difference is unphysical and is a consequence of the particular convention adopted.

The PMC scale eliminates this conventional dependence (i.e. this RS dependence). Scheme independent relations between two effective charges can be achieved by ‘‘commensurate scale relations’’ (CSR) [86, 108] as discussed in Sec.3.

For b -quark production, setting the mass to $m_Q = 4.89$ GeV, we obtain the scale $Q_h = 7.11$ GeV for the non-Coulomb correction, and its value larger than the conventional choice $\mu_r = m_Q$. The scale for the Coulomb correction depends on the velocity v , we show the Q_v scale versus the center-of-mass energy \sqrt{s} in the V-scheme in Fig. 8.4. The exponent disappears in Eq. 8.22 compared to the scale in Eq. 8.13 in the $\overline{\text{MS}}$ scheme. The scale Q_v becomes soft for $v \rightarrow 0$, and $Q_v \rightarrow 2m_Q$ for $v \rightarrow 1$, showing the correct physical behavior.

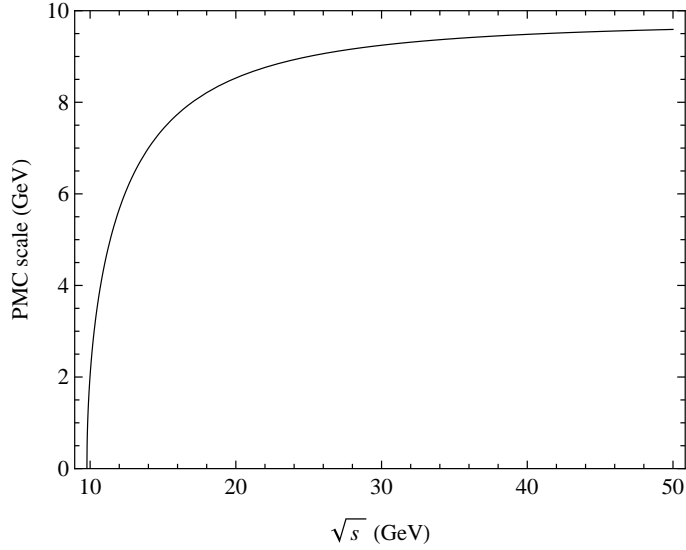


Figure 8.4: The PMC scale Q_v versus the center-of-mass energy \sqrt{s} for the b quark pair production in the V-scheme [169]. $m_Q = 4.89$ GeV.

As in the case of the $\overline{\text{MS}}$ scheme, the v -dependent behavior of the coefficients $\Delta_h^{(2)}$ of the non-Coulomb correction in the V-scheme using conventional and PMC scale settings is the same. The two-loop coefficients $(\pi/v)\Delta_v^{(2)}$ of the Coulomb correction in the V-scheme using conventional and PMC scale settings are presented in Fig. 8.5. Figure 8.5 shows that close to the threshold region, the v -dependent behavior of the coefficients $(\pi/v)\Delta_v^{(2)}$ using conventional and PMC scale settings is dramatically different. When the quark velocity $v \rightarrow 0$, the coefficient is $(\pi/v)\Delta_v^{(2)} \rightarrow +\infty$ due to the presence of the term $-\ln v/v$ using conventional scale setting. After applying PMC scale setting, the coefficient is $(\pi/v)\Delta_v^{(2)} \rightarrow -\infty$ due to the term $\ln v$ vanishes and the term $-1/v$ remains in the conformal coefficient. Thus, multiplying by the v -factor in the LO cross section $\sigma^{(0)}$, the contribution of the Coulomb correction for $v \rightarrow 0$ is not finite using conventional scale setting and is finite after using PMC scale setting. It is noted that quark-pair and lepton-pair production in e^+e^- annihilation near the threshold region should show similar physical behavior. This dramatically different behavior of the $(\pi/v)\Delta_v^{(2)}$ between conventional and PMC scale settings near the threshold region should be checked in QED.

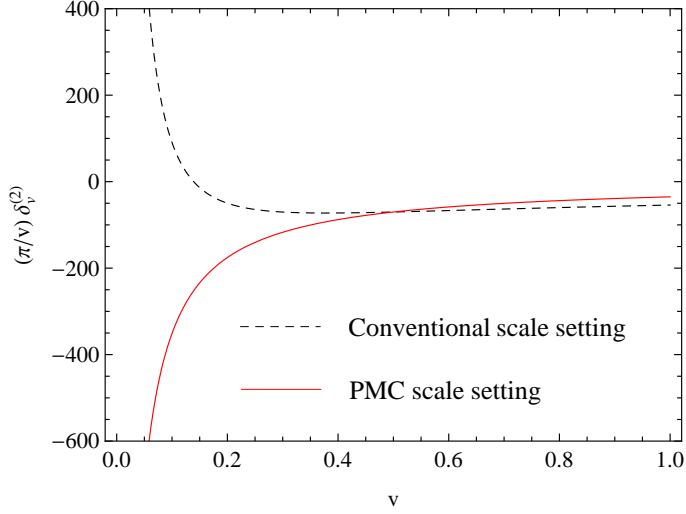


Figure 8.5: The two-loop coefficients $(\pi/v)\Delta_v^{(2)}$ of the Coulomb correction in the V-scheme for the b quark pair production, where $\Delta_v^{(2)} = (\Delta_{v,in}^{(2)}|_V + \Delta_{v,n_f}^{(2)}|_V n_f)$ is for conventional scale setting and $\Delta_v^{(2)} = \Delta_{v,sc}^{(2)}|_V$ is for PMC scale setting [169].

8.3 Lepton pair production

Similar to quark-pair production, the lepton-pair production cross section for the QED process $e^+e^- \rightarrow \gamma^* \rightarrow l\bar{l}$ is expanded in the QED fine structure constant α . According to the previous analysis, we can split the cross section into non-Coulomb and Coulomb parts. Perturbative coefficients for the lepton-pair production cross section can be obtained from Eq. 8.6 by replacing the QCD color factors: $C_A = 3$, $C_F = 4/3$ and $T_R = 1/2$ with the corresponding QED [166, 174, 175]: $C_A = 0$, $C_F = 1$ and $T_R = 1$.

Applying the PMC, vacuum-polarization corrections can be absorbed into the QED running coupling, according to:

$$\alpha(Q) = \alpha \left[1 + \left(\frac{\alpha}{\pi} \right) \sum_{i=1}^{n_f} \frac{1}{3} \left(\ln \left(\frac{Q^2}{m_i^2} \right) - \frac{5}{3} \right) \right], \quad (8.23)$$

where m_i is the mass of the light virtual lepton, and is far smaller than the final-state lepton mass m_l .

The resulting PMC scales can be written as

$$Q_i = m_l \exp \left[\frac{5}{6} + \frac{3}{2} \frac{\Delta_{i,n_f}^{(2)}}{\Delta_i^{(1)}} \right], \quad (8.24)$$

where, $i = h$ and v stand for the non-Coulomb and Coulomb corrections, respectively. After absorbing the vacuum polarization corrections into the QED running coupling, the coefficients $\Delta_{i,n_f}^{(2)}$ vanish. According to the replacements $C_A = 0$, $C_F = 1$ and $T_R = 1$ for QED, the PMC scales become:

$$Q_h = e^{3/8} m_l \quad (8.25)$$

for the non-Coulomb correction, and

$$Q_v = 2 v m_l \quad (8.26)$$

for the Coulomb correction.

PMC scales show the same physical behavior from QCD to QED. It is noted that PMC scales in Eqs. 8.21 and 8.22 for QCD in the V-scheme coincide with the QED scales in Eqs. 8.25) and 8.26, respectively. This result was expected for self-consistency, given that the PMC method in QCD agrees with the standard Gell-Mann-Low method [4] in QED. We also point out that the V-scheme provides a natural scheme for the QCD process for quark-pair production.

In the following, we take τ -lepton pair production as an example to make a detailed analysis near the threshold region. Taking $m_\tau = 1.777$ GeV [152], we obtain the scale $Q_h = 2.59$ GeV, which is larger than the scale m_τ for non-Coulomb correction. For the Coulomb correction, as in the case of QCD, the scale becomes soft for $v \rightarrow 0$ and $Q_v \rightarrow 2m_l$ for $v \rightarrow 1$. The PMC scales thus rigorously yield the correct physical behavior for the lepton pair production near the threshold region.

Non-Coulomb corrections have the same v -dependent behavior for the coefficients $\Delta_h^{(2)}$ independently of the use of conventional or PMC scale settings, as for the QCD case. For the Coulomb correction, we show the coefficients $(\pi/v)\Delta_v^{(2)}$ using conventional and PMC scale settings in Fig. 8.6.

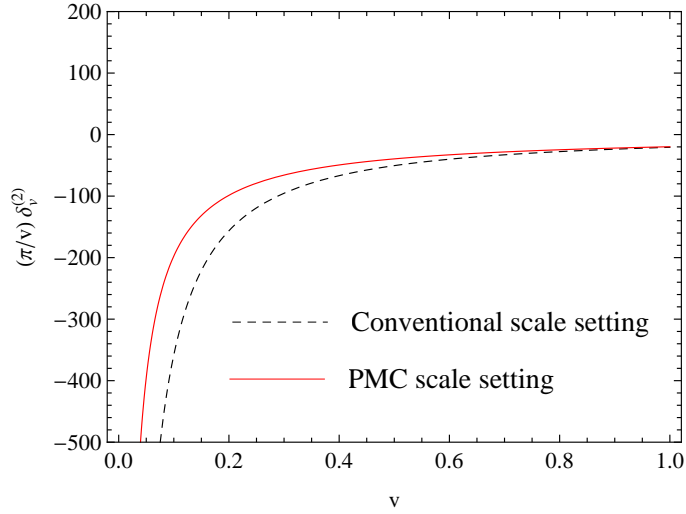


Figure 8.6: The two-loop coefficients $(\pi/v)\Delta_v^{(2)}$ of the Coulomb correction for the τ lepton pair production, where $\Delta_v^{(2)} = (\Delta_{v,in}^{(2)} + \Delta_{v,n_f}^{(2)} n_f)$ is for conventional scale setting and $\Delta_v^{(2)} = \Delta_{v,in}^{(2)}$ is for PMC scale setting ([169]).

It is noted that in contrast with the QCD case, using the CSS, when the quark velocity $v \rightarrow 0$, the coefficient $(\pi/v)\Delta_v^{(2)} \rightarrow -\infty$ due to the presence of the term $\ln v/v$; while using the PMC the coefficient $(\pi/v)\Delta_v^{(2)} \rightarrow -\infty$ due to the presence of the term $-1/v$. Multiplying by the v -factor in the LO cross section $\sigma^{(0)}$, the contribution of the Coulomb correction is given by: $(\sigma^{(0)} (\pi/v) \Delta_v^{(2)} (\alpha/\pi)^2) \rightarrow -\infty$ for $v \rightarrow 0$ using conventional scale setting, and is a finite for $v \rightarrow 0$ using PMC scale setting. We note that using different scale setting we achieve opposite behaviors, as shown in Figs. 8.3, 8.5 and 8.6, but only the PMC is in agreement with the QED results of the GM-L scheme. Moreover, scale setting affects results for the Coulomb corrections that are finite when using the PMC scale setting, and in contrast diverge when using conventional scale setting for both QCD and QED.

Summary

We briefly summarize here the results.

- I) In section 5 we have illustrated the PMC_∞ method and how it applies to either numerical or analytical calculated observables. The approach of the PMC_∞ is totally general and can be applied to any perturbative calculation, such as fully integrated cross sections and also differential distributions. This new approach preserves intrinsic conformality (iCF), which introduces a new concept of scale invariance: ordered scale invariance, i.e. the scale invariance of any combination of conformal subsets. In this approach scale invariance is preserved perturbatively, analogously to gauge invariance.

In this thesis we have also presented a new procedure to identify the conformal coefficients and the PMC_∞ -scales valid to all orders, which can be applied to either numerical or analytical calculations. The PMC_∞ preserves the (A,B,C,D,E,F) properties of the BLM/PMC method: it eliminates renormalon growth $\alpha_s^{n+1}\beta_0^n n!$, scheme dependence and all uncertainties related to the scale ambiguity up to the order of accuracy. The iCF/ PMC_∞ scales are identified by the lowest order logarithm related to the β_0 -term at each order and all the physics of the process is contained in the conformal coefficients. This is in complete agreement with QED and with the Gell-Mann and Low scheme [17, 32].

We have discussed why iCF should be considered a strict requirement for a theory in order to preserve the scale invariance of the observables and we have

shown that iCF is consistent with the single-variable thrust and C-parameter distributions. We point out that other conformal aspects of QCD resulting from different sectors such as Commensurate Scale Relations-CSR [86] or dual theories as AdS/CFT [176] might also be related to the intrinsic conformality. We underline that the iCF property in a theory would have two main remarkable consequences: first, it indicates the correct coupling constant at each order as a function of the intrinsic conformal scale μ_N , and second, since only the conformal and the β_0 coefficients need to be identified in the observables at each order, by means of the PMC_∞ method the iCF would reveal its predictive feature for the coefficients of the higher order color factors. We point out that in many cases implementation of the iCF in a multi-loop calculations procedure would lead to a significant reduction of the color-factor coefficients and it would speed up the calculations for higher order corrections.

- II) In section 5.5 we have shown results for thrust and the C-parameter for $e^+e^- \rightarrow 3jets$, comparing the two methods for setting the renormalization scale in pQCD: the Conventional Scale Setting (CSS) and the infinite-order scale setting based on the Principle of Maximum Conformality (PMC_∞). The PMC_∞ has been applied to the NNLO thrust and C-parameter distributions and the results show perfect agreement with the experimental data. The evaluation of theoretical errors using standard criteria show that the PMC_∞ significantly improves the theoretical predictions over the entire spectra of the shape variables. We have shown that PMC_∞ works particularly well for the case of the event shape variables, where we found an extremely good agreement of the n_f coefficients with the iCF parametrization. We point out that in fixed order calculations the PMC_∞ last scale is set to the kinematic scale of the process: in this case $\mu_{III} = \sqrt{s} = M_Z$. As shown in Eq. 5.6, the scale dependence on the initial scale is totally confined in the last subset σ_n . Thus the the last term in the iCF determines the level of *conformality* reached by

the expansion and is entangled with theoretical uncertainties given by higher order uncalculated terms. Any variation of the last scale has to be intended to evaluate theoretical uncertainties given by higher order contributions and not as an ambiguity of the PMC_∞ method [177]. Evaluation of the theoretical errors using standard criteria shows that the PMC_∞ significantly improves the precision of the pQCD calculations for thrust and C-parameter. We remark that an improved analysis of theoretical errors might be obtained by giving a prediction of the contributions of higher order terms using a statistical approach as shown in Refs. [178,179]. This would lead to a more rigorous method to evaluate errors and thus to restrict the range of the last PMC_∞ scale that, as we have shown here, can also be fixed to the last known PMC_∞ one leading to precise and stable predictions.

- III) In section 6 we have investigated, for the first time, the thrust distribution in the conformal window of pQCD and in the QED limit. Assuming, for phenomenological reasons, the physical value of the strong coupling to be that of the Z^0 mass scale, it restricts the conformal window range, at two loops, to be within $\frac{34N_c^3}{13N_c^2-3} < N_f < \bar{N}_f$ with $\bar{N}_f \simeq 15.22$. The closer N_f is to the higher value, the more perturbative and conformal the system is. In this region, we have shown that the PMC_∞ leads to a higher precision with a theoretical error that tends to zero. Moreover, results for the thrust distribution in the conformal window have similar shapes to those of the physical values of N_f and the position of the peak is preserved when one applies the PMC_∞ method. Comparison with the experimental data indicates also that PMC_∞ agrees with the expected number of flavors. A good fit with experimental data is shown by the PMC_∞ results for the range $5 < N_f < 6$, which agrees with the active number of flavors of the Standard Model. Outside the pQCD conformal window the PMC_∞ leads to a higher precision with respect to the CSS. In addition, calculations for the QED thrust shown in section 6.2 reveal a perfect

consistency of the PMC_∞ with QED when taking the QED limit of QCD for both the PMC_∞ scale and for the regularization η parameter which tends to the same QCD value.

IV) In section 7 we have presented a novel method to determine the strong coupling constant from event-shape variables. Though the event-shape variables, especially those for the process $e^+e^- \rightarrow 3jets$, are particularly suitable for the determination of the strong coupling constant $\alpha_s(M_Z)$, results obtained by using CSS do not match the experimental average value and event-shape distributions underestimate the experimental data at NNLO. Some extracted α_s from event shapes by the CSS may also seem quite unrealistic. Our analysis suggests that these conventional difficulties can be overcome by using the PMC renormalization scale setting leading to a comprehensive and self-consistent analysis for both the differential distributions and the mean values for event shapes. The physical observable should be independent of the choice of renormalization scale. The PMC scale yields the renormalization scale-independent physical behavior and reflects the virtuality of the QCD dynamics. Thus the PMC provides a remarkable way to verify the running of $\alpha_s(Q)$ from the event shape differential measurement at a single energy of \sqrt{s} . The values of $\alpha_s(M_Z)$ determined are consistent with the world average and are more precise than the values obtained from previous analysis performed on the same data. Recently in Ref. [180], this method has also been extended to the other event-shape variables B_W, B_T, ρ .

V) In section 8 we have investigated heavy-fermion pair production in e^+e^- annihilation as a fundamental process of the SM. In the kinematic region close to threshold, two major distinct contributions arise in perturbative calculations given by the static Coulomb-like rescattering potential and non-Coulomb hard-gluon virtual corrections. The conventional procedure of simply setting the renormalization scale as $\mu_r = m_f$ violates the physical behavior and leads

to unreliable predictions near the threshold region. In contrast, the PMC scale-setting method provides a self-consistent analysis, and reveals perfect agreement for the physical behavior of the scale near the threshold region, between QED and QCD. This fundamental process shows a peculiar situation where two distinctly different scales are applied using the PMC. The scale determined for the hard virtual correction is of order the fermion mass m_f ; the scale determined for the Coulomb rescattering is of order $v m_f$, which becomes soft at the threshold, given that $v \rightarrow 0$. This reflects the physical virtuality of the exchanged gluons (or photons), given by the dynamics of the underlying physical QCD (or QED) process.

- While non-Coulomb corrections for fermion pair production are suppressed near the threshold region, the Coulomb corrections diverge in this kinematic region, using CSS. In contrast, the v -dependent behavior of the scale changes after using PMC scale setting, turning into a perfectly consistent behavior from QCD to QED. The divergence is given only by the higher-order $(\pi/v)^n a_s^n$ -Coulomb terms, and the proper resummation using the Sommerfeld (SGS) rescattering formula leads to a finite result. A finite prediction can also be obtained using the PMC scale setting in both QCD and in QED.
- A straight comparison between QED and QCD is obtained using the V-scheme, which provides a natural scheme for the QCD calculation for the quark pair production process. Converting the QCD calculations in the $\overline{\text{MS}}$ scheme to the V-scheme, the resulting PMC predictions in the QED limit are consistent with the GM-L scheme. QCD and QED scales differ only by a scheme factor: $Q_{\text{QCD}}^2/Q_{\text{QED}}^2 = e^{-5/3}$; this factor converts the underlying scale predictions in the $\overline{\text{MS}}$ scheme used in QCD to the scale of the V-scheme conventionally used in QED [108]. In fact, the PMC scales are: $Q_h = e^{3/8} m_f$ for the hard virtual correction and $Q_v = 2 v m_f$ for Coulomb rescattering for both QCD and QED. The predictions in the V-scheme based on the conventional scale-setting

method do not agree with the QED limit where the renormalization scale can be set unambiguously by using the GM-L method. The PMC scale-setting method in QCD can be reduced in the Abelian limit $N_c \rightarrow 0$ to the Gell-Mann-Low method. This consistency provides strong support for the PMC scale-setting method.

Conclusions

In this thesis we have introduced a new scale setting procedure, namely PMC_∞ , which stems from the general Principle of Maximum Conformality (PMC) and preserves a particular property that we have defined as *intrinsic conformality* (iCF). The iCF is a particular parametrization of the perturbative series that preserves exactly the scale invariance of an observable perturbatively. The PMC_∞ solves the conventional renormalization-scale ambiguity in QCD, it preserves not only the iCF but also all the features of the PMC approach and leads to a final conformal series at any order of the perturbative calculation. In fact, the final series is given by perturbative conformal coefficients with the couplings determined at conformal renormalization scales. This method agrees with the BLM/PMC_m approach at LO and given the uniqueness of the iCF, any other alternative method, e.g. the method proposed in Ref. [177], which we indicate as “PMCa”, to fix a scale in order to obtain a perturbative scale-invariant quantity leads to the same results as the PMC_∞ , as shown in Ref. [181]. Unlike the previous BLM/PMC approaches, the PMC_∞ scales are not perturbatively calculated, but are conformal functions of the physical scale/scales of the process and any other non-integrated momentum/variable, e.g. the event-shape variable $(1 - T)$ or C .

The PMC_∞ is totally independent of the initial scale μ_0 used for renormalization in perturbative calculations and it preserves the scale invariance at any stage of calculation, independently of the kinematic boundary conditions, independently of the starting order of the observable or the order of the truncated expansion.

The iCF improves the general BLM/PMC procedure and the point “3” of sec-

tion 3.4. In the same section, we have suggested that an improvement and simplification of the perturbatively calculated BLM/PMC scales, would be achieved by setting the renormalization scale μ_R directly to the physical scale Q of the process, before applying the BLM/PMC procedure. This would remove the initial scale μ_0 dependence from the perturbatively calculated BLM/PMC scales.

We underline that in contrast with the other PMCm and PMCs approach the PMC_∞ preserves the iCF, thus scales are set automatically in kinematic regions where kinematic constraints cancel the effects of the lower order conformal coefficients. These effects are particularly visible in the case of event-shape variables in the multi-jet regions. The iCF effects in these kinematic regions are neglected by the PMCm and PMCs approach, unless an *ad hoc* prescription is introduced. As recently shown in Refs. [182] and [181], application of the PMC_∞ improves the theoretical predictions for $\Gamma(H \rightarrow gg)$, $R_{e^+e^-}$, R_τ , $\Gamma(H \rightarrow b\bar{b})$ with respect to the CSS. It has been noted in Ref. [181] that in general also the PMCs approach works remarkably well especially for fully integrated quantities.

We point out that this approach may have an effect of averaging the differences of the PMCm/ PMC_∞ scales arising at each order, which might be significant for the precision of a prediction at a certain level of accuracy.

However, given the small differences that we have found in the first two consecutive PMC_∞ scales, i.e. μ_I, μ_{II} , in the LO allowed kinematic region, i.e. $0 < (1 - T) < 1/3$ and in $0 < C < 0.75$, we may argue that in the same accessible kinematic domain two consecutive PMC_∞ scales have such small differences that a single-scale approach, such as the PMCs, would be justified leading to analogously precise predictions.

We recall that only the n_f terms related to the UV diverging diagrams (i.e. the N_f terms) must be reabsorbed into the PMC_∞ scales. Thus PMC_∞ perfectly agrees with the PMCm when an observable has a manifest iCF form. We remark that the iCF underlies scale invariance perturbatively, i.e. the ordered scale invariance. We also remark that PMC_∞ agrees with the single-scale approach PMCs in the

case of an observable with a particular iCF form with all scales equal, i.e. $\mu_I = \mu_{II} = \mu_{III} \dots = \mu_N$. In this sense the PMCM and PMCs may be considered more as “optimization procedures” that follow the purpose of the maximal conformal series by transforming the original perturbative series into an iCF-like final series by using the PMC scales. In contrast, the PMC_∞ does not indicate any particular value of the renormalization scale to be used, but indicates the final limit obtained by each conformal subset and then by the perturbative expansion once all the terms related to each conformal subset are resummed. The PMC_∞ is RG invariant at each order of accuracy, which means we can perform a change of scale at any stage and reobtain the initial perturbative quantity. In this sense PMC_∞ is not to be understood as an “optimization procedure”, but as an explicit RG invariant form to parametrize a perturbative quantity that leads faster to the conformal limit. By setting the renormalization scale of each subset to the corresponding PMC_∞ scale, one simply cancels the infinite series of β terms, leading to the same conformal result as the original series. Given that both scales and coefficients are conformal in the PMC_∞ , also the scheme and scale dependence is completely removed in the perturbative series up to infinity. It has been pointed out in Ref. [181], that the PMC_∞ scale might become quite small at a certain order and that PMC_∞ retains the second kind of scale dependence. We underline that the last scale in the PMC_∞ controls the level of convergence and the conformality of the perturbative series and is thus entangled with the theoretical error of a given prediction. According to the PMC_∞ procedure the last scale must be set to the invariant physical scale of the process, given by $\sqrt{s}, M_H \dots$. We have shown in this thesis that the usual PMC practice of setting the last scale equal to the last unknown scale is consistent also for the PMC_∞ and leads to precise and stable results. At the moment, improvements to these points are under investigation.

We remark that the evaluation of the theoretical errors using standard criteria, shows that the PMC_∞ significantly improves the precision of the pQCD calculations and eliminates the scheme and scale ambiguities. An improved analysis of

theoretical errors might be obtained by using a statistical approach for evaluating the contributions of the uncalculated higher order terms as shown in Refs. [178,179]. This approach would lead to a more rigorous method to evaluate errors giving also indications on the possible range of values for the last unknown PMC_∞ scale.

Bibliography

- [1] Charalampos Anastasiou, Claude Duhr, Falko Dulat, Elisabetta Furlan, Thomas Gehrmann, Franz Herzog, Achilleas Lazopoulos, and Bernhard Mistlberger. High precision determination of the gluon fusion Higgs boson cross-section at the LHC. *JHEP*, 05:058, 2016.
- [2] Stefano Catani, Simone Devoto, Massimiliano Grazzini, Stefan Kallweit, and Javier Mazzitelli. Bottom-quark production at hadron colliders: fully differential predictions in NNLO QCD. *JHEP*, 03:029, 2021.
- [3] Ernst Carl Gerlach Stueckelberg de Breidenbach and Andreas Petermann. Normalization of constants in the quanta theory. *Helv. Phys. Acta*, 26:499–520, 1953.
- [4] Murray Gell-Mann and F. E. Low. Quantum electrodynamics at small distances. *Phys. Rev.*, 95:1300–1312, 1954.
- [5] A. Peterman. Renormalization Group and the Deep Structure of the Proton. *Phys. Rept.*, 53:157, 1979.
- [6] Curtis G. Callan, Jr. Broken scale invariance in scalar field theory. *Phys. Rev. D*, 2:1541–1547, 1970.
- [7] K. Symanzik. Small distance behavior analysis and Wilson expansion. *Commun. Math. Phys.*, 23:49–86, 1971.

- [8] William Celmaster and Richard J. Gonsalves. The Renormalization Prescription Dependence of the QCD Coupling Constant. *Phys. Rev. D*, 20:1420, 1979.
- [9] Andrzej J. Buras. Asymptotic Freedom in Deep Inelastic Processes in the Leading Order and Beyond. *Rev. Mod. Phys.*, 52:199, 1980.
- [10] Paul M. Stevenson. Resolution of the Renormalization Scheme Ambiguity in Perturbative QCD. *Phys. Lett. B*, 100:61–64, 1981.
- [11] Paul M. Stevenson. Optimized Perturbation Theory. *Phys. Rev. D*, 23:2916, 1981.
- [12] Paul M. Stevenson. Optimization and the Ultimate Convergence of QCD Perturbation Theory. *Nucl. Phys. B*, 231:65–90, 1984.
- [13] P. Stevenson. Sense and Nonsense in the Renormalization Scheme Dependence Problem. *Nucl. Phys. B*, 203:472–492, 1982.
- [14] G. Grunberg. Renormalization Group Improved Perturbative QCD. *Phys. Lett. B*, 95:70, 1980. [Erratum: *Phys.Lett.B* 110, 501 (1982)].
- [15] G. Grunberg. Renormalization Scheme Independent QCD and QED: The Method of Effective Charges. *Phys. Rev. D*, 29:2315–2338, 1984.
- [16] G. Grunberg. On Some Ambiguities in the Method of Effective Charges. *Phys. Rev. D*, 40:680, 1989.
- [17] Stanley J. Brodsky, G. Peter Lepage, and Paul B. Mackenzie. On the Elimination of Scale Ambiguities in Perturbative Quantum Chromodynamics. *Phys. Rev. D*, 28:228, 1983.
- [18] L. F. Abbott. Choosing an Expansion Parameter for QCD. *Phys. Rev. Lett.*, 44:1569, 1980.

- [19] G. 't Hooft. The Whys of Subnuclear Physics. In *Proc. Intern. School of Subnuclear Physics (Erice, 1977)*, page 943. ed. A. Zichichi (Plenum, New York, 1979).
- [20] C. F. Berger, Z. Bern, Lance J. Dixon, Fernando Febres Cordero, D. Forde, T. Gleisberg, H. Ita, D. A. Kosower, and D. Maitre. Next-to-Leading Order QCD Predictions for W+3-Jet Distributions at Hadron Colliders. *Phys. Rev. D*, 80:074036, 2009.
- [21] Xing-Gang Wu, Stanley J. Brodsky, and Martin Mojaza. The Renormalization Scale-Setting Problem in QCD. *Prog. Part. Nucl. Phys.*, 72:44–98, 2013.
- [22] Alexandre Deur, Stanley J. Brodsky, and Guy F. de Teramond. The QCD Running Coupling. *Nucl. Phys.*, 90:1, 2016.
- [23] G. Kramer and B. Lampe. Jet production rates at LEP and the scale of alpha-s. *Z. Phys. A*, 339:189–193, 1991.
- [24] Stanley J. Brodsky and Xing-Gang Wu. Self-Consistency Requirements of the Renormalization Group for Setting the Renormalization Scale. *Phys. Rev. D*, 86:054018, 2012.
- [25] Stanley J. Brodsky and Leonardo Di Giustino. Setting the Renormalization Scale in QCD: The Principle of Maximum Conformality. *Phys. Rev. D*, 86:085026, 2012.
- [26] Stanley J. Brodsky and Xing-Gang Wu. Scale Setting Using the Extended Renormalization Group and the Principle of Maximum Conformality: the QCD Coupling Constant at Four Loops. *Phys. Rev. D*, 85:034038, 2012. [Erratum: *Phys.Rev.D* 86, 079903 (2012)].
- [27] Stanley J. Brodsky and Xing-Gang Wu. Eliminating the Renormalization Scale Ambiguity for Top-Pair Production Using the Principle of Maximum Conformality. *Phys. Rev. Lett.*, 109:042002, 2012.

- [28] Matin Mojaza, Stanley J. Brodsky, and Xing-Gang Wu. Systematic All-Orders Method to Eliminate Renormalization-Scale and Scheme Ambiguities in Perturbative QCD. *Phys. Rev. Lett.*, 110:192001, 2013.
- [29] Stanley J. Brodsky, Matin Mojaza, and Xing-Gang Wu. Systematic Scale-Setting to All Orders: The Principle of Maximum Conformality and Commensurate Scale Relations. *Phys. Rev. D*, 89:014027, 2014.
- [30] Xing-Gang Wu, Yang Ma, Sheng-Quan Wang, Hai-Bing Fu, Hong-Hao Ma, Stanley J. Brodsky, and Matin Mojaza. Renormalization Group Invariance and Optimal QCD Renormalization Scale-Setting. *Rept. Prog. Phys.*, 78:126201, 2015.
- [31] Xing-Gang Wu, Jian-Ming Shen, Bo-Lun Du, Xu-Dong Huang, Sheng-Quan Wang, and Stanley J. Brodsky. The QCD renormalization group equation and the elimination of fixed-order scheme-and-scale ambiguities using the principle of maximum conformality. *Prog. Part. Nucl. Phys.*, 108:103706, 2019.
- [32] Stanley J. Brodsky and Patrick Huet. Aspects of $SU(N(c))$ gauge theories in the limit of small number of colors. *Phys. Lett. B*, 417:145–153, 1998.
- [33] Stanley J. Brodsky, John R. Ellis, Einan Gardi, Marek Karliner, and Mark. A. Samuel. Pade approximants, optimal renormalization scales, and momentum flow in Feynman diagrams. *Phys. Rev. D*, 56:6980–6992, 1997.
- [34] P. A. Zyla et al. Review of Particle Physics. *PTEP*, 2020(8):083C01, 2020.
- [35] Keith A. Brueckner. Meson-Nucleon Scattering and Nucleon Isobars. *Phys. Rev.*, 86:106–109, 1952.
- [36] Michael E. Peskin and Daniel V. Schroeder. *An Introduction to quantum field theory*. Addison-Wesley, Reading, USA, 1995.

- [37] Yan-Rui Liu, Hua-Xing Chen, Wei Chen, Xiang Liu, and Shi-Lin Zhu. Pentaquark and Tetraquark states. *Prog. Part. Nucl. Phys.*, 107:237–320, 2019.
- [38] Robert L. Jaffe. Perhaps a Stable Dihyperon. *Phys. Rev. Lett.*, 38:195–198, 1977. [Erratum: *Phys.Rev.Lett.* 38, 617 (1977)].
- [39] Glennys R. Farrar. Stable Sexaquark. 8 2017. hep-ph/1708.08951.
- [40] T. Kinoshita. Mass singularities of Feynman amplitudes. *J. Math. Phys.*, 3:650–677, 1962.
- [41] T. D. Lee and M. Nauenberg. Degenerate Systems and Mass Singularities. *Phys. Rev.*, 133:B1549–B1562, 1964.
- [42] Gerard 't Hooft and M. J. G. Veltman. Regularization and Renormalization of Gauge Fields. *Nucl. Phys. B*, 44:189–213, 1972.
- [43] G. M. Cicuta and E. Montaldi. Analytic renormalization via continuous space dimension. *Lett. Nuovo Cim.*, 4:329–332, 1972.
- [44] C. G. Bollini and J. J. Giambiagi. Dimensional Renormalization: The Number of Dimensions as a Regularizing Parameter. *Nuovo Cim. B*, 12:20–26, 1972.
- [45] William A. Bardeen, A. J. Buras, D. W. Duke, and T. Muta. Deep Inelastic Scattering Beyond the Leading Order in Asymptotically Free Gauge Theories. *Phys. Rev. D*, 18:3998, 1978.
- [46] Gerard 't Hooft. Dimensional regularization and the renormalization group. *Nucl. Phys. B*, 61:455–468, 1973.
- [47] Steven Weinberg. New approach to the renormalization group. *Phys. Rev. D*, 8:3497–3509, 1973.
- [48] Sidney R. Coleman and David J. Gross. Price of asymptotic freedom. *Phys. Rev. Lett.*, 31:851–854, 1973.

- [49] G. M. Prosperi, M. Raciti, and C. Simolo. On the running coupling constant in QCD. *Prog. Part. Nucl. Phys.*, 58:387–438, 2007.
- [50] Guido Altarelli. The QCD Running Coupling and its Measurement. *PoS, Corfu2012:002*, 2013.
- [51] David J. Gross and Frank Wilczek. Ultraviolet Behavior of Nonabelian Gauge Theories. *Phys. Rev. Lett.*, 30:1343–1346, 1973.
- [52] H. David Politzer. Reliable Perturbative Results for Strong Interactions? *Phys. Rev. Lett.*, 30:1346–1349, 1973.
- [53] William E. Caswell. Asymptotic Behavior of Nonabelian Gauge Theories to Two Loop Order. *Phys. Rev. Lett.*, 33:244, 1974.
- [54] D. R. T. Jones. Two Loop Diagrams in Yang-Mills Theory. *Nucl. Phys. B*, 75:531, 1974.
- [55] E. Egorian and O. V. Tarasov. Two Loop Renormalization of the QCD in an Arbitrary Gauge. *Teor. Mat. Fiz.*, 41:26–32, 1979.
- [56] Martin Mojaza, Claudio Pica, and Francesco Sannino. Hot Conformal Gauge Theories. *Phys. Rev. D*, 82:116009, 2010.
- [57] S. A. Larin and J. A. M. Vermaseren. The Three loop QCD Beta function and anomalous dimensions. *Phys. Lett. B*, 303:334–336, 1993.
- [58] T. van Ritbergen, J. A. M. Vermaseren, and S. A. Larin. The Four loop beta function in quantum chromodynamics. *Phys. Lett. B*, 400:379–384, 1997.
- [59] P. A. Baikov, K. G. Chetyrkin, and J. H. Kühn. Five-Loop Running of the QCD coupling constant. *Phys. Rev. Lett.*, 118(8):082002, 2017.
- [60] Oleg Antipin and Francesco Sannino. Conformal Window 2.0: The large N_f safe story. *Phys. Rev. D*, 97(11):116007, 2018.

- [61] Tom Banks and A. Zaks. On the Phase Structure of Vector-Like Gauge Theories with Massless Fermions. *Nucl. Phys. B*, 196:189–204, 1982.
- [62] Einan Gardi, Georges Grunberg, and Marek Karliner. Can the QCD running coupling have a causal analyticity structure? *JHEP*, 07:007, 1998.
- [63] Thomas A. Ryttov and Robert Shrock. Scheme-independent calculations of physical quantities in an $N = 1$ supersymmetric gauge theory. *Phys. Rev. D*, 96(10):105018, 2017.
- [64] Leonardo Di Giustino, Francesco Sannino, Sheng-Quan Wang, and Xing-Gang Wu. Thrust distribution for 3-jet production from $e+e-$ annihilation within the QCD conformal window and in QED. *Phys. Lett. B*, 823:136728, 2021.
- [65] Einan Gardi. Why Padé approximants reduce the renormalization scale dependence in QFT? *Phys. Rev. D*, 56:68–79, 1997.
- [66] B. A. Kniehl, A. V. Kotikov, A. I. Onishchenko, and O. L. Veretin. Strong-coupling constant with flavor thresholds at five loops in the anti-MS scheme. *Phys. Rev. Lett.*, 97:042001, 2006.
- [67] Philippe Boucaud, F. de Soto, J. P. Leroy, A. Le Yaouanc, J. Micheli, H. Moutarde, O. Pene, and J. Rodriguez-Quintero. Artefacts and $\langle A^{**2} \rangle$ power corrections: Revisiting the MOM Z $\psi(p^{**2})$ and $Z(V)$. *Phys. Rev. D*, 74:034505, 2006.
- [68] K. G. Chetyrkin and A. Retey. Three loop three linear vertices and four loop similar to MOM beta functions in massless QCD. hep-ph/0007088.
- [69] Thomas Appelquist, Michael Dine, and I. J. Muzinich. The Static Potential in Quantum Chromodynamics. *Phys. Lett. B*, 69:231–236, 1977.
- [70] W. Fischler. Quark - anti-Quark Potential in QCD. *Nucl. Phys. B*, 129:157–174, 1977.

- [71] Markus Peter. The Static quark - anti-quark potential in QCD to three loops. *Phys. Rev. Lett.*, 78:602–605, 1997.
- [72] York Schroder. The Static potential in QCD to two loops. *Phys. Lett. B*, 447:321–326, 1999.
- [73] Alexander V. Smirnov, Vladimir A. Smirnov, and Matthias Steinhauser. Fermionic contributions to the three-loop static potential. *Phys. Lett. B*, 668:293–298, 2008.
- [74] Alexander V. Smirnov, Vladimir A. Smirnov, and Matthias Steinhauser. Three-loop static potential. *Phys. Rev. Lett.*, 104:112002, 2010.
- [75] C. Anzai, Y. Kiyo, and Y. Sumino. Static QCD potential at three-loop order. *Phys. Rev. Lett.*, 104:112003, 2010.
- [76] A. L. Kataev and V. S. Molokoedov. Fourth-order QCD renormalization group quantities in the V scheme and the relation of the β function to the Gell-Mann–Low function in QED. *Phys. Rev. D*, 92(5):054008, 2015.
- [77] M. Gockeler, R. Horsley, V. Linke, Paul E. L. Rakow, G. Schierholz, and H. Stuben. Is there a Landau pole problem in QED? *Phys. Rev. Lett.*, 80:4119–4122, 1998.
- [78] S. A. Larin, T. van Ritbergen, and J. A. M. Vermaseren. The Large quark mass expansion of $\Gamma(Z^0 \rightarrow \text{hadrons})$ and $\Gamma(\tau \rightarrow \tau\text{-neutrino} + \text{hadrons})$ in the order α_s^3 . *Nucl. Phys. B*, 438:278–306, 1995.
- [79] K. G. Chetyrkin, Bernd A. Kniehl, and M. Steinhauser. Strong coupling constant with flavor thresholds at four loops in the $\overline{\text{MS}}$ scheme. *Phys. Rev. Lett.*, 79:2184–2187, 1997.

- [80] Stanley J. Brodsky, Guy F. de Teramond, Hans Gunter Dosch, and Joshua Erlich. Light-Front Holographic QCD and Emerging Confinement. *Phys. Rept.*, 584:1–105, 2015.
- [81] S. Catani and L. Trentadue. Resummation of the QCD Perturbative Series for Hard Processes. *Nucl. Phys. B*, 327:323–352, 1989.
- [82] Leonardo Di Giustino, Giulia Ricciardi, and Luca Trentadue. Minimal prescription corrected spectra in heavy quark decays. *Phys. Rev. D*, 84:034017, 2011.
- [83] Guido Altarelli. Introduction to renormalons. In *5th Hellenic School and Workshops on Elementary Particle Physics*, pages 221–236, 1996.
- [84] M. Beneke. Renormalons. *Phys. Rept.*, 317:1–142, 1999.
- [85] Stanley J. Brodsky, Einan Gardi, Georges Grunberg, and Johan Rathsman. Disentangling running coupling and conformal effects in QCD. *Phys. Rev. D*, 63:094017, 2001.
- [86] Hung-Jung Lu and Stanley J. Brodsky. Relating physical observables in QCD without scale - scheme ambiguity. *Phys. Rev. D*, 48:3310–3318, 1993.
- [87] Farrukh Chishtie, D. G. C. McKeon, and T. N. Sherry. Renormalization Scheme Dependence in a QCD Cross Section. *Phys. Rev. D*, 94(5):054031, 2016.
- [88] F. A. Chishtie and D. G. C. McKeon. Renormalization Scheme Dependence and the Renormalization Group Beta Function. *Phys. Rev. D*, 95(11):116013, 2017.
- [89] David J. Gross and Andre Neveu. Dynamical Symmetry Breaking in Asymptotically Free Field Theories. *Phys. Rev. D*, 10:3235, 1974.

- [90] B. E. Lautrup. On High Order Estimates in QED. *Phys. Lett. B*, 69:109–111, 1977.
- [91] S. Catani, G. Turnock, B. R. Webber, and L. Trentadue. Thrust distribution in $e^+ e^-$ annihilation. *Phys. Lett. B*, 263:491–497, 1991.
- [92] S. Catani, L. Trentadue, G. Turnock, and B. R. Webber. Resummation of large logarithms in $e^+ e^-$ event shape distributions. *Nucl. Phys. B*, 407:3–42, 1993.
- [93] Stefano Catani, Michelangelo L. Mangano, Paolo Nason, and Luca Trentadue. The Resummation of soft gluons in hadronic collisions. *Nucl. Phys. B*, 478:273–310, 1996.
- [94] Ugo Aglietti, Leonardo Di Giustino, Giancarlo Ferrera, and Luca Trentadue. Resummed Mass Distribution for Jets Initiated by Massive Quarks. *Phys. Lett. B*, 651:275–292, 2007.
- [95] Andrea Banfi, Heather McAslan, Pier Francesco Monni, and Giulia Zanderighi. A general method for the resummation of event-shape distributions in e^+e^- annihilation. *JHEP*, 05:102, 2015.
- [96] Riccardo Abbate, Michael Fickinger, Andre H. Hoang, Vicent Mateu, and Iain W. Stewart. Thrust at N^3LL with Power Corrections and a Precision Global Fit for $\alpha_s(m_Z)$. *Phys. Rev. D*, 83:074021, 2011.
- [97] A. L. Kataev. Riemann $\zeta(3)$ - terms in perturbative QED series, conformal symmetry and the analogies with structures of multiloop effects in N=4 supersymmetric Yang-Mills theory. *Phys. Lett. B*, 691:82–86, 2010.
- [98] A. Dhar and V. Gupta. A New Perturbative Approach to Renormalizable Field Theories. *Phys. Rev. D*, 29:2822, 1984.

- [99] V. Gupta, D. V. Shirkov, and O. V. Tarasov. New perturbative approach to general renormalizable quantum field theories. *Int. J. Mod. Phys. A*, 6:3381–3397, 1991.
- [100] S. G. Gorishnii, A. L. Kataev, and S. A. Larin. The $O(\alpha_s^3)$ -corrections to $\sigma_{tot}(e^+e^- \rightarrow hadrons)$ and $\Gamma(\tau^- \rightarrow \nu_\tau + hadrons)$ in QCD. *Phys. Lett. B*, 259:144–150, 1991.
- [101] N. V. Krasnikov. Analyticity and Renormalization Group. *Nucl. Phys. B*, 192:497–508, 1981.
- [102] G. Grunberg and A. L. Kataev. On Some possible extensions of the Brodsky-Lepage-MacKenzie approach beyond the next-to-leading order. *Phys. Lett. B*, 279:352–358, 1992.
- [103] G. Grunberg. Method of effective charges and BLM criterion. *Phys. Rev. D*, 46:2228–2239, 1992.
- [104] Stanley J. Brodsky, Mandeep S. Gill, Michael Melles, and Johan Rathsmann. An Analytic extension of the $\overline{\text{MS}}$ -bar renormalization scheme. *Phys. Rev. D*, 58:116006, 1998.
- [105] Hung Jung Lu and C. A. R. Sa de Melo. Dressed skeleton expansion and the coupling scale ambiguity problem. *Phys. Lett. B*, 273:260–267, 1991. [Erratum: *Phys.Lett.B* 285, 399 (1992)].
- [106] Hung Jung Lu. Dressed skeleton expansion in (1+1)-dimensional field theory models. *Phys. Rev. D*, 45:1217–1232, 1992.
- [107] S. J. Brodsky, A. H. Hoang, Johann H. Kuhn, and T. Teubner. Angular distributions of massive quarks and leptons close to threshold. *Phys. Lett. B*, 359:355–361, 1995.

- [108] Stanley J. Brodsky and Hung Jung Lu. Commensurate scale relations in quantum chromodynamics. *Phys. Rev. D*, 51:3652–3668, 1995.
- [109] R. J. Crewther. Nonperturbative evaluation of the anomalies in low-energy theorems. *Phys. Rev. Lett.*, 28:1421, 1972.
- [110] David J. Broadhurst and A. L. Kataev. Connections between deep inelastic and annihilation processes at next to next-to-leading order and beyond. *Phys. Lett. B*, 315:179–187, 1993.
- [111] P. A. Baikov, K. G. Chetyrkin, and J. H. Kuhn. Adler Function, Bjorken Sum Rule, and the Crewther Relation to Order α_s^4 in a General Gauge Theory. *Phys. Rev. Lett.*, 104:132004, 2010.
- [112] S. J. Brodsky, G. T. Gabadadze, A. L. Kataev, and H. J. Lu. The Generalized Crewther relation in QCD and its experimental consequences. *Phys. Lett. B*, 372:133–140, 1996.
- [113] P.N. Burrows, H. Masuda, D. Muller, and Y. Ohnishi. Application of 'optimized' perturbation theory to determination of $\alpha_s(M_Z^2)$ from hadronic event shape observables in e+e- annihilation. *Physics Letters B*, 382(1):157–164, 1996.
- [114] M. Beneke and Vladimir M. Braun. Naive nonAbelianization and resummation of fermion bubble chains. *Phys. Lett. B*, 348:513–520, 1995.
- [115] Patricia Ball, M. Beneke, and Vladimir M. Braun. Resummation of (beta0 alpha-s)**n corrections in QCD: Techniques and applications to the tau hadronic width and the heavy quark pole mass. *Nucl. Phys. B*, 452:563–625, 1995.
- [116] Matthias Neubert. Scale setting in QCD and the momentum flow in Feynman diagrams. *Phys. Rev. D*, 51:5924–5941, 1995.

- [117] S. V. Mikhailov. Generalization of BLM procedure and its scales in any order of pQCD: A Practical approach. *JHEP*, 06:009, 2007.
- [118] A. L. Kataev and S. V. Mikhailov. Generalization of the Brodsky-Lepage-Mackenzie optimization within the β -expansion and the principle of maximal conformality. *Phys. Rev. D*, 91(1):014007, 2015.
- [119] Huan-Yu Bi, Xing-Gang Wu, Yang Ma, Hong-Hao Ma, Stanley J. Brodsky, and Martin Mojaza. Degeneracy Relations in QCD and the Equivalence of Two Systematic All-Orders Methods for Setting the Renormalization Scale. *Phys. Lett. B*, 748:13–18, 2015.
- [120] Xu-Dong Huang, Xing-Gang Wu, Qing Yu, Xu-Chang Zheng, Jun Zeng, and Jian-Ming Shen. Generalized Crewther relation and a novel demonstration of the scheme independence of commensurate scale relations up to all orders. *Chin. Phys. C*, 45:103104, 2021.
- [121] Xing-Gang Wu, Sheng-Quan Wang, and Stanley J. Brodsky. Importance of proper renormalization scale-setting for QCD testing at colliders. *Front. Phys. (Beijing)*, 11(1):111201, 2016.
- [122] Jian-Ming Shen, Xing-Gang Wu, Bo-Lun Du, and Stanley J. Brodsky. Novel All-Orders Single-Scale Approach to QCD Renormalization Scale-Setting. *Phys. Rev. D*, 95(9):094006, 2017.
- [123] Xing-Gang Wu, Jian-Ming Shen, Bo-Lun Du, and Stanley J. Brodsky. Novel demonstration of the renormalization group invariance of the fixed-order predictions using the principle of maximum conformality and the C -scheme coupling. *Phys. Rev. D*, 97(9):094030, 2018.
- [124] Stefan Weinzierl. NNLO corrections to 3-jet observables in electron-positron annihilation. *Phys. Rev. Lett.*, 101:162001, 2008.

- [125] Stefan Weinzierl. Event shapes and jet rates in electron-positron annihilation at NNLO. *JHEP*, 06:041, 2009.
- [126] Michael Binger and Stanley J. Brodsky. The Form-factors of the gauge-invariant three-gluon vertex. *Phys. Rev. D*, 74:054016, 2006.
- [127] Stefan Kluth. Tests of Quantum Chromo Dynamics at e+ e- Colliders. *Rept. Prog. Phys.*, 69:1771–1846, 2006.
- [128] A. Heister et al. Studies of QCD at e+ e- centre-of-mass energies between 91-GeV and 209-GeV. *Eur. Phys. J. C*, 35:457–486, 2004.
- [129] J. Abdallah et al. A Study of the energy evolution of event shape distributions and their means with the DELPHI detector at LEP. *Eur. Phys. J. C*, 29:285–312, 2003.
- [130] G. Abbiendi et al. Measurement of event shape distributions and moments in e+ e- \rightarrow hadrons at 91-GeV - 209-GeV and a determination of $\alpha(s)$. *Eur. Phys. J. C*, 40:287–316, 2005.
- [131] P. Achard et al. Studies of hadronic event structure in e^+e^- annihilation from 30-GeV to 209-GeV with the L3 detector. *Phys. Rept.*, 399:71–174, 2004.
- [132] K. Abe et al. Measurement of $\alpha_s(M(Z)^{**2})$ from hadronic event observables at the Z0 resonance. *Phys. Rev. D*, 51:962–984, 1995.
- [133] R. Keith Ellis, D. A. Ross, and A. E. Terrano. The Perturbative Calculation of Jet Structure in e+ e- Annihilation. *Nucl. Phys. B*, 178:421–456, 1981.
- [134] Zoltan Kunszt. Comment on the $O(\alpha^{**2-S})$ Corrections to Jet Production in e+ e- Annihilation. *Phys. Lett. B*, 99:429–432, 1981.
- [135] J. A. M. Vermaseren, K. J. F. Gaemers, and S. J. Oldham. Perturbative QCD Calculation of Jet Cross-Sections in e+ e- Annihilation. *Nucl. Phys. B*, 187:301–320, 1981.

- [136] K. Fabricius, I. Schmitt, G. Kramer, and G. Schierholz. Higher Order Perturbative QCD Calculation of Jet Cross-Sections in $e^+ e^-$ Annihilation. *Z. Phys. C*, 11:315, 1981.
- [137] W. T. Giele and E. W. Nigel Glover. Higher order corrections to jet cross-sections in $e^+ e^-$ annihilation. *Phys. Rev. D*, 46:1980–2010, 1992.
- [138] S. Catani and M. H. Seymour. The Dipole formalism for the calculation of QCD jet cross-sections at next-to-leading order. *Phys. Lett. B*, 378:287–301, 1996.
- [139] A. Gehrmann-De Ridder, T. Gehrmann, E. W. N. Glover, and G. Heinrich. EERAD3: Event shapes and jet rates in electron-positron annihilation at order α_s^3 . *Comput. Phys. Commun.*, 185:3331, 2014.
- [140] A. Gehrmann-De Ridder, T. Gehrmann, E. W. N. Glover, and G. Heinrich. Second-order QCD corrections to the thrust distribution. *Phys. Rev. Lett.*, 99:132002, 2007.
- [141] A. Gehrmann-De Ridder, T. Gehrmann, E. W. N. Glover, and G. Heinrich. NNLO corrections to event shapes in $e^+ e^-$ annihilation. *JHEP*, 12:094, 2007.
- [142] Vittorio Del Duca, Claude Duhr, Adam Kardos, Gábor Somogyi, Zoltán Szőr, Zoltán Trócsányi, and Zoltán Tulipánt. Jet production in the CoLoRFulNNLO method: event shapes in electron-positron collisions. *Phys. Rev. D*, 94(7):074019, 2016.
- [143] Vittorio Del Duca, Claude Duhr, Adam Kardos, Gábor Somogyi, and Zoltán Trócsányi. Three-Jet Production in Electron-Positron Collisions at Next-to-Next-to-Leading Order Accuracy. *Phys. Rev. Lett.*, 117(15):152004, 2016.
- [144] Ugo Aglietti, Leonardo Di Giustino, Giancarlo Ferrera, Alessandro Renzaglia, Giulia Ricciardi, and Luca Trentadue. Threshold Resummation in $B \rightarrow X(c) l \nu(l)$ Decays. *Phys. Lett. B*, 653:38–52, 2007.

- [145] Leonardo Di Giustino, Stanley J. Brodsky, Sheng-Quan Wang, and Xing-Gang Wu. Infinite-order scale-setting using the principle of maximum conformality: A remarkably efficient method for eliminating renormalization scale ambiguities for perturbative QCD. *Phys. Rev. D*, 102(1):014015, 2020.
- [146] Sheng-Quan Wang, Stanley J. Brodsky, Xing-Gang Wu, and Leonardo Di Giustino. Thrust Distribution in Electron-Positron Annihilation using the Principle of Maximum Conformality. *Phys. Rev. D*, 99(11):114020, 2019.
- [147] K. G. Chetyrkin, Johann H. Kuhn, and M. Steinhauser. RunDec: A Mathematica package for running and decoupling of the strong coupling and quark masses. *Comput. Phys. Commun.*, 133:43–65, 2000.
- [148] Thomas Gehrmann, Niklaus Häfliger, and Pier Francesco Monni. BLM Scale Fixing in Event Shape Distributions. *Eur. Phys. J. C*, 74(6):2896, 2014.
- [149] Sheng-Quan Wang, Stanley J. Brodsky, Xing-Gang Wu, Jian-Ming Shen, and Leonardo Di Giustino. Novel method for the precise determination of the QCD running coupling from event shape distributions in electron-positron annihilation. *Phys. Rev. D*, 100(9):094010, 2019.
- [150] Dennis D. Dietrich and Francesco Sannino. Conformal window of SU(N) gauge theories with fermions in higher dimensional representations. *Phys. Rev. D*, 75:085018, 2007.
- [151] Giacomo Cacciapaglia, Claudio Pica, and Francesco Sannino. Fundamental Composite Dynamics: A Review. *Phys. Rept.*, 877:1–70, 2020.
- [152] M. Tanabashi et al. Review of Particle Physics. *Phys. Rev. D*, 98(3):030001, 2018.
- [153] G. Dissertori, A. Gehrmann-De Ridder, T. Gehrmann, E. W. N. Glover, G. Heinrich, G. Luisoni, and H. Stenzel. Determination of the strong cou-

- pling constant using matched NNLO+NLLA predictions for hadronic event shapes in e+e- annihilations. *JHEP*, 08:036, 2009.
- [154] André H. Hoang, Daniel W. Kolodrubetz, Vicent Mateu, and Iain W. Stewart. Precise determination of α_s from the C -parameter distribution. *Phys. Rev. D*, 91(9):094018, 2015.
- [155] Mrinal Dasgupta and Gavin P. Salam. Event shapes in e+ e- annihilation and deep inelastic scattering. *J. Phys. G*, 30:R143, 2004.
- [156] André H. Hoang, Daniel W. Kolodrubetz, Vicent Mateu, and Iain W. Stewart. C -parameter distribution at N³LL' including power corrections. *Phys. Rev. D*, 91(9):094017, 2015.
- [157] G. Abbiendi et al. Measurement of the running of the QED coupling in small-angle Bhabha scattering at LEP. *Eur. Phys. J. C*, 45:1–21, 2006.
- [158] A. Gehrmann-De Ridder, T. Gehrmann, E. W. N. Glover, and G. Heinrich. NNLO moments of event shapes in e+e- annihilation. *JHEP*, 05:106, 2009.
- [159] Stefan Weinzierl. Moments of event shapes in electron-positron annihilation at NNLO. *Phys. Rev. D*, 80:094018, 2009.
- [160] Christoph Johannes Pahl. *Untersuchung perturbativer und nichtperturbativer Struktur der Momente hadronischer Ereignisformvariablen mit den Experimenten JADE und OPAL*. PhD thesis, Munich, Max Planck Inst., 2007.
- [161] D. M. Asner et al. Physics at BES-III. *Int. J. Mod. Phys. A*, 24:S1–794, 2009.
- [162] V. A. Novikov, L. B. Okun, Mikhail A. Shifman, A. I. Vainshtein, M. B. Voloshin, and Valentin I. Zakharov. Sum Rules for Charmonium and Charmed Mesons Decay Rates in Quantum Chromodynamics. *Phys. Rev. Lett.*, 38:626, 1977. [Erratum: *Phys.Rev.Lett.* 38, 791 (1977)].

- [163] V. A. Novikov, L. B. Okun, Mikhail A. Shifman, A. I. Vainshtein, M. B. Voloshin, and Valentin I. Zakharov. Charmonium and Gluons: Basic Experimental Facts and Theoretical Introduction. *Phys. Rept.*, 41:1–133, 1978.
- [164] M. B. Voloshin. Precision determination of α_s and $m(b)$ from QCD sum rules for b anti- b . *Int. J. Mod. Phys. A*, 10:2865–2880, 1995.
- [165] Katja Seidel, Frank Simon, Michal Tesar, and Stephane Poss. Top quark mass measurements at and above threshold at CLIC. *Eur. Phys. J. C*, 73(8):2530, 2013.
- [166] Andrzej Czarnecki and Kirill Melnikov. Two loop QCD corrections to the heavy quark pair production cross-section in e^+e^- annihilation near the threshold. *Phys. Rev. Lett.*, 80:2531–2534, 1998.
- [167] M. Beneke, A. Signer, and Vladimir A. Smirnov. Two loop correction to the leptonic decay of quarkonium. *Phys. Rev. Lett.*, 80:2535–2538, 1998.
- [168] W. Bernreuther, R. Bonciani, T. Gehrmann, R. Heinesch, T. Leineweber, P. Mastrolia, and E. Remiddi. Two-Parton Contribution to the Heavy-Quark Forward-Backward Asymmetry in NNLO QCD. *Nucl. Phys. B*, 750:83–107, 2006.
- [169] Sheng-Quan Wang, Stanley J. Brodsky, Xing-Gang Wu, Leonardo Di Giustino, and Jian-Ming Shen. Renormalization scale setting for heavy quark pair production in e^+e^- annihilation near the threshold region. *Phys. Rev. D*, 102(1):014005, 2020.
- [170] Werner Bernreuther, Long Chen, Oliver Dekkers, Thomas Gehrmann, and Dennis Heisler. The forward-backward asymmetry for massive bottom quarks at the Z peak at next-to-next-to-leading order QCD. *JHEP*, 01:053, 2017.
- [171] A. Sommerfeld. *Atombau und Spektrallinien*. F. Vieweg & Sohn, 1921.

- [172] G. Gamow. Zur Quantentheorie des Atomkernes. *Z. Phys.*, 51:204–212, 1928.
- [173] Andrei D. Sakharov. Interaction of an Electron and Positron in Pair Production. *Zh. Eksp. Teor. Fiz.*, 18:631–635, 1948.
- [174] A. H. Hoang, Johann H. Kuhn, and T. Teubner. Radiation of light fermions in heavy fermion production. *Nucl. Phys. B*, 452:173–187, 1995.
- [175] A. H. Hoang. Two loop corrections to the electromagnetic vertex for energies close to threshold. *Phys. Rev. D*, 56:7276–7283, 1997.
- [176] Stanley J. Brodsky and Guy F. de Téramond. Light-front hadron dynamics and AdS/CFT correspondence. *Phys. Lett. B*, 582:211–221, 2004.
- [177] Herschel A. Chawdhry and Alexander Mitov. Ambiguities of the principle of maximum conformality procedure for hadron collider processes. *Phys. Rev. D*, 100(7):074013, 2019.
- [178] Marco Bonvini. Probabilistic definition of the perturbative theoretical uncertainty from missing higher orders. *Eur. Phys. J. C*, 80(10):989, 2020.
- [179] Claude Duhr, Alexander Huss, Aleksas Mazeliauskas, and Robert Szafron. An analysis of Bayesian estimates for missing higher orders in perturbative calculations. *JHEP*, 09:122, 2021.
- [180] Sheng-Quan Wang, Chao-Qin Luo, Xing-Gang Wu, Jian-Ming Shen, and Leonardo Di Giustino. New analyses of event shape observables in electron-positron annihilation and the determination of α_s running behavior in perturbative domain. 12 2021. hep-ph/2112.06212.
- [181] Xu-Dong Huang, Jiang Yan, Hong-Hao Ma, Leonardo Di Giustino, Jian-Ming Shen, Xing-Gang Wu, and Stanley J. Brodsky. Detailed Comparison of Renormalization Scale-Setting Procedures based on the Principle of Maximum Conformality. 9 2021. hep-ph/2109.12356.

- [182] Chu-Tian Gao, Xing-Gang Wu, Xu-Dong Huang, and Jun Zeng. The Higgs-boson decay $H \rightarrow gg$ using the infinite-order scale-setting approach based on the intrinsic conformality. 9 2021. hep-ph/2109.11754.